

AD-A172 996

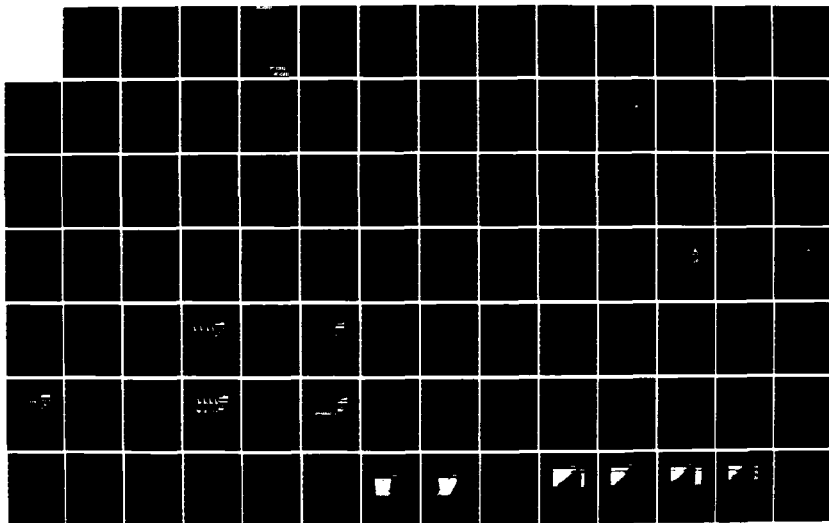
FREE ELECTRON LASER THEORY(U) BERKELEY RESEARCH  
ASSOCIATES INC CA W B COLSON 10 JUL 86 DRA-86-313R  
AFOSR-TR-86-0912 F49620-85-C-0007

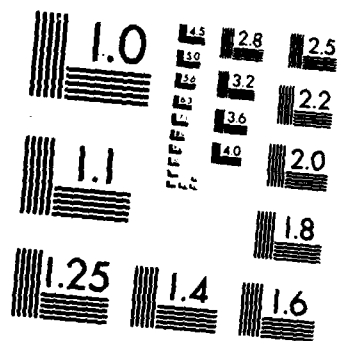
1/2

UNCLASSIFIED

F/G 20/5

NL





MICROCOPY RESOLUTION TEST CHART  
NATIONAL BUREAU OF STANDARDS-1963-A

AD-A172 996



# BERKELEY RESEARCH ASSOCIATES, INC.

AFOSR-TR- 86 - 0912

BRA - 86 - 313R

July 1986

## FREE ELECTRON LASER THEORY

W. B. Colson

Berkeley Research Associates  
P. o. Box 241  
Berkeley, CA 94701

Approved for release;  
distribution unlimited.

AIR FORCE OFFICE OF SCIENTIFIC RESEARCH (AFOSR)  
NOTED FOR DISTRIBUTION TO DTIC  
This report has been reviewed and is  
approved for public release IAW AFR 100-12.  
Distribution is unlimited.

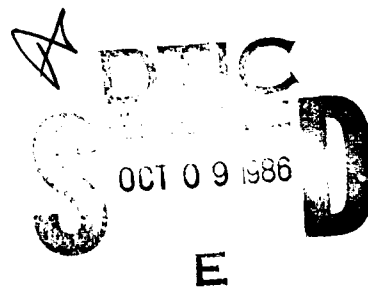
WILLIAM J. KEEFER

Chief, Technical Information Division

Final Scientific Report  
Contract No. F49620-85-C-0087

Prepared for

Air Force Office of Scientific Research  
Bolling Air Force Base  
Washington, DC 20332



86 10 6 084

**Air Force Office of Scientific Research**

**AFOSR F49620-85-C-0087**

*W. B. Colson*

Berkeley Research Associates, P.O. Box 241, Berkeley, CA 94701

Accession For	
NTIS GRA&I	<input checked="checked" type="checkbox"/>
DTIC TAB	<input type="checkbox"/>
Unannounced	<input type="checkbox"/>
Justification	
By _____	
Distribution/	
Availability Codes	
Dist	Avail and/or Special
A-1	

**Abstract**

Free electron laser (FEL) theory is extended to explain several effects associated with high gain operation. The trapped-particle instability is reviewed for short pulse FELs, FEL oscillators, and FEL amplifiers. A new FEL theory exactly includes the effect of an arbitrary electron distribution function and an explanation is given for optical self-guiding.

**Final Scientific Report**

1. Introduction
2. Panel Discussion on Long Undulators
3. Review Article
4. The Trapped-Particle Instability
5. Electron Beam Energy Spread and Emittance
6. Optical Self-Guiding

**Documents**

"Free Electron Lasers", W. B. Colson and A. M. Sessler, Annual Reviews of Nuclear and Particle Science 35, 25 (1985).

"The Trapped-Particle Instability in Free-Electron Laser Oscillators and Amplifiers", W. B. Colson, Proceedings of the 1985 Free-Electron Laser Conference, Lake Tahoe CA (1986).

"The Effect of Electron Trapping in Free-Electron Laser Oscillators and Amplifiers", W. B. Colson, Proceedings of the 1985 International Conf. on LASERs, Las Vegas CA (1986).

"Free-Electron Laser Gain Degradation and Electron Beam Quality", W. B. Colson, J. C. Gallardo and P. M. Bosco, submitted to Physical Review A.

**Invention (Patent) Report**

**UNCLASSIFIED**

## REPORT DOCUMENTATION PAGE

1a. REPORT SECURITY CLASSIFICATION <b>Approved for public release, distribution unlimited</b>		1b. RESTRICTIVE MARKINGS	
2a. SECURITY CLASSIFICATION AUTHORITY		3. DISTRIBUTION/AVAILABILITY OF REPORT <b>Approved for public release, distribution unlimited</b>	
2b. DECLASSIFICATION/DOWNGRADING SCHEDULE		5. MONITORING ORGANIZATION REPORT NUMBER(S) <b>AFOSR-TR-86-0012</b>	
4. PERFORMING ORGANIZATION REPORT NUMBER(S) <b>BRA - 86 - 313R</b>		7a. NAME OF MONITORING ORGANIZATION <b>Air Force Office of Scientific Research</b>	
6a. NAME OF PERFORMING ORGANIZATION <b>Berkeley Research Associates</b>	6b. OFFICE SYMBOL (if applicable)	7b. ADDRESS (City, State, and ZIP Code) <b>Bolling Air Force Base Washington, DC 20032</b>	
8a. NAME OF FUNDING/SPONSORING ORGANIZATION <b>AFOSR</b>	8b. OFFICE SYMBOL (if applicable) <b>NP</b>	9. PROCUREMENT INSTRUMENT IDENTIFICATION NUMBER <b>79A606-85-C-0087</b>	
8c. ADDRESS (City, State, and ZIP Code) <b>AFOSR/NP, Bldg 410 Bolling AFB DC 20332-6148</b>		10. SOURCE OF FUNDING NUMBERS PROGRAM ELEMENT NO. <b>61102F</b> PROJECT NO. <b>0301</b> TASK NO. <b>A1</b> WORK UNIT ACCESSION NO. <b>N/A</b>	
11. TITLE (Include Security Classification) <b>Free Electron Laser Theory</b>			
12. PERSONAL AUTHOR(S) <b>W. B. Colson</b>			
13a. TYPE OF REPORT <b>Final Scientific</b>	13b. TIME COVERED FROM <b>5/65/81</b> TO <b>7/9/81</b>	14. DATE OF REPORT (Year, Month, Day) <b>86/10/01</b>	15. PAGE COUNT <b>1</b>
16. SUPPLEMENTARY NOTATION			
17. COSATI CODES FIELD GROUP SUB-GROUP		18. SUBJECT TERMS (Continue on reverse if necessary and identify by block number) <b>free electron laser; laser amplifiers; trapped particle instability; long undulators; laser oscillators; review article.</b>	
19. ABSTRACT (Continue on reverse if necessary and identify by block number) <b>Free electron laser (FEL) theory is extended to explain several effects associated with high gain operation. The trapped-particle instability is reviewed for short pulse FELs, FEL oscillators, and FEL amplifiers. A new FEL theory exactly includes the effect of an arbitrary electron distribution function and an explanation is given for optical self-guiding.</b>			
20. DISTRIBUTION/AVAILABILITY OF ABSTRACT <input checked="" type="checkbox"/> UNCLASSIFIED/UNLIMITED <input type="checkbox"/> SAME AS RPT. <input type="checkbox"/> DTIC USERS		21. ABSTRACT SECURITY CLASSIFICATION <b>UNCLASSIFIED</b>	
22a. NAME OF RESPONSIBLE INDIVIDUAL <b>HOWARD R. SCHLOSSBERG</b>		22b. TELEPHONE (Include Area Code) (if applicable) <b>202/762-4906</b>	

**UNCLASSIFIED**

## Final Scientific Report: F49620-85-C-0087

May 1, 1985 to April 30, 1986

### Introduction

The proposed research was partially funded and the following reports on the resulting scientific progress. We have continued to work closely with the experimental free electron laser (FEL) projects in Universities and National Research Labs with emphasis on the high-power configurations at LANL and LLNL as well as the short wavelength configurations at Stanford and LANL. One aspect of the work has been to characterize the FEL trapped-particle instability. An especially important result is a new theoretical procedure solving the FEL wave and electron equations in weak optical fields for an arbitrary electron distribution function.

The slowly-varying, self-consistent wave and electron equations of motion provide the basic theory. The complex optical field strength is  $a(\vec{x}, \tau)$ , and the electron phase is  $\zeta(\vec{x}, \tau)$ . The optical wave envelope is then described by the parabolic wave equation:

$$\left[ -\frac{i}{4} \nabla_{\perp}^2 + \frac{\partial}{\partial \tau} \right] a(\vec{x}, \tau) = - \langle j(\vec{x}) \exp(-i \zeta(\vec{x}, \tau)) \rangle , \quad (1)$$

where the dimensionless current density is  $j(\vec{x}, \tau)$  and  $\nabla_{\perp}^2$  is the transverse Laplacian. FELs amplify the radiation with a co-propagating relativistic electron beam traveling along the axis of a long, undulating magnetic field. For the periodic undulator, we can describe the electron dynamics at a site in the beam with the self-consistent pendulum equation:

$$\ddot{\zeta}(z + \tau) = \dot{v}(z + \tau) = \frac{1}{2} [ a(z) \exp(i \zeta(z + \tau)) + a^*(z) \exp(-i \zeta(z + \tau)) ] . \quad (2)$$

The slippage of the optical field with respect to the electrons is indicated by  $(z + \tau)$ . The longitudinal variables have been normalized to the slippage distance and all variables have been reduced to a meaningful dimensionless form.

While simple in form, these equations contain a large array of important effects describing FEL operation. The goals of high optical power or short optical wavelengths both have in common the need for increasing the current density  $j(\vec{x})$  above. This coupling between the electrons and light can be increased by increasing the undulator length and/or the physical electron current density.

#### **Panel Discussion on Long Undulators**

Several members of the FEL community reviewed the possible limitations of long undulators containing up to  $10^3$  periods. The panel members were K. Halbach, B. Kincaid, B. Newman, D. A. G. Deacon, and myself (panel discussion leader). The general conclusion was that the expected improvements in the design of currently proposed undulators will make it possible to reach the long lengths desired. The tasks will be difficult, but not forbidden by serious physical limitations. The reference is

"Long Wigglers for Free Electron Lasers: A Maximum Limit?", First International Laser Science Conference, Dallas TX (1985).

#### **FEL Review Article**

Some work on a major review article fell into this contracting period. FELs were reviewed starting with their historical development from microwave tubes and atomic lasers. Data describing all operating FEL experiments was presented in a table format. The basic FEL theory is reviewed with extensions to include many of the complicated effects in equations (1) and (2). The high-gain growth rate is derived for the first time from the single-particle equations of motion. Specific accelerators suitable for driving FELs are reviewed in a table format. The linac driven FEL, induction linac driven FEL, and the storage-ring FEL are described in more detail. The extensions of the FEL undulator designs and new configurations are summarized. The reference is

W. B. Colson and A. M. Sessler, "Free Electron Lasers", Annual Reviews of Nuclear and Particle Science 35, 25 (1985).

A document report on this paper follows.

#### **The Trapped-Particle Instability**

Several simulations and simulation techniques have been developed describing the trapped-particle instability in free-electron laser oscillators and amplifiers. There are distinct differences in the physics in these two cases. The electrons in a high-power free-electron laser can become trapped and oscillate in deep potential wells formed by the combined optical and undulator field forces. The trapped current oscillates at the synchrotron frequency, and can drive the optical wave at sideband frequencies around the fundamental. This "trapped-particle instability" can occur in both the oscillator and amplifier configurations. The gain in the trapped-particle sideband frequencies has been calculated at saturation and agrees well with the simulation results. General features of the trapped-particle instability in free-electron laser

oscillators and amplifiers have been summarized. Dimensionless parameters are used to clarify the trends for a wide range of FEL designs. The instability was first observed in the simulation of short pulse oscillators, and then extended to long pulse oscillators. In this research, the trends of the trapped-particle instability in short pulse oscillators, long pulse oscillators, and now long pulse amplifiers is compared. This research made the first simulations of the sideband instability in the LLNL long pulse amplifiers. There are two publications:

"The Trapped-Particle Instability in Free-Electron Laser Oscillators and Amplifiers", W. B. Colson, Proc. of the 1985 Free-Electron Laser Conference, Lake Tahoe CA (1986).

"The Effect of Electron Trapping in Free-Electron Laser Oscillators and Amplifiers", W. B. Colson, Proceedings of the 1985 International Conf. on LASERs, Las Vegas CA (1986).

These two documents are included at the end of this report.

#### **Electron Beam Energy Spread and Emittance**

In an FEL, maintaining the coherence of the electron bunches over a significant interaction length imposes important restrictions on the electron beam quality. An energy or angular spread (due to emittance) contributes a random component to the electron motion that decreases the coherent bunching in time. Some of the earliest FEL experiments used electron beams that were essentially monoenergetic, but practically all subsequent experiments have made use of higher current sources with significant energy spread or emittance. Many accelerators present a design trade-off between high current and high beam quality. This makes it essential to accurately evaluate the effects of beam quality in present and future experiments. It is particularly important for FELs designed to operate at XUV or X-ray wavelengths.

The theory presented here uses a convenient, yet powerful, method of including an arbitrary electron distribution function in a self-consistent integral equation for the complex optical field. FEL gain and the effects of beam quality can then be calculated analytically or integrated on a small computer. Since the basic equations solved here are the same as in computer simulations or the plasma dispersion methods, specific physical results have been shown to agree with those methods when a direct comparison is possible. The computer simulations have proved to be a useful method of understanding many aspects of the FEL interaction, but one of the most difficult effects to accurately characterize is that of electron beam quality. Even a prohibitively large number of sample particles is far short of the number in a real experiment, and yet introduces a large amount of numerical noise when distributed over a large volume of phase-space. To reproduce some of the results shown later in this paper, we found the simulation method to be several hundred to a thousand times less efficient. While many other FEL topics are most

efficiently studied through simulations, the detrimental effects of beam quality are probably better handled through a combination of analytic and numerical techniques.

The stability analysis used to obtain plasma dispersion relations usually calculates the reduced FEL growth rates due to poor beam quality. This method can lead to analytical expressions, but depends upon specific models for the electron beam distribution, and does not easily describe more complicated transient behavior where the FEL growth rate is not constant; the FEL is often designed to operate in this regime. In addition, the exact formulation presented here works smoothly between different regimes of operation like high and low gain. The only requirement is weak optical fields.

An FEL with arbitrary beam quality is accurately described by the Lorentz-Maxwell equations solved self-consistently in weak optical fields. The integral equation is formed by summing over all electrons in the beam. The result has no reference to the electron phases and only involves the optical field evolution. High gain growth rates can be recovered from the integral equation analytically; the integral can be solved numerically for more complicated cases. Contour maps are used to show the gain degradation due to an electron beam energy spread and an electron beam angular spread. In the limit of low gain, the gain spectrum is related to the spontaneous emission line-shape through successively higher derivatives. In the limit of high gain, it is shown that the growth rate becomes less susceptible to degradation from the electron beam quality. The reference is

"Free-Electron Laser Gain Degradation and Electron Beam Quality", W. B. Colson, J. C. Gallardo and P. M. Bosco, submitted to Physical Review A.

The document report is included at the end of this report.

#### **Understanding the Free Electron Laser Optical Self-Guiding Effect**

In the free electron laser (FEL) interaction the optical light wave and electrons travel together through the periodic magnetic field of the undulator. Without the electron beam interaction, the optical wavefronts propagate in vacuum and diffract according to Maxwell's wave equation. Depending on the wavelength, diffraction can provide an important limitation to the effective interaction length of the undulator. This would reduce the coupling of the electrons and light, because the light diffracts away the smaller electron beam.

An important FEL effect is the optical guiding of light which focuses the light wave back into the electron beam so the interaction strength can remain strong over long undulators. The existence of this effect is crucial to XUV application and high power FELs. This brief section contains a simple understanding of how the self-guiding effect can work favorably for FELs.

We start with the full optical wave equation

$$\left[ \nabla_{\perp}^2 + \frac{\partial^2}{\partial z^2} - \frac{1}{c^2} \frac{\partial^2}{\partial t^2} \right] \vec{A} = -\frac{4\pi}{c} \vec{J}_{\perp} \quad (3)$$

Using the slowly varying amplitude and phase approximation, the longitudinal derivatives in the wave operator can be reduced to single derivatives,  $ik(\partial_z + c^{-1}\partial_t)$  where  $k$  is the optical wavenumber. With the coordinate changes  $s = z - ct$  and  $\tau = ct/L$  we have  $(\partial_z + c^{-1}\partial_t) \rightarrow L^{-1}\partial_{\tau}$ , where  $L$  is the length of the FEL undulator. The full wave equation is now reduced to the parabolic wave equation,

$$\left[ -\frac{i}{4} \nabla_{\perp}^2 + \frac{\partial}{\partial \tau} \right] a(x, y, \tau) = r.h.s. \quad (4)$$

where  $x = X(k/2L)^{1/2}$  and  $y = Y(k/2L)^{1/2}$  are dimensionless transverse coordinates, and a long electron pulse has been assumed to give translational invariance in the  $z$  dimension. The interacting current on the right hand side (*r.h.s.*) of the wave equation is determined by the Lorentz force. The transverse motion of electrons is given by  $\beta_{\perp} = e\vec{B}_m / \gamma mc^2 k_0$  where  $\gamma mc^2$  is the electron energy  $\lambda_0 = 2\pi/k_0$  is the undulator wavelength and  $\vec{B}_m$  is the transverse undulator magnetic field. The current is not examined in detail here, except to say that in the absence of diffraction, the FEL interaction causes the optical phase to increase,  $\Delta\phi_{FEL} > 0$  at the wavelength of maximum gain. This is true in either the high or low gain regimes, has been observed in many simulations, and can be shown analytically.

In order to study the modification of FEL interaction to diffraction we first try to understand the diffraction process itself. So, the discussion proceeds with  $\vec{J}_{\perp} = 0$  in (3) and *r.h.s.* = 0 in (4). The exact solution of (4) in this case over a finite time interval  $\Delta\tau$  is

$$a(x, y, \tau + \Delta\tau) = e^{\frac{i}{4} \nabla_{\perp}^2 \Delta\tau} a(x, y, \tau) \quad (5)$$

There is no restriction in (5) that the time interval  $\Delta\tau$  is small, but the equation does require derivatives to infinite order. If the time interval  $\Delta\tau$  is small, then an approximate solution is

$$a(x, y, \tau + \Delta\tau) \approx a(x, y, \tau) + \frac{i}{4} \nabla_{\perp}^2 a(x, y, \tau) \Delta\tau + \dots \quad (4)$$

The Laplacian  $\nabla_{\perp}^2 = \partial_x^2 + \partial_y^2$  can be evaluated including only nearest neighbors. Propagation of the real and imaginary parts of the optical field  $ar(x, y)$  and  $ai(x, y)$  is accomplished with one step for the following statements in Fortran.

```

_#_ _statement_
1 do 8 x=1,n-1
2 do 8 y=1,n-1
3 artmp=ar(x,y)
4 ardif=ar(x+1,y)+ar(x-1,y)+ar(x,y+1)+ar(x,y-1)
5 aidif=ai(x+1,y)+ai(x-1,y)+ai(x,y+1)+ai(x,y-1)
6 ar(x,y)=ar(x,y)-C*(aidif-4*ai(x,y))
7 ai(x,y)=ai(x,y)+C*(ardif-4*artmp)
8 continue

```

The first two steps set up Fortran loops to line 8 over the array surface  $0 < x < n$  and  $0 < y < n$ . The arrays  $a = (ar, ai)$  are dimensioned from 0 to  $n$ . In order to avoid sampling array elements outside the window of width  $w$ , the loops only cover sites inside the edge. The third step temporarily saves the real part of the field at the point  $(x, y)$  to update the imaginary part in step 7. Steps 4 and 5 evaluate the Laplacian for the real and imaginary parts of  $a(x, y)$  using the nearest neighbor differences at  $x \pm 1$  and  $y \pm 1$ . The real part of  $a(x, y)$  is updated in step 6 with the coefficient  $C = \Delta\tau/4dx^2$  where  $dx = w/n$ . The number of time steps  $1/\Delta\tau$ , and the window width,  $w$ , must both be large enough so that  $C$  is a small number. The sampling in  $n$  cannot be too large. The reason for this is that diffraction in one time step must not take significant light past nearest neighbors.

We see that the important small quantity in this expansion is  $\Delta\tau/4dx^2$ . This algorithm has been used on an IBM PC to explore diffraction properties in the free electron laser. In order to understand the step by step process of diffraction, now rewrite the diffraction equations for one small step  $\Delta\tau$  in a slightly different form.

The sum of surrounding nearest neighbor points divided by 4 is defined as the average value of the real or imaginary parts of the field  $\bar{a}$ . The step equation for any field point  $a(x, y)$  is then affected by its nearest neighbors  $\Delta a = -i(a - \bar{a}) \Delta\tau/dx^2$ . The optical phase is given by  $\Delta\phi = -(a_r - \bar{a}_r) \Delta\tau / |a| dx^2$ . It is the optical phase over the wavefront that determines that diffraction focuses the wave into or out of the the electron beam.

A wavefront that has curvature such that  $a_r < \bar{a}_r$ , then the optical phase shift will be positive. This corresponds to focusing of the wave. If  $a_r > \bar{a}_r$ , then the phase shift will be negative and the wave expands in size away from the electron beam reducing coupling.

The FEL interaction also changes the optical phase with  $\Delta\phi_{FEL}$ , but opposite in sign to natural diffraction. Diffraction causes a negative phase change while the FEL interaction causes a positive phase change. The FEL interaction therefore decreases the effect of natural diffraction and focuses the wave back into the electron beam.

**Invention (Patent) Report**

There are no inventions to report during this contracting period. The form DD 882 is attached.

## REPORT DOCUMENTATION PAGE

1a. REPORT SECURITY CLASSIFICATION			1b. RESTRICTIVE MARKINGS		
2a. SECURITY CLASSIFICATION AUTHORITY			3. DISTRIBUTION/AVAILABILITY OF REPORT		
2b. DECLASSIFICATION/DOWNGRADING SCHEDULE					
4. PERFORMING ORGANIZATION REPORT NUMBER(S)			5. MONITORING ORGANIZATION REPORT NUMBER(S)		
6a. NAME OF PERFORMING ORGANIZATION Berkeley Research Associates		6b. OFFICE SYMBOL (if applicable)	7a. NAME OF MONITORING ORGANIZATION Air Force Office of Scientific Research		
6c. ADDRESS (City, State, and ZIP Code) P. O. Box 241 Berkeley, CA 94701			7b. ADDRESS (City, State, and ZIP Code) Bolling Air Force Base Washington, DC 20332		
8a. NAME OF FUNDING/SPONSORING ORGANIZATION		8b. OFFICE SYMBOL (if applicable)	9. PROCUREMENT INSTRUMENT IDENTIFICATION NUMBER		
8c. ADDRESS (City, State, and ZIP Code)			10. SOURCE OF FUNDING NUMBERS		
		PROGRAM ELEMENT NO.	PROJECT NO.	TASK NO.	WORK UNIT ACCESSION NO.
11. TITLE (Include Security Classification) Free Electron Lasers					
12. PERSONAL AUTHOR(S) W. B. Colson, A. M. Sessler					
13a. TYPE OF REPORT Final Scientific		13b. TIME COVERED FROM _____ TO _____		14. DATE OF REPORT (Year, Month, Day)	
15. PAGE COUNT					
16. SUPPLEMENTARY NOTATION					
17. COSATI CODES			18. SUBJECT TERMS (Continue on reverse if necessary and identify by block number)		
FIELD	GROUP	SUB-GROUP	free electron laser optical klystron longitudinal effects		
			review article accelerators laser amplifier		
			tapered wiggler transverse effects laser oscillator		
19. ABSTRACT (Continue on reverse if necessary and identify by block number) Free electron lasers (FELs) are reviewed starting with their historical development. All operating FEL experiments are presented in a table. The basic theory is reviewed with extensions to include betatron focussing, optical diffraction, optical self-guiding, short pulse propagation, and the trapped-particle instability. In addition, specific accelerators used with FELs are reviewed. The linac driven FEL, induction linac driven FEL, and the FEL storage-ring are described in detail. The extensions of the FEL undulator designs and new configurations are summarized.					
20. DISTRIBUTION/AVAILABILITY OF ABSTRACT <input type="checkbox"/> UNCLASSIFIED/UNLIMITED <input type="checkbox"/> SAME AS RPT. <input type="checkbox"/> DTIC USERS			21. ABSTRACT SECURITY CLASSIFICATION		
22a. NAME OF RESPONSIBLE INDIVIDUAL			22b. TELEPHONE (Include Area Code)		22c. OFFICE SYMBOL

# FREE ELECTRON LASERS

*W. B. Colson*

Berkeley Research Associates, P. O. Box 241, Berkeley, California 94701

*A. M. Sessler*

Lawrence Berkeley Laboratory, University of California, Berkeley, California 94720

## CONTENTS

1. Introduction
2. Generalities
  - 2.1 History
  - 2.2 Basic Concepts
  - 2.3 Transverse Effects
  - 2.4 Longitudinal Effects
3. Free Electron Laser Systems
  - 3.1 The Linac Oscillator
  - 3.2 The Linac Amplifier
  - 3.3 Storage Rings
  - 3.4 Extensions

## 1. INTRODUCTION

The free electron laser (FEL) uses a high quality relativistic beam of electrons passing through a periodic magnetic field to amplify a co-propagating optical wave (1-4). In an oscillator configuration, the light is stored between the mirrors of an open optical resonator, as shown in Figure 1. In an amplifier configuration, the optical wave and an intense electron beam pass through a transversely undulating magnetic field to achieve high gain. In either case, the electrons must spatially overlap the optical mode for good coupling. Typically, the peak electron beam current varies from several amperes to many hundreds of amperes, and the electron energy ranges from a few MeV to a few GeV. The electrons are the power source in a FEL, and provide from a megawatt to more than a gigawatt flowing through the resonator or amplifier system. The undulator resonantly couples the electrons to the transverse electrical field of the optical wave in vacuum.

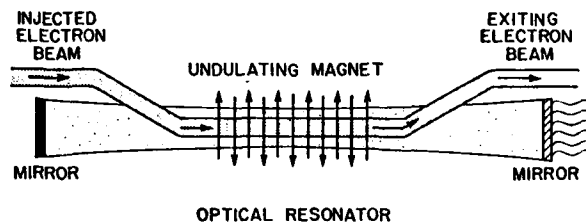


Figure 1. The basic elements of a free electron laser (FEL) oscillator are a high quality relativistic electron beam, an undulator magnet that causes the electrons to wiggle, and the resonant optical cavity to provide feedback.

The basic mechanism of the coherent energy exchange is the bunching of the electrons at optical wavelengths. Since the power source is large, even small coupling can result in a powerful laser. Energy extraction of 5% of the electron beam energy has already been demonstrated. The electron beam quality is crucial in maintaining the coupling over a significant interaction distance, and of central importance to all FEL systems is the magnetic undulator. The peak undulator field strength is usually several kG and can be constructed from coil windings or permanent magnets. In the top part of Figure 2, the Halbach undulator design is shown for one period. The field can be achieved, to a good approximation, using permanent magnets made out of rare earth compounds, a technique developed by K. Halbach (5) and now employed in most undulators. The undulator wavelength is in the range of a few centimeters and the undulator length extends for a few meters, so that there are several hundreds periods for the interaction (6-8). The polarization of the undulator can be either linear or circular or a combination (9). The optical wave has the same polarization as the undulator driving it. This is an illustration of the FEL's most important attribute--the flexibility of its design characteristics.

The transverse undulations of electrons with energy  $\gamma mc^2$  generate spontaneous emission in a forward cone of angular width  $\gamma^{-1}$ . When the undulator fields are strong enough so that the amplitude of the cone's oscillation off-axis is comparable to the cone's width, a detector on-axis at infinity will begin to see several radiation harmonics (10). If the angular deviations of the cone are larger, then the spectrum becomes broad-band like the synchrotron emission from a bending magnet. The total emission energy from a bending magnet and a FEL undulator are similar, but the FEL spectrum is confined to a relatively narrow bandwidth because the electron motion is periodic and the radiation cone stays on the undulator axis. The FEL gain-bandwidth falls within the narrow spontaneous emission spectrum that is determined by the number of undulator

periods. The laser line-width can be much narrower than the spontaneous line-width as in an atomic laser; the narrow line and long coherence length are established by mode competition.

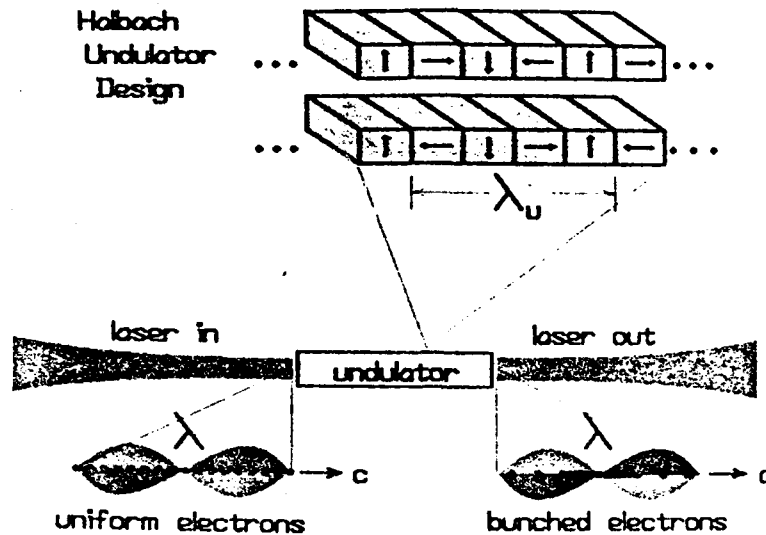


Figure 2. A practical design for constructing the undulator field is shown at the top where eight permanent magnets are used to form one undulator period. The arrows show the directions of the permanent magnetic field. The interaction of an initially azimuthally uniform electron beam with the radiation in a FEL causes the electron beam to bunch in an optical wavelength. It is this bunching that causes coherent radiation.

The laser frequencies driven by the FEL mechanism are much higher than the oscillation frequency of the electrons in the undulator. This is due to a large Lorentz contraction of the undulator wavelength and a large relativistic Doppler shift of the emitted radiation in the forward direction. The relation between the undulator wavelength  $\lambda_u$ , the optical wavelength  $\lambda$ , and the electron beam energy is then  $\lambda \approx \lambda_u / 2\gamma^2$  and the mechanism can be described as stimulated Compton backscattering. It is the relativistic factor  $2\gamma^2$  that allows the FEL to reach short wavelengths. Low energy beams (5 MeV) are being used to reach wavelengths longer than atomic lasers (500  $\mu\text{m}$ ) and high energy beams (1 GeV) are used for x-rays (500  $\text{\AA}$ ), as shown in Table 1 (11-27). The FEL system is also continuously tunable merely by changing the electron energy of the electron source. Figure 3 shows some FEL system configurations, which are explained more fully in Section 2.

Table 1. Operation of free electron lasers

Name (Ref.)	Year of first operation	Wavelength	Peak power	Type <sup>a</sup>
Stanford (11)	1976,1977	10 $\mu\text{m}$ , 3.4 $\mu\text{m}$	130 kW	A,O
Columbia (25)	1977	1.5 mm	8 MW	ASE
NRL (26)	1977	400 $\mu\text{m}$	1 MW	ASE
NRL/Columbia (23)	1978	400 $\mu\text{m}$	1 MW	ASE,O
LANL (13)	1981,82	10.6 $\mu\text{m}$	10 MW	A,O
NRL (12)	1981	4.6-3.1 mm	75 MW	ASE
	1983	35 GHz	17 MW	A
Orsay (15)	1981,1983	6500 $\text{\AA}$	60 mW	A,O
MSNW (14)	1982	10.6 $\mu\text{m}$	<sup>b</sup>	A
Frascati (22)	1983	5145 $\text{\AA}$	<sup>c</sup>	A,O
TRW (16)	1983	1.57 $\mu\text{m}$	1.2 MW	O
NRL (17)	1984	1 cm	20 MW	ASE
MIT (19)	1984	4.3-1.7 cm	100 kW	A
USCB (20)	1984	0.4 mm	8 kW	O
LLNL (18)	1984	8.6 mm	80 MW	A
Hughes (21)	1984	1 cm	60 kW	O
Erevan (24)	1984	20-40 $\mu\text{m}$	10 W	O
Novosibirsk (27)	1984	6000 $\text{\AA}$	<sup>d</sup>	A,O

<sup>a</sup> A = amplifier, O = oscillator, ASE = amplified spontaneous emission.

<sup>b</sup> Output power not measured, but peak loss of electron energy was observed to be 9%.

<sup>c</sup> With an input laser power of 6 W, a gain of  $3 \times 10^{-4}$  was measured.

<sup>d</sup> A gain of 1.5% was measured.

Figure 2 illustrates the basic bunching mechanism used to obtain coherent radiation. The electrons leaving the accelerator are randomly positioned over many optical wavelengths. There are typically  $10^7$  electrons, or more, in each section of the electron beam one optical wavelength long. As the light and electrons interact at the beginning of the undulator, some electrons gain energy and some lose energy. Those that gain energy move a little faster longitudinally and those that lose energy move a little slower; this creates one bunch in each optical wavelength.

## Some FEL Configurations

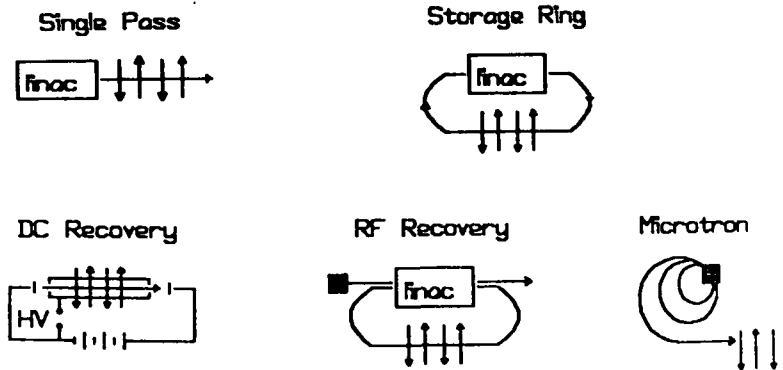


Figure 3. Free electron lasers can be in a variety of configurations, as depicted here. In fact, three of the five types have already operated.

FELs have been described in a number of articles in the general scientific press (28-37). In addition, there is a textbook and a number of review articles on the subject (38-40) and two special issues of *IEEE Journal of Quantum Electronics* contained many papers on FELs (41, 42). Finally, there are six volumes of conference proceedings that contain hundreds of papers and provide a good introduction to the FEL literature (43-48).

## 2. GENERALITIES

### 2.1 History

The historical development of FELs can be traced back to the microwave tubes, backward wave oscillators, traveling-wave tubes, magnetrons, and klystrons of the 1940s, shown at the top of Figure 4. The traveling-wave tubes were similar in structure to the FEL in that they used mildly relativistic electrons traveling through periodically undulating electric or magnetic fields inside a wave guide. The radiation wavelengths produced were in the centimeter range. A characteristic of all such devices was the closed structure used to store the radiation. These electron tubes were tunable by changing the electron energy and using higher harmonics, and high efficiencies were common. While the Motz (49) tubes used the same configuration as the FEL, the operating mechanism was different. A tube that used the same mechanism as that in a FEL was invented

by Phillips (50), but J.M.J. Madey, the inventor of the FEL, was unaware of the Phillips tube, although he did know of Motz's work. Shorter wavelengths could not be reached because electrons did not oscillate fast enough and the closed resonator could not be made small enough.

## GENERAL HISTORY



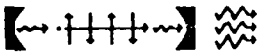
- **Electron Tubes (1930's -> 1960's)** 
  - free non-relativistic electrons
  - microwave cavity
  - long wavelengths, tunable, efficient
- **Atomic & Molecular Lasers (1960's -> now)** 
  - bound electrons
  - optical resonator
  - short wavelengths
- **Free-Electron Lasers (1976 -> now)** 
  - free relativistic electrons
  - optical resonator
  - short wavelengths, tunable, efficient

Figure 4. FELs grew out of the development of electron tubes and atomic lasers. They retain some of the good qualities of both.

Atomic lasers were invented in the 1960s and made use of two new concepts (51): excited electrons in the bound states of atoms or molecules oscillated rapidly to produce optical radiation and this radiation was stored in open optical resonator.

J.M.J. Madey's conception of the FEL (1) came from a mixture of the attributes of microwave tubes and the atomic laser: the Motz undulator and the optical resonator. The relativistic Lorentz contraction and the Doppler shift produced high frequencies from the slower oscillations of the electrons traveling near the speed of light. The FEL is tunable just as the early electron tubes were but it works at short wavelengths.

Independently, R. Palmer, P. Csonka, and K. Robinson were working on the coherent emission of radiation by relativistic electron beams (52).

## 2.2 Basic Concepts

A good theoretical approach to FELs is to solve the relativistic particle dynamics and couple the solutions to the optical wave equation. The more sophisticated analytical methods employed in the analysis of plasmas and lasers are appropriate, but generally not needed. The first classical theory was introduced by M.O. Scully, F. Hopf, et al [53].

The initial electron density has no structure on the scale of the FEL optical wavelength. Individual electrons are only influenced by the radiation field, the undulator magnetic field, and possibly the Coulomb fields of other electrons if the density is large enough. For typical undulator fields and wavelengths, the radiation emitted spontaneously after just one pass is sufficient to define a classical wave. The Lorentz force equations for an electron are

$$\frac{d}{dt}(\gamma \vec{\beta}) = -\frac{e}{mc} [\vec{E}_r + \vec{\beta} \times (\vec{B}_u + \vec{B}_r)]$$

$$\frac{d\gamma}{dt} = -\frac{e}{mc} \vec{\beta} \cdot \vec{E}_r \quad (1b)$$

$$\gamma^{-2} = 1 - \vec{\beta} \cdot \vec{\beta} \quad (1c)$$

where  $\vec{E}_r$  and  $\vec{B}_r$  are the optical electric and magnetic fields,  $\vec{B}_u$  is the undulator field,  $e = |e|$  is the electron charge magnitude,  $c$  is the speed of light,  $m$  is the electron mass,  $\vec{\beta}c$  is the electron velocity, and  $\gamma mc^2$  is the electron energy. Only four of the five equations (Equations 1) are needed to completely specify the problem. The undulator axis is taken along the  $z$  axis so that the transverse optical force with contributions from both  $\vec{E}_r$  and  $\vec{B}_r$  is proportional to  $|\vec{E}_r|(1 - \beta_z)$ . For relativistic electrons  $(1 - \beta_z) \approx 1/2\gamma^2$ , so that the transverse optical force is small; the optical electric and magnetic forces combine almost to cancel when  $\gamma \gg 1$ .

In order to couple energy out of the electron beam, the time average of  $\vec{\beta} \cdot \vec{E}_r$  must be nonzero during the interaction time in the undulator. The role of the undulator is to rotate the transverse electron velocity as the field  $\vec{E}_r$  passes over it. Note that in Equation (1a) the transverse electron motion is determined primarily by the undulator magnet since the transverse optical force is small. However, a randomly distributed electron beam will have  $\langle \vec{\beta} \cdot \vec{E}_r \rangle = 0$  with no net energy transfer. But, an energy modulation alters the electron  $z$  velocities to cause bunching and coherent emission. While deflections off the mode axis are necessary for coupling, they cannot be too large, since the optical mode has a limited radial extent.

A suitable undulator field (6) around the mode axis is

$$\begin{aligned} B_x &\approx -B \{ [1 + k_u^2 (3x^2 + y^2) / 8] \cos(k_u z) - [k_u^2 xy / 4] \sin(k_u z) \} \\ B_y &\approx B \{ [1 + k_u^2 (x^2 + 3y^2) / 8] \sin(k_u z) - [k_u^2 xy / 4] \cos(k_u z) \} \\ B_z &\approx -B [1 + k_u^2 (x^2 + y^2) / 8] [x \sin(k_u z) + y \cos(k_u z)] \end{aligned} \quad (2)$$

where  $B$  is the peak field strength and  $\lambda_u = 2\pi/k_u$  is the undulator wavelength. The electron beams suitable for FELs must be sufficiently aligned so that the transverse excursions are small compared to  $\lambda_u$ . The average magnetic field strength increases off-axis so that the electrons are focused toward the axis. When electrons are focused back toward the undulator axis, the transverse oscillations are called betatron oscillations. Typical transverse excursions are small enough that  $k_u x$  and  $k_u y$  are negligible.

With a small, high quality beam, the undulator field sampled by electrons is  $(B \cos(k_u z), B \sin(k_u z), 0)$  and the orbits which are helical, are

$$\vec{\beta} = [(-K/\gamma) \cos(k_u z), (-K/\gamma) \sin(k_u z), \beta_z] \quad (3)$$

where  $\beta_z \approx 1 - (1 + K^2)/2\gamma^2$  and  $K = eB \lambda_u / 2\pi mc^2$ . Typically  $K \approx 1$  and one sees that the transverse oscillations are small.

The optical field polarization that best couples to the above trajectory is given by the vector potential

$$\vec{A}(z, t) = \frac{E(t)}{k} \{ \sin[kz - \omega t + \phi(t)], \cos[kz - \omega t + \phi(t)], 0 \} \quad (4)$$

where  $E(t)$  is the electric field magnitude,  $\lambda = 2\pi c / \omega = 2\pi / k$  is the optical carrier wavelength, and  $\phi(t)$  is the optical phase. No  $x$  or  $y$  dependence is included in  $\vec{A}$ , for now, since we assume the electrons remain well inside the optical mode waist. The optical electric field is  $\vec{E}_r = -c^{-1} \partial \vec{A} / \partial t$ . Inserting  $\vec{E}_r$  and Equation (3) into Equation (1b) we have

$$\frac{d\gamma}{dt} = \left[ \frac{eKE}{\gamma mc} \right] \cos[(k_u + k)z - \omega t + \phi] \quad (5)$$

A particularly useful form of Equation (5) may be obtained in the case where the fractional energy change  $\delta\gamma / \gamma \ll 1$ . Define the electron phase  $\zeta(t) = (k_u + k)z(t) - \omega t$ , then eliminate  $\dot{\gamma}(t)$  from Equation (5) to get

$$\frac{d^2\zeta}{d\tau^2} = \frac{dv}{d\tau} = |a| \cos(\zeta + \phi) \quad , \quad (6)$$

where  $|a| = 4\pi N_e K L E / \gamma^2 m c^2$  is the dimensionless optical field strength,  $\tau = ct/L$  is the dimensionless time,  $L = N\lambda_u$  is the undulator length so that  $0 \leq \tau \leq 1$ , and  $v = d\zeta/d\tau$  is the electron phase velocity. The electron dynamics have been put in the form of a pendulum equation [54].

The evolution of each electron entering the FEL undulator follows Equation (6). Individual electrons are identified by their initial conditions  $\zeta(0) = \zeta_0$  and  $v(0) = v_0 = L[k_u + k]\beta_z(0) - k$ . In weak fields  $|a| \ll \pi$ , and when  $|a| \gg \pi$ , the fields are considered strong because the phases evolve significantly in the time  $\tau \leq 1$ . Experiments are usually designed so that the spread in electron velocities does not cause a spread in  $v_0$  greater than  $\pi$ . This can be adjusted by keeping the length  $L$  small enough, but a better beam quality allows a greater length  $L$  and much more gain.

The optical wave is governed by the wave equation driven by the current  $\vec{J}_\perp$ :

$$\left[ \frac{\partial^2}{\partial z^2} - \frac{1}{c^2} \frac{\partial^2}{\partial t^2} \right] \vec{A}(z, t) = - \frac{4\pi}{c} \vec{J}_\perp(z, t) \quad , \quad (7)$$

where the  $(x, y)$  dependence has been dropped (see Section 5). The transverse electron current is the sum of all particle currents

$$\vec{J} = -ec \sum_m \vec{\beta}_\perp \delta^{(3)}[\vec{x} - \vec{r}_m(t)] \quad , \quad (8)$$

where  $\vec{r}_m(t)$  is the trajectory of the  $m$ th electron and  $\vec{\beta}_\perp = (\beta_x, \beta_y, 0)$ . Even the spontaneous emission spectrum in a FEL has a long coherence length so that the field  $E(t)$  and phase  $\phi(t)$  can be taken to vary slowly over an optical period,  $\omega^{-1}$ . Then, the terms containing second derivatives in Equation (7) are negligible compared to terms with single derivatives and

$$\frac{d}{d\tau} (E e^{i\phi}) = \frac{L}{c} \frac{d}{d\tau} (E e^{i\phi}) = -\pi e K L \sum_m \frac{e^{-i\zeta}}{\gamma} \delta^{(3)}[\vec{x} - \vec{r}_m(t)] \quad .$$

Then, the wave equation has the simple form

$$\frac{da}{d\tau} = -j \langle e^{-i\zeta} \rangle \quad , \quad (9)$$

where  $a = |a| e^{i\phi}$ , the dimensionless current density is  $j = 8N(\pi e K L)^2 \rho / \gamma^3 m c^2$ ,  $\rho$  is the electron particle density, and the angular brackets represent a normalized average over the electrons. If

electrons are bunched at the phase  $\pi$ , then the optical amplitude is driven with strength  $j$  during the time  $0 < \tau < 1$  and there is gain. If the phase  $\pi/2$  is overpopulated, then the optical phase  $\phi$  grows with little gain. Usually, it is a combination of  $|a|$  and  $\phi$  that is driven because the electron bunching is not perfect.

Figure 5 shows the phase space evolution of a periodic section of the electron beam in the  $(\zeta, \nu)$  coordinates. The separatrix path shown is given by  $\nu_s^2 = 2|a| [1 + \sin(\zeta_s + \phi)]$ ; the peak-to-peak height is  $4|a|^{1/2}$  and the horizontal position is determined by  $\phi$ . The "fluid" of electrons starts equally populating all phases and at the phase velocity  $v_0 = 2.6$  for maximum gain. As the electron fluid evolves in Figure 5 it becomes darker, becoming black at  $\tau = 1$ . The final bunching is near the phase  $\pi$  and the gain and optical phase shift evolution are shown at the right. The initial optical field is weak  $a(0) = a_0 = 1$ , and the final gain determined numerically is  $G \equiv [|a(1)|^2 - a^2(0)]/a^2(0) = 0.135j$ .

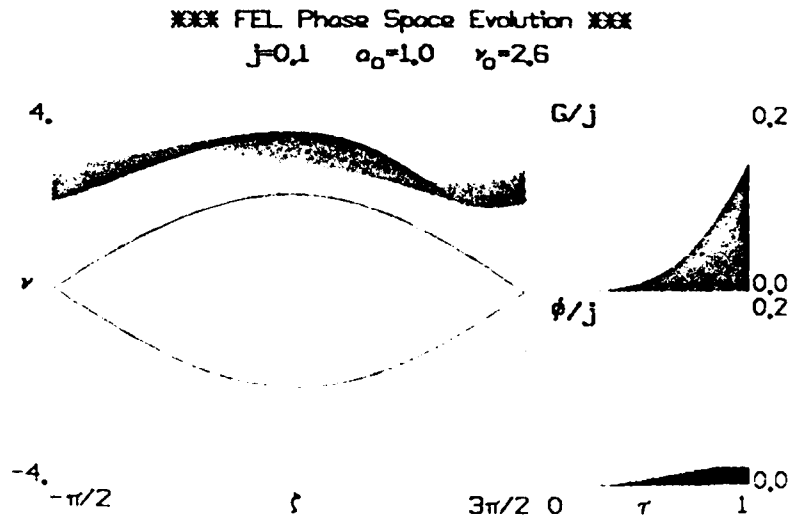


Figure 5. The electron phase space follows sample electrons through the undulator. The separatrix is shown as a guide to the phase space paths. The electron fluid grows darker as it passes through the undulator. (The same representation is employed in Figures 6 and 8.) Bunching at the phase  $\pi$  leads to gain, but also affects the optical phase.

While we have made a few assumptions, the "pendulum" and wave equations (Equations 6 and 9) form a simple, powerful description of the FEL (54). They are valid for both weak ( $|a| \ll \pi$ ) and strong ( $|a| \gg \pi$ ) optical fields in either high ( $j \gg 1$ ) or low ( $j \ll 1$ ) gain conditions. It is generally important that both the optical field amplitude and phase are included in the description.

When the optical fields are weak, Equations (6) and (9) can be easily linearized in  $a(\tau)$ :

$$\dot{a} = ij \langle \exp[-i(\zeta_0 + \nu_0 \tau)] \zeta_1 \rangle; \quad \ddot{\zeta}_1 = |a| \cos(\zeta_0 + \nu_0 \tau + \phi) \quad , \quad (10)$$

where  $(\dot{\phantom{x}}) = d(\phantom{x})/d\tau$ ,  $\zeta = \zeta_0 + \nu_0 \tau + \zeta_1$ , and  $\zeta_1$  is  $\zeta$  expanded to lowest order in  $|a|$ . For a uniform beam distribution, the average of any quantity  $f$  is given by

$$\langle f \rangle = \int_0^{2\pi} d\zeta_0 (f) / 2\pi \quad ,$$

the electron coordinates can be removed from Equation (10) and the optical field is determined by the roots to the cubic equation

$$\alpha_r^3 - i\nu_0 \alpha_r^2 - \left[ \frac{i}{2} \right] j = 0 \quad , \quad (11)$$

with the field of the form

$$a = a_0 \exp(-i\nu_0 \tau) \sum_{r=1}^3 c_r \exp(\alpha_r \tau) \quad ,$$

where the  $c_r$  are determined by initial conditions. If  $|\nu_0| \gg \pi$  so that the FEL is far off-resonance, the driving term  $j$  is negligible and the trivial uninteresting solution  $a \approx a_0$  is obtained, i.e., no gain. If the current density  $j$  is large, so that  $\nu_0$  is negligible, the important real root is  $\alpha_r = (j/2)^{1/3} \sqrt{3}/2$  giving exponential growth. The complex field is then described by  $a(\tau) = (a_0/3) \exp[(j/2)^{1/3} (\sqrt{3} + i)\tau/2]$ , and the gain is exponential after an initial bunching time.

Figure 6 shows the phase space evolution in the high gain case where  $j = 100$ . The electrons are started at  $\nu_0 = 0$  to show how gain is achieved on-resonance. Bunching occurs at the phase  $\pi/2$ , but in the high gain case a significant optical phase shift changes the position of the separatrix so that, relative to the optical wave, bunching is at phase  $\pi$ . The resulting exponential growth and phase evolution are shown on the right. The exponential gain only occurs after bunching is established.

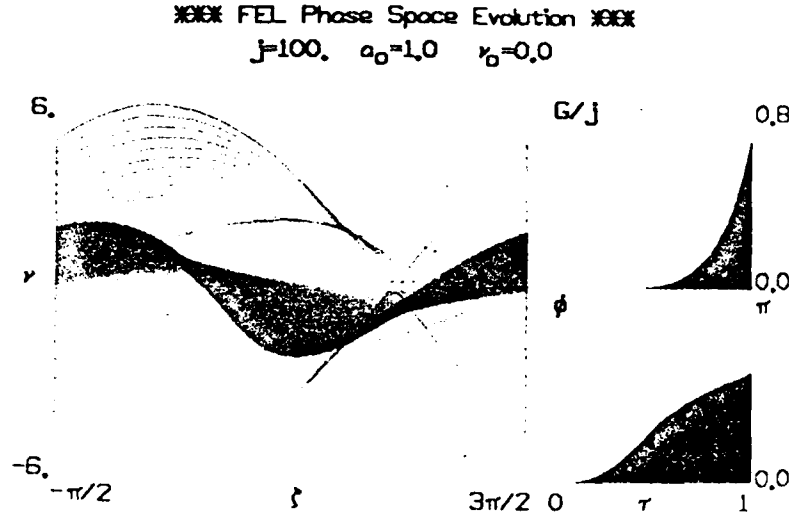


Figure 6. In the high gain case, there is a substantial optical phase change shift, which then shifts the separatrix. The height of the separatrix is proportional to the  $|a|^{1/2}$  and grows with the high gain.

In the low gain case, both  $v_0$  and  $j$  are important in Equation (11). The gain is no longer exponential and all three roots are needed to find the final gain at  $\tau = 1$ , which is given by

$$G(v_0) = -j \frac{[2 - 2\cos v_0 - v_0 \sin v_0]}{v_0^3} = -\frac{j}{2} \frac{d}{dv_0} \left[ \frac{\sin(v_0/2)}{(v_0/2)} \right]^2 \quad (12)$$

The gain is antisymmetric in  $v_0$  and peaks at  $G = 0.135j$  with  $v_0 = 2.6$ . Figure 7 shows the plot of  $G(v_0)$  above the accompanying optical phase shift  $\phi(v_0) = j[2\sin v_0 - v_0(1 + \cos v_0)]/v_0^3$ . Note that the gain spectrum can be written as the derivative of the spontaneous emission spectrum  $[\sin(v_0/2)/(v_0/2)]^2$ . This remains true for a large class of undulator designs and is known as the Madey theorem [55]. The theorem states that when an undulator design produces a spectrum  $s(v_0)$  the gain is proportional to the slope of the spectrum  $ds(v_0)/dv_0$ . A second theorem relates the "second moment of the mean electron energy loss evaluated to first order in the optical field strength,"  $\langle [\delta\gamma^{(1)}]^2 \rangle$ , to the "mean energy loss evaluated to second order in the optical field strength,"  $\langle \delta\gamma^{(2)} \rangle$ :

$$\langle \delta\gamma^{(2)} \rangle = \frac{1}{2} \frac{\partial}{\partial \gamma} \langle [\delta\gamma^{(1)}]^2 \rangle.$$

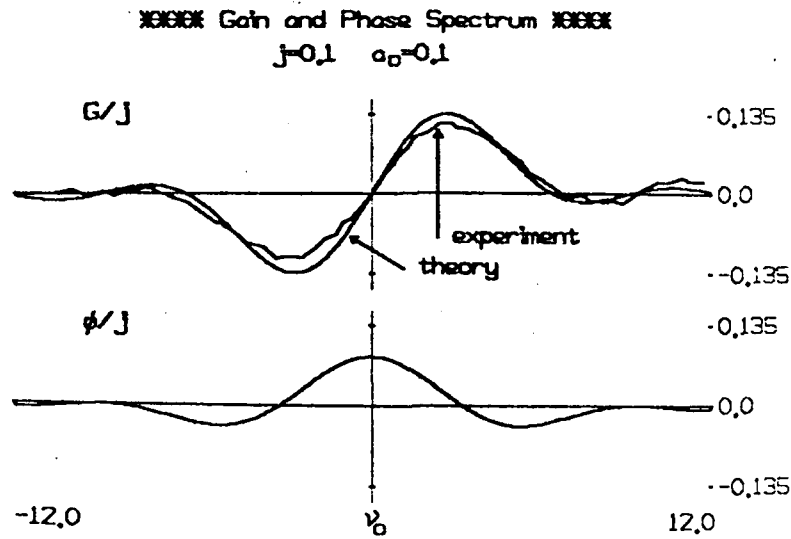


Figure 7. The final gain and phase of the optical wave are plotted as a function of  $\nu_0$ . Experimental points are superimposed to show agreement between small amplitude theory and experiment (Orsay) (89).

In the FEL oscillator, gain over many passes leads to strong fields. The spontaneous fields either experience exponential growth or the repeated gain of Equation 12. In stronger fields where  $|a| \geq \pi$ , the gain process changes and begins to depend on  $|a|$ . Electron phases now evolve too far in phase space and bunching is difficult to maintain. Figure 8 shows electrons in a strong field  $a_0 \equiv |a(0)| = 8$ . The separatrix is now large and electrons are trapped in the closed orbit region of phase space. Those near the harmonic circular paths oscillate around the phase  $\pi/2$  at a frequency  $|a|^{1/2}$ ; these oscillations are called synchrotron oscillations. There is a decrease in gain, i.e., saturation. When the gain is reduced to equal the FEL system losses, steady-state operation is established.

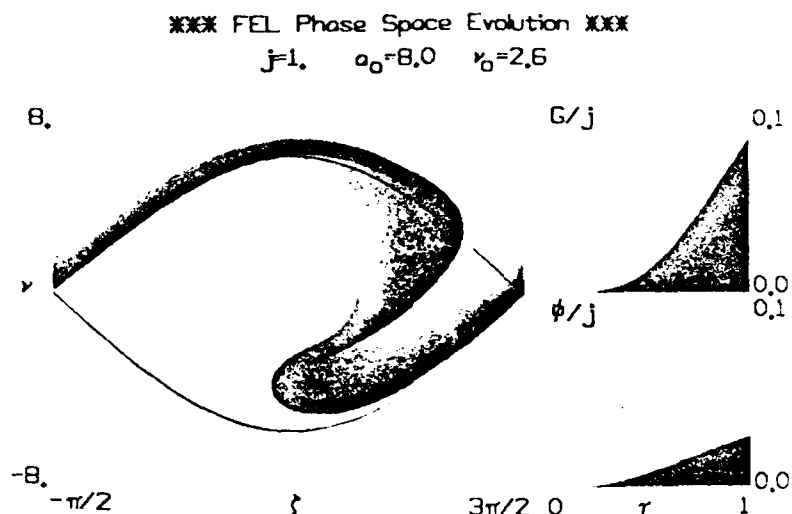


Figure 8. Phase space evolution in the strong field regime. The "synchrotron" motion of the particles has led to saturation and energy is no longer transferred from the electrons to the optical wave. Even in saturation the phases of the optical wave evolves.

A method used to extend the saturation limit of FELs was proposed by Kroll, Morton & Rosenbluth (56) and is called the tapered undulator. As electrons lose energy to the optical wave, the undulator properties can be modified to accommodate the new electron energy. As  $\gamma$  decreases either the modulator wavelength,  $\lambda_u$ , or field strength  $B$ , can be decreased to maintain resonance. A simple case is that in which both  $B$  and  $\lambda_u$  change along the undulator so that  $K$  is constant. When such a taper is included, the pendulum equation acquires an accelerating term,  $\delta = L^2 dk_u(z)/dz$ ,

$$\ddot{\zeta} = \delta + |a| \cos(\zeta + \phi). \quad (13)$$

In the absence of the field  $|a|$ , electrons appear to be "accelerated" to higher phase velocities. In strong fields, about half the electron phases are trapped near the phase  $\pi$ , which drives the optical amplitude and gain. Figure 9 shows the final position of electrons in phase space after trapping has occurred in strong fields  $a_0 \approx 40$  and with tapering such that  $\delta = 6\pi$ . The untrapped electrons are seen at the top of the phase space picture spread over the phase axis randomly. The gain is higher than would be possible at this field strength without tapering. The tapered undulator is a good example of the design flexibility of FELs. The undulator structure [length, polarization,

wavelength profile, field profile  $B(z)$ , etc] are all features that can be modified to enhance performance for a particular FEL application.

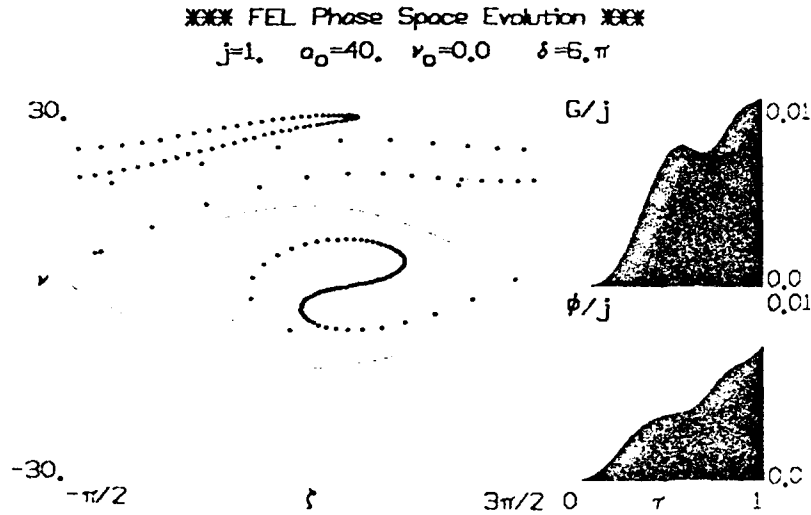


Figure 9. In a tapered FEL some electrons are trapped near the phase that drives the optical wave. The untrapped electrons are distributed over many phases and do not drive the wave.

An example proposed by Vinokurov & Shrinsky (57) is the klystron FEL (sometimes called a transverse optical klystron FEL, or TOK) where the undulator is split into two sections separated by a drift or dispersive section. The purpose is to achieve higher gain for a given interaction length  $L$ . The dispersive section acts like the bending magnet of an electron energy analyzer. Small variations in the electron phase velocity  $v$  caused by the first undulator section are translated into phase changes  $\Delta\zeta = Dv$  at the end of the dispersive magnet and the parameter  $D$  measures the strength of the dispersive field. The theoretical description of the field and the electrons uses Equations 6 and 9 with  $\Delta\zeta = Dv$  applied to each electron at  $\tau = 1/2$ . This results in a higher degree of bunching, and therefore greater gain than given by Equation 12.

When the undulator is designed to have linear polarization, only the definitions of variables in Equations 6 and 9 change while the form of the equations remains the same. The modifications are  $a \rightarrow a[J_0(\xi) - J_1(\xi)]$ ,  $j \rightarrow j[J_0(\xi) - J_1(\xi)]^2$ , where  $\xi = K^2/2(1 + K^2)$ , and  $B$  becomes the rms undulator field strength.

### 2.3 Transverse Effects

The one-dimensional analysis, which we have employed up to this point, leaves out all transverse effects except the simple periodic undulator motion.

First we discuss electron beam transverse effects. A helical undulator provides focusing of the electrons in both transverse planes. Sometimes a longitudinal, solenoidal field is employed so as to give even more focusing. For some devices the cyclotron resonance in this field coincides, or almost coincides, with the FEL resonance and makes the interpretation of these experiments more complicated (12). On the other hand this juxtaposition appears to enhance the gain, but is limited to long wavelength applications because of the upper limit on attainable solenoidal field strengths.

For planar undulators there is only "natural" focusing in the plane perpendicular to the sinusoidal motion and the betatron wave number is  $k_{\beta y} = eB/\sqrt{2}mc\gamma$  in the non-wiggle plane, where  $B$  is the peak field. The resonance condition is maintained as a particle undergoes betatron oscillations. In the wiggle plane, generally some focusing is required (50, 58, 59). Quadrupoles, although they give focusing, seriously degrade FEL performance. A planar undulator field is

$$\vec{B} = -B \cosh(k_u y) \cos(k_u z) \vec{y} + B \sinh(k_u y) \sin(k_u z) \vec{z},$$

so that the motion is

$$x' \equiv \frac{dx}{dz} = \frac{B}{\gamma} \left[ 1 + \frac{k_u^2 y^2}{2} + \dots \right] \sin(k_u z) ,$$

and hence increases as  $y$  increases. This increase with  $y$  just balances the decrease of  $y' \equiv dy/dz$  when  $y$  increases and causes  $\beta_x$  to be constant. E. T. Scharlemann (60) has shown how shaping the undulator pole faces with a slight parabolic curvature provides horizontal focusing while maintaining  $\beta_x$  a constant of the motion. The curvature causes the field to increase off-axis and provides focusing in both  $x$  and  $y$ . If the pole face is given by  $y(x) = Y_0(1 - k_u^2 x^2/4)$ , then the focusing will be the same in  $x$  and  $y$  and the electron beam cross section will be round.

It is necessary, in any real FEL, to avoid resonances between the various frequencies to which the particles are subject. For example, one must avoid a resonance between betatron oscillations and integral multiples of  $\lambda_u$ . Also, one must avoid the usual coupling resonances between the betatron oscillations in  $x$  and  $y$ . There is another kind of resonance that must also

be avoided: a synchro-betatron resonance between the "synchrotron motion" of trapped electrons and transverse betatron motion (61, 62).

We turn now to transverse effects of the electromagnetic wave. The simplest effect is the excitation of cavity modes in an oscillator. Figure 10 shows this phenomenon in a computer simulation of the original Stanford experiment where the electron beam has been moved off-axis to excite a combination of higher order modes.

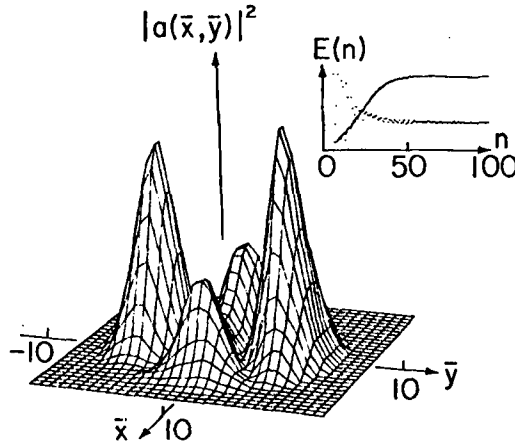


Figure 10. Typically FELs are made to produce the fundamental mode in an optical resonator with a Gaussian shape in  $x$  and  $y$ . A higher order mode is excited here by moving the electron beam off of the resonator axis. The theoretical calculation employed the parameters of the original Stanford FEL (11).

The Rayleigh range is a measure of the effect of diffraction. For a light beam of radius  $w$ , the Rayleigh range  $z_r = \pi w^2 / \lambda$  is the propagation distance over which the optical wavefront doubles its area. In a proper FEL design one wants good overlap between the electron beam and the light beam over the whole interaction length so that  $z_r$  should be comparable to  $L$ . However, if the FEL has sufficiently high gain it can provide "guiding" to the light and keep it within the electron beam for many Rayleigh lengths, as in an optical fiber (63, 64). This is seen, dramatically, in Figure 11.

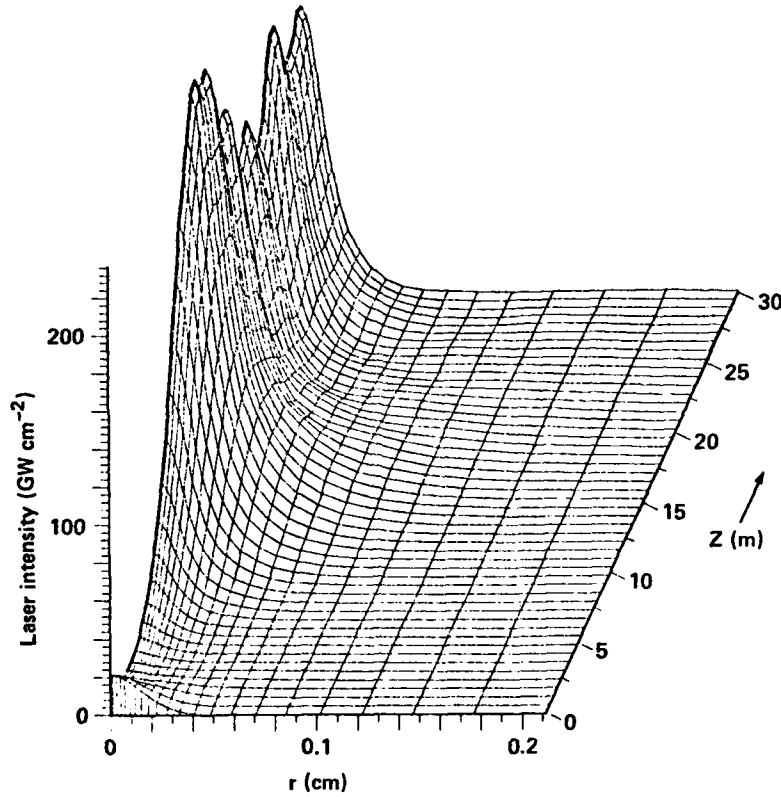


Figure 11. Intense electron beams going through a FEL can provide optical guiding of the radiation. In the absence of guiding, the radiation would diffract out of the electron beam long before the end of the undulator.

A FEL provides an effective index of refraction,  $n$ , by changing the optical phase along the interaction length:

$$\text{Re}(n) - 1 \equiv \frac{1}{k} \frac{d\phi}{dz} = \frac{j}{|a| Lk} \langle \sin(\zeta + \phi) \rangle ,$$

and

$$\text{Im}(n) \equiv \frac{1}{k |a|} \frac{d|a|}{dz} = \frac{-j}{|a| Lk} \langle \cos(\zeta + \phi) \rangle .$$

For an optical fiber, guiding occurs if  $\text{Re}(V^2) + \text{Im}(V^2)/2 > 1$ , where the (complex) fiber parameter,  $V$ , is given by  $V^2 = (n^2 - 1)b^2 k^2$ , where  $b$  is the electron beam radius. Thus one can readily determine when guiding takes place, provided one can evaluate the averages over particles of

$\sin(\zeta + \phi)$  and  $\cos(\zeta + \phi)$ . When there is gain, we know that the averages of sin and cos are nonzero.

In the exponential growth regime one can evaluate the averages analytically (63-65). One simply augments the wave equation, Equation 7, with  $\nabla_{\perp}^2$  and then approximates this transverse derivative with

$$\nabla_{\perp}^2 E \approx -\frac{2kE}{z_r}.$$

The result is that Equation 11 becomes for  $v_0 = 0$ ,

$$\alpha_r^3 + i\alpha_r^2(L/z_r) - (i/2)j = 0,$$

where the length of the undulator is  $L$ . Thus the effect of diffraction and optical guiding are included in a one-dimensional theory. Extension to a warm beam and to  $v_0 \neq 0$  can be found in the quoted literature (63-65).

## 2.4 Longitudinal Effects

The simple pendulum and wave equations (Equations 6 and 9) are valid for a single complex field  $a = |a|e^{i\phi}$  with only a single frequency, the carrier frequency  $\omega$ . A realistic FEL oscillator, or amplifier, produces a spectrum of frequencies surrounding the carrier wave. Usually, the coherence length extends over several optical wavelengths so that the slowly varying amplitude and phase approximation remain valid. To generalize the optical field representation to many modes, the single complex field  $a(\tau)$  becomes  $a(k, \tau)$  or  $a(z, \tau)$ .

Driving the carrier phase  $\phi$  in the center of the optical wavefront will focus the light along the electron beam path. Even in low gain, diffraction couples the transverse and longitudinal waves. The phase profile  $\phi(z)$  in a low gain oscillator is determined by the resonator mirrors and their Rayleigh length  $z$ . This causes a shift in frequency and a shift in the gain spectrum in an oscillator (66).

Often, the lack of distinct electron energy levels leads to questions about the ultimate coherence capabilities of FELs. In both the FEL and atomic laser, a long coherence length and narrow frequency spectrum is determined by mode competition, not by energy levels. In the low gain case, the weak field gain per pass in each mode is given by Equation 12. The number of modes within the gain bandwidth is about  $\gamma^2$  (typically  $\gamma^2 \gg 1$ ). Figure 12 shows the evolution of 100 optical wavelengths, around resonance. The spontaneous emission above resonance

experiences gain on every pass, while other wavelengths receive less gain or absorption. The vertical scale follows the photon number  $\eta(\lambda)$  over six orders of magnitude in 100 passes. The spectrum clearly narrows as mode competition continues. The photon number evolves as  $\exp[G(\lambda)n_p]$ , where  $n_p$  is the pass number in the low gain oscillator where modes are uncoupled.

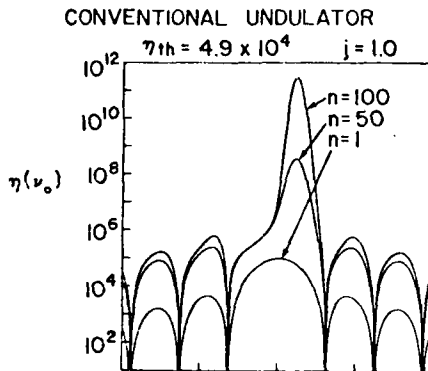


Figure 12. The growth of coherence in the optical wave is shown by following 100 modes from spontaneous emission. The photon density at the wavelengths near peak gain grows more rapidly than the densities at surrounding wavelengths. This narrows the spectrum after only 100 passes. Evidently the laser can become narrow-band.

Short pulse effects (67) in FELs can also be described by generalizing the field to  $a(k)$ . An essential concept is "slippage"; this is the distance that light travels over the electron beam while the electrons travel through the undulator. It is given by  $L(1 - \beta_z) \approx N\lambda$  using the FEL resonance condition. The ratio of the slippage distance  $N\lambda$  to the electron pulse length  $\sigma_z$  determines whether or not short effects are important. If  $N\lambda \ll \sigma_z$ , then the pulse is considered long, and each part of the pulse experiences gain proportional to the local density. If  $N\lambda \gg \sigma_z$ , then the FEL has short pulses and the modal structure of the pulse is comparable to the gain bandwidth,  $\approx N^{-1}$ .

Since electrons bunch when they reach the trailing edge of the optical pulse, the optical pulse receives more gain on its trailing edge than on its leading edge and behaves as if it is traveling slower than the speed of light,  $c$ . This effect is called "lethargy" (68) and must be considered in the oscillator FEL, where the resonator mirror spacing and the electron pulse repetition time must be synchronized (69, 70). The range of mirror positions to achieve synchronism is astonishingly small: only a 4- $\mu\text{m}$  range was observed in the Stanford experiment. The amount of synchronism within the working range is important in determining the laser line-width and power.

Other longitudinal effects involve long pulses in the FEL. One is the "trapped particle" instability analyzed by Kroll & Rosenbluth (71). The synchrotron frequency  $|a|^{1/2}$  can mix with

the carrier wave and produce sideband gain in the FEL. Figure 13 shows the growth of sideband structure in  $|a(z)|$  and  $\phi(z)$ . A window section of a long pulse is four slippage distances long ( $-2 < z/N\lambda < 2$ ). The field  $|a(z)|$  is plotted at the top left, with bright regions indicating an intense field and dark regions indicating a low field region. The pass number is plotted along the vertical axis. The "trapped particle" instability starts a modulation in the field magnitude  $|a(z)|$  and the phase  $\phi(z)$  with a period equal to the slippage distance. The final spectrum, the Fourier transform of  $a(z)$ , is shown with its sideband on the bottom right; above is the weak field gain spectrum for reference. The final electron energy spectrum is shown above the gain spectrum. The power and net gain evolution are plotted on the upper right as a function of pass number  $n$ . The trapped particle instability is expected in nearly all FELs that saturate because of strong fields.

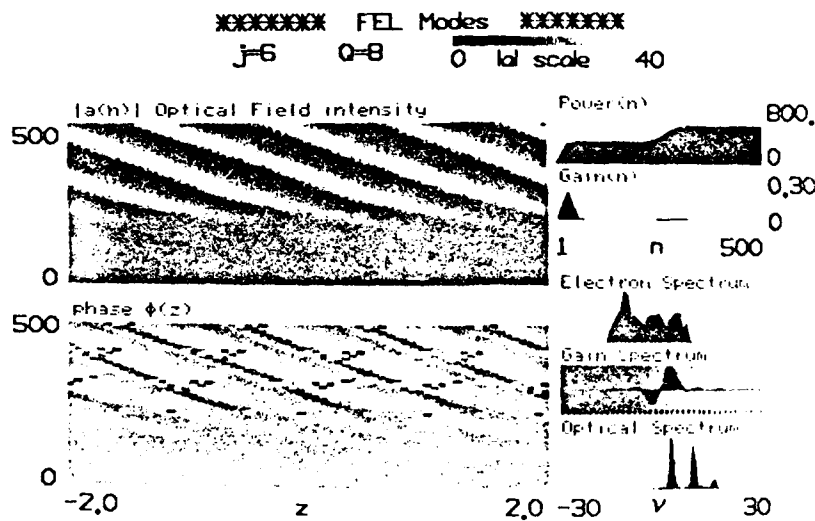


Figure 13. When the electron synchrotron oscillations mix with the carrier wave, sidebands can be formed. Over many passes the optical wave develops a modulation whose period matches the synchrotron period. The optical power increases with the addition of energy of the sideband.

In a linearly polarized undulator, the electron  $z$  motion is more complex than in the helical case because there is a periodic oscillation of the electron  $z$  velocity even when injected perfectly. The oscillation in  $z, \Delta z$ , is given by  $k \Delta z \approx -\xi \sin(2k_u ct)$  where  $\xi = K^2/2(1 + K^2)$ . Since typically  $K \approx 1$ , the oscillations are a sizeable fraction of the optical carrier wavelength and lead to spontaneous emission and gain in higher optical harmonics (72). To generalize Equations 6 and 9 for a harmonic  $hk$ , make the replacements  $\zeta \rightarrow h\zeta$ ,  $\nu \rightarrow h\nu$ ,

$$a \rightarrow ah [J_{(h-1)/2}(h\xi) - J_{(h+1)/2}(h\xi)], \quad \text{and } j \rightarrow jh [J_{(h-1)/2}(h\xi) - J_{(h+1)/2}(h\xi)]^2.$$

The form of the equations stays the same, only the couplings are modified. Note that there is gain only in the odd harmonics  $h = 1, 3, 5, \dots$ . If the undulator field is large enough so that  $K \geq 2$ , then the coupling to higher harmonics is very strong. Several of the FEL experiments to date have observed coherent emission into higher harmonics, and it should prove to be a useful technique for reaching shorter wavelengths in a FEL.

### 3. Free Electron Laser Systems

FELs can be made in a variety of configurations as is depicted schematically in Figure 3. In Section 2 we describe in more detail a particular linac oscillator, a linac amplifier, and a storage ring oscillator experiment. FEL systems are rapidly evolving and in the future can be expected to be quite different from those described here.

In Table 1 we presented a compendium of those FELs that have operated. Many more FEL devices are under construction and, as one can see from the dates in Table 1, these devices are being brought into operation at an ever-increasing rate. In Table 2 (73-87) we present a representative list of FEL accelerators.

Of great importance to FELs are electron beams of high quality. Two figures of merit of quality, for a given current, are energy spread and brightness. The brightness is defined by  $J = \pi^2 I / \gamma^2 \delta^4 V$ , and becomes a measure of "goodness," where  $I$  is the current enclosed within the transverse 4-volume ( $\delta^4 V \equiv \delta x \delta x' \delta y \delta y'$ ). For uniform phase space density, the brightness can be approximated by  $J \approx 2I / \gamma^2 \delta x \delta x' \delta y \delta y'$ . The quality of a beam depends upon the parameters of the accelerator, the type of accelerator, and, of course, with what care it is aligned, etc. In Table 2 we present brightness and energy spread for a number of accelerators. As one can deduce, the expected performance of FELs far exceeds present achievements.

The development of FELs has been the result of both theoretical advances, which we emphasized in this article, and of experimental advances. In fact, without the latter, we would only have an empty theoretical structure. The experimentalists who have been instrumental in the

development of FELs are many in number and, of course, are cited in the references, but special note should be taken of the work of C. A. Brau, D. Prosnitz, D. A. G. Deacon, J. Eckstein, L. Elias, E. Shaw, S. Skrinski, B. Kincaid, C. Pellegrini, J. M. Ortega, M. W. Poole, A. Renieri, P. Elleaume, T. Smith, A. Gover, J. A. Edighoffer, J. M. Slater, D. Dattoli, V. Granatstein, B. Newman, R. Warren, T. Marshall, J. Walsh, R. Pantell, J. Pasour, and Y. Petroff.

Some FEL accelerators

Accelerator <sup>a</sup>	Beam energy (MeV)	Peak beam current(A)	Pulse length	Pulse rep. rate (Hz)	Beam brightness (A/cm <sup>2</sup> rad <sup>2</sup> )	$\Delta\gamma/\gamma$
ETA (IL)	5	1,000	15 ns	1.0 (at 2.5 MeV) <sup>b</sup>	2x10 <sup>4</sup>	<sup>d</sup>
ATA (IL)	50	1,000-10,000	50 ns	1.0 (at 4 MeV) <sup>b</sup>	5-6x10 <sup>4</sup>	<sup>d</sup>
Osaka (RF)	20-38	1,000-3,000	16 ps	1.0-720	1.8-5.4x10 <sup>7</sup>	7x10 <sup>-3</sup>
LANL (RF)	20	35-65	40 ps (micro) 100 $\mu$ s (macro)	1.0	7.0x10 <sup>5</sup>	2x10 <sup>-2</sup>
UC Santa Barbara (DC)	2.5	1.25	30 $\mu$ -dc		3.8x10 <sup>6b</sup>	<sup>d</sup>
Stanford SCA (RF)	80-120	4	2 ps (micro) 10 ms (macro)	10	8x10 <sup>6c</sup>	10 <sup>-4</sup>
LLNL High Brightness Test Stand (IL)	2	20-900	70 ns	1	1.5x10 <sup>5</sup>	<sup>d</sup>
Bell Labs Microtron	10-20	1-5 10 $\mu$ s (macro)	10 ps (micro)	100	4.2x10 <sup>2e</sup>	
UK RF Linac (RF)	30-100	10.0	60 ps (micro) 8.5 $\mu$ s (macro)	100	2.5x10 <sup>4</sup>	10 <sup>-2</sup>
Frascati ENEA Microtron	20	6.5	23 ps (micro) 12 $\mu$ s (macro)	10	4.5x10 <sup>4</sup>	1.2x10 <sup>-3</sup>
NRL Induction (IL)	0.55-0.75	200	2 $\mu$ s	single shot	6.4x10 <sup>3</sup>	3x10 <sup>-2</sup>
MIT Pulsed Device	2.0	1,100	20 ns	0.01	1.4x10 <sup>6</sup>	<0.01
Orsay ACO (SR)	163	3.3	0.5-1 ns	27 MHz	3.8x10 <sup>6c</sup>	10 <sup>-3</sup>
Stanford SXRC Ring (SR)	1.2GeV	270	33 ps	20 MHz	4x10 <sup>8c</sup>	6x10 <sup>-4</sup>
Orsay Super ACO (SR)	400	50	25-300 ps	4.8 MHz	1.7x10 <sup>8c</sup>	3x10 <sup>-4</sup>
LBL Design (SR)	750	327	41 ps	2 MHz	2.8x10 <sup>9c</sup>	2x10 <sup>-3</sup>

<sup>a</sup> IL = induction linac, RF = rf linac, SR = storage ring, DC = DC accelerator.

<sup>b</sup> Edge emittance, i.e. area of  $x-x'$  phase space that includes all of the beam.

<sup>c</sup>  $1/e$  in  $x$  and  $1/e$  in  $x'$  emittance, or approximately 9 times edge brightness.

<sup>d</sup>  $\Delta\gamma/\gamma$  unmeasurably small; variation of  $\gamma$  during a pulse.

<sup>e</sup> estimated.

### 3.1 The Linac Oscillator

The experiment of the TRW Group (15) serves to illustrate the linac oscillator. The superconducting accelerator at Stanford has a bunch length 4.2 ps, a peak current of 0.5 - 2.5 A, and at 66 MeV an energy spread of 0.03% and a beam emittance of  $1.5\pi \times 10^{-3}$  cm · rad. The optical cavity had mirrors 12.68 m apart with a 7.5-m radius of curvature. At the optical wavelength of 1.57  $\mu$ m, the reflectivity was 99.84%. The undulator consisted of pairs of linear arrays of  $\text{SmCO}_5$  permanent magnets with wavelength  $\lambda_u = 3.6$  cm and a peak field of 2.9 kG.

The experiment was designed to study the effect of tapering. Furthermore they devised an optical klystron so the multicomponent undulator had the following structure. First, there was a prebuncher section of 15 periods, then a magnetic dispersion section of two periods and a total length of 58.6 cm. Then 90 periods followed that could be tapered and, finally, 15 periods of constant undulator. The tapered part was varied to be a 0, 1, and 2% taper in energy. Beam diagnostics consisted of 14 insertable fluorescent screens so as to be sure the beam was steered properly and the mirrors were aligned using a green light laser.

With a 1% taper, the FEL had an average output laser power of 4W and the peak power was 1.2 MW. Since the mirror transmission was 0.13% on each end of the cavity, the intracavity optical power was 11 GW cm<sup>-2</sup>. The repetition rate was 10 Hz and the macro-pulse length 5 ms with the micropulse of 4 ps. The radiation fundamental was at 1.57 $\mu$ m and the laser bandwidth was 1.3%.

Above threshold for the laser, the power increased by a factor of  $10^{10}$  over that of the spontaneous radiation! The FEL took 305 passages at a gain of 7% per pass to get to 10% of the saturated level. The experimenters also observed coherent radiation at the second and third harmonic of 1.6  $\mu$ m.

A study was made of the effect of tapering the undulator. For an untapered case the electron transfer of energy, efficiency, should be  $(1/2N)$ . The efficiency was measured to be 0.4%, which compares well with the expected value. With a 1% taper the electrons clearly divided into two groups: trapped and untrapped. Most of the electrons (60%) were trapped and decelerated 1-1.8% while the untrapped electrons were unchanged in energy. Thus the beneficial effect of tapering was demonstrated.

### 3.2 The Linac Amplifier

The experiment of the LBL / LLNL is representative of linac amplifier FELs (18,88). The FEL was run as a single-pass amplifier in the microwave range at 34.6 GHz. The input signal was supplied by a magnetron of peak power 60 kW and a pulse length of 500 ns.

Use was made of the LLNL Experimental Test Accelerator (ETA) (73) to provide a 6-kA, 3.3 MeV beam with emittance of  $0.23 \pi \text{ cm} \cdot \text{rad}$ . An emittance filter was used to reduce the beam current to approximately 500 A with a normalized edge emittance of  $0.47 \pi \text{ cm} \cdot \text{rad}$ . The highly chromatic transport of the ETA beam-line and matching quadrupoles results in a 15-ns, nearly monoenergetic, beam delivered to the interaction region.

The undulator magnet was three meters long, and the undulator period was 9.8 cm. The longitudinal variation of the undulator field provided strong vertical focusing. Horizontally focusing quadrupole magnets, surrounding the undulator, provided horizontal focusing while only slightly reducing the vertical focusing and negligibly affecting the FEL resonance condition.

The interaction waveguide was a rectangular, oversized waveguide immersed in the undulator. The inside dimensions of the waveguide were 9.83 cm wide by 2.91 cm high. The electric field was horizontal and coupled to the  $\text{TE}_{01}$  waveguide mode, which was excited by the input microwave signal.

The signal gain in the amplified spontaneous emission mode (no microwave input signal) was measured and it was found that the microwave signal grew at a rate of 13.4 dB per meter for a beam current of 450 A. Extrapolating this growth back to the origin, one finds that the effective input noise was 0.35 W.

The amplifier gain was studied both as a function of undulator magnetic field intensity and as a function of undulator length. The peak output power of 80 MW was achieved for both the 2 m and 3 m long undulator. The amplifier went into saturation at 2.2 m; beyond this point, the amplified output power first decreased and then near 3 m started to increase again. The gain as a function of undulator length showed an exponential gain of approximately  $15.6 \text{ dB m}^{-1}$  up to saturation. This was in close agreement with the small signal gain measurement. The gain curves for the 1-m and 2-m undulators are relatively symmetric about the peak, while the gain

curve for the 3 m long wiggler shows a marked asymmetry with a plateau on the long wavelength side of the curve. This asymmetry at saturation is also shown in the numerical simulations.

Study of excitation of other than the  $TE_{01}$  mode and study of the effect of varying the undulator parameters (so as to avoid saturation at 80 MW) are to be undertaken in the near future. What has been shown, so far, is that a FEL can be operated in the high gain regime (Gain  $\geq 2500$ ).

### 3.3 Storage Rings

The first, and so far the only, operation of a storage ring FEL oscillator was achieved by the Orsay-Stanford collaboration using the Orsay ring ACO (16, 89). This laser operated in the visible range, at  $6500^\circ$ , and produced 75  $\mu$ W average power or 60 mW output peak power. The intracavity peak optical power was 2 kW.

The ACO storage ring has a circumference of 22 m and was operated between 160 and 166 MeV. Two bunches were employed, with the average current between 16 and 100 mA. The rms bunch length was (in time units) 0.5 to 1 ns and the energy spread (rms)  $0.9 \times 10^{-3}$  to  $1.3 \times 10^{-3}$ . Because of the strong radiation damping, the transverse size (rms) was 0.3 to 0.5 mm, corresponding to an angular spread of 0.1 to 0.2 mrad.

The optical cavity was 5.5 m long so the round-trip time resonated with the 11 m between electron bunches. The mirror radius was 3 m, the Rayleigh range 1 m. Although the mirror transmission was only  $3 \times 10^{-5}$ , the round-trip cavity loss was  $7 \times 10^{-4}$ , primarily because of absorption in the mirror dielectric. In fact, there was mirror degradation due to the radiation harmonics of the undulator, which forced the experimentalists to operate ACO at a reduced energy (originally they had expected to be at 240 MeV) and to operate the undulator at reduced magnetic field ( $K = 1.1$  to  $1.2$ ), both effects tending, of course, to reduce the flux at higher harmonics.

The permanent magnet undulator had 17 periods with a period of 7.8 cm, and a total length of 1.33 m. It was operated as an optical klystron in order to increase the gain per pass. This increased the gain by a factor of 2 to 7 so as to reach  $2 \times 10^{-4}$  per pass. Lasing with such low gain

required careful alignment of the electron beam onto the axis of the optical cavity, high quality mirrors, as well as precise synchronism between the light pulse reflections and the electron bunch revolution frequency. The detuning curve gave only a  $1.6 \mu\text{m}$  full width at half maximum near laser threshold.

The laser time pulse structure was a series of pulses and showed the electron rf synchrotron frequency (13 kHz), and the 27.2-MHz bunch frequency. The time sequence of pulses is understood as a consequence of theoretical study (90). In frequency space the laser had three lines (near  $6500 \text{ \AA}$ ) with the dominant one at  $6475 \text{ \AA}$ . All the lines, corresponding to maximum gains in the klystron FEL, were in the  $\text{TEM}_{00}$  mode. The width of the lines was  $2\text{-}4 \text{ \AA}$ . Tunability was over  $150 \text{ \AA}$  and limited by mirror reflectivity.

The storage ring FEL is the only configuration mentioned where the FEL feeds back on the electron source. On each pass the working FEL "heats" the electron beam by introducing an energy spread. Synchrotron radiation  $P_{\text{syn}}$  from the bending magnets in the ring damps the excitations. The laser power at saturation is determined by thermodynamic equilibrium, which results in weak fields; this is the Renieri limit (91),  $P_{\text{laser}} = P_{\text{syn}}/2N$ . The efficiency of the FEL was only  $2.4 \times 10^{-5}$ , which is 0.4 of the prediction of Renieri for this case.

### 3.4 Extensions

We have seen that FELs can be expected to be efficient, powerful, reliable, tunable sources of radiation in a wide range of wavelengths. In fact, FELs have already been made to operate from the microwave range down to the visible range. It is reasonable to expect that soon we shall have FELs readily available, for many different applications, from microwave wavelengths to soft x-ray wavelengths. When augmented with atomic and molecular lasers and conventional radio tube sources, we can expect to have coherent radiation sources throughout the radiation spectrum (currently, one can see one's way to  $300 \text{ \AA}$ ).

Why then should one develop even more devices? Clearly, because they can be design for special purposes, have special properties, be less expensive, more efficient, etc. The development of FELs is far from completed and really only starting; a number of extensions of

FELs appear to be possible. Here, we mention a few of them and refer the interested reader to the appropriate literature.

In the microwave range it is possible to apply a longitudinal magnetic field of sufficient strength that the cyclotron frequency resonates with the radiation frequency. Thus one can arrange a device where there is coincidence between the FEL resonance and the cyclotron resonance as described in Section 2.3 (12, 92, 93).

It is possible to replace the undulator with an electromagnetic field. The attainable magnetic field of an rf wave is less than that of a static or pulsed magnetic field, but the wavelength of the "undulator" can be made less than that of a conventional undulator. Thus, one can get to short wavelengths with a low energy electron beam. The use of an rf wave as an undulator has already been demonstrated (94) and demonstration has been made of an electromagnetic wave undulator FEL by an NRL group (95). This group had the electron beam produce 500 MW of 12.5-GHz radiation through a backward wave oscillator mechanism, and then used this radiation as an undulator for FEL action. In this manner they produced 200-GHz radiation with peak power, not yet optimized, of 0.35 MW. The Santa Barbara group (96) plans to employ the same idea, but use the FEL mechanism to generate the rf field of an "undulator" in a "two-stage FEL."

We have concentrated upon so-called "Compton regime FELs" where there is a strong interaction between the electrons and the optical wave, but where the interaction between electrons is small. In the opposite case, where the electrons interact strongly through Coulomb forces so that a density fluctuations, or plasmon, description of the electron beam is more appropriate, the FEL is said to be in the "Raman regime." An understanding of the collective regime, the Raman regime, is more difficult than that of the Compton regime but offers distinctive features. Experiments (12) have demonstrated 6% conversion efficiency, and large power emission (75 MW) in this regime. One can expect more development of these devices in future years (97).

An interesting extension of the FEL is to operate in a dielectric media (98, 99). Gas loading, for this is the manner proposed to realize the dielectric media, changes the phase-matching condition and so allows a wider parameter space than the vacuum FEL. In fact, this extension

can be nontrivial and would appear to allow operation, for example, at smaller undulator magnetic fields than in the conventional FEL. The resonance condition, for relativistic electrons is  $n - 1 + \lambda / \lambda_u = (1 + K^2) / 2\gamma^2$ , for a medium having an index of refraction  $n$ . Note that the  $(n - 1)$  term can easily be comparable to the usual  $(1/2\lambda^2)$  FEL term. One can think of this device as being a suitable combination of the Cerenkov effect and the FEL resonance.

Another interesting extension of a conventional FEL is to have an undulator in an isochronous storage ring (100, 101) in which particles with different energies take exactly the same time to go around the ring. Thus bunching at optical wavelengths is preserved around the ring. Most rings do not have this property and thus the electron bunch on entering the undulator is essentially a "new bunch" with random phases. Rings can be made isochronous, to some degree, so that the bunching of a FEL can be preserved. Clearly this is advantageous, and it can be done so as preserve far-infrared wavelength bunching as has been shown on BESSY (102). A FEL using this concept has not yet been made; it is doubtful that the technique can be extended into the visible, but for the infrared it could make a very interesting device.

Finally, it should be emphasized that "pushing" FELs to shorter and shorter wavelengths, as has been spearheaded by J. M. J. Madey and C. Pellegrini, may require no "new inventions," but nevertheless be difficult and a significant extension. This subject, as one might expect, has received considerable attention (85, 87, 103, 104). Suffice it to say here that it appears possible to construct a FEL oscillator down to about 500 Å, and a single-pass FEL growing from noise to about 300 Å. Just what the limits are remains to be seen, but extending the Orsay achievement by an order of magnitude appears to be possible.

#### ACKNOWLEDGEMENTS

We are grateful for support from the US Air Force Office of Scientific Research Grant No. AFOSR-84-0079 (W.B.C.) and from the Office of Energy Research, US Department of Energy under contract DE-AC03-76SF 00098 (A.M.S.).

#### Literature Cited

1. Madey, J.M.J. *J. Appl. Phys.* 42:1906 (1971).
2. Madey, J.M.J. Stimulated emission of radiation in periodically deflected electron beam. *US Patent 3,822,410* (1974).
3. Elias, L.R., Fairbank, W.M., Madey, J.M.J., Schwettman, H.A., Smith, T.I. *Phys. Rev. Lett.* 36:717 (1976).
4. Deacon, D.A.G., et al. *Phys. Rev. Lett.* 38:892 (1977).
5. Halbach, K. See Ref. 47, p. C1-211.
6. Blewett, J.P., Chasman, R. *J. Appl. Phys.* 48:2692 (1977).
7. Elias, L.R., Madey, J.M.J. *Rev. Sci. Instrum.* 50:1339 (1979).
8. Diamant, P., *Phys. Rev. Lett. A* 23:2537 (1981).
9. Kim, K.-J. *Nucl. Instrum. Method* 219:425 (1984).
10. Colson, W.B. *Free electron laser theory*, PhD dissertation, Stanford Univ. (1977).
11. Deacon, D.A.G., et al. *Phys. Rev. Lett.* 38:892 (1977).
12. Gold, S.M., et al. See Ref. 48, p. 350.
13. Newman, B.E., et al. *Phys. Rev. Lett.* 38:118 (1977); Newman, B.E., Hohla, K., Warren, R., Goldstein, J.C. *IEEE J. Quantum Electron.* QE17:1480 (1981).
14. Grossman, W.M., et al. *Phys. Rev. Lett.* 38:52 (1977).
15. Edighoffer, J.A., et al. *Phys. Rev. Lett.* 52:344 (1984).
16. Billardon, M., et al. *Phys. Rev. Lett.* 51:1652 (1983).
17. Pasour, J.A., Lucey, R.F., Kapetanakis, C.A. *Phys. Rev. Lett.* 53:1728 (1984).
18. Orzechowski, T. J., et al. *Phys. Rev. Lett.* 54:889 (1985).
19. Fajans, J., Bekefi, G., Yin, Y.Z., Lax, B. *Phys. Rev. Lett.* 53: 246 (1984).
20. Robinson, A.L. Reported in *Science* 226:154 (1984).
21. Dolezal, F., Harvey, R., Palmer, A. Paper presented at *9th Int. Conf. on Infrared and Millimeter Waves*, Osaka (Oct. 1984).
22. Barbini, R., et al. See Ref. 47, p. C1-1.
23. McDermott, B.D., et al. *Phys. Rev. Lett.* 41:1368 (1978).
24. Omatuni, T.S., Petrosian, M.L., Petrosian, B.V., Shahbazian, N.T., Oganessian, K.B. *Erevan EPI-727* (42)-84 (unpublished 1984).
25. Marshall, T., et al. *Appl. Phys. Lett.* 31:320 (1977).

26. Granatstein, V., et al. *Appl. Phys. Lett.* 30:384 (1977).
27. Artamonov, et al. *Nucl. Instrum. Methods* 177:247 (1980); Kornyuikhin, G.A. et al. *Inst. Nucl. Phys., Novosibirsk, Internal Report* (unpublished).
28. Rothenberg, M.S. *Phys. Today* 29:17 (Feb. 1976).
29. "The Free Electron Laser." *Sci. Am.* 236:62 (Jun. 1977).
30. Schwarzschild, B. *Phys. Today* 36:17 (Dec. 1983).
31. *Lasers and Applications* 2:40 (Oct. 1983).
32. Robinson, A. *Science* 221:937 (Sep. 1983).
33. Robinson, A. *Science* 226:153 (Oct. 1984).
34. Schwarzschild, B. *Phys. Today* 37:19 (Nov. 1984).
35. Schwarzschild, B. *Phys. Today* 37:21 (Nov. 1984).
36. Robinson, A. *Science* 226:1300 (Dec. 1984).
37. Thomsen, D.E. *Sci. News* 126:359 (Dec. 1984).
38. Marshall, T.C. *Free Electron Lasers*. New York: MacMillan (1985).
39. Prosnitz, D. "Free electron lasers." In *CRC Handbook of Laser Science and Technology I*, ed. M.J. Weber, p. 425. Boca Raton: CRC Press (1982).
40. Pellegrini, C. *IEEE Trans. Nucl. Sci.* NS-26:3791 (1979); Morton, P.L. *IEEE Trans. Nucl. Sci.* NS-28:3125 (1981).
41. *IEEE J. Quantum Electron.*, Vol. QE-17, No. 8 (Aug. 1981).
42. *IEEE J. Quantum Electron.*, Vol. QE-19, No. 3 (Mar. 1983).
43. Jacobs, S.F., Sargent, M. III, Scully, M.O., eds. Novel sources of coherent radiation. In *Physics of Quantum Electronics*, Vol. 5, Reading, Mass: Addison-Wesley (1978).
44. Jacobs, S.F., Pilloff, H.S., Sargent, M. III, Scully, M.O., Spitzer, R., eds. Free electron generators of coherent radiation. In *Physics of Quantum Electronics*, Vol. 7, Reading, Mass: Addison-Wesley (1980).
45. Jacobs, S.F., Pilloff, H.S., Sargent, M. III, Scully, M.O., Spitzer, R., eds. Free electron generators of coherent radiation. In *Physics of Quantum Electronics*, Vol. 8, Reading, Mass: Addison-Wesley (1982).
46. Jacobs, S.F., Pilloff, H.S., Sargent, M. III, Scully, M.O., Spitzer, R., eds. Free electron generators of coherent radiation. In *Physics of Quantum Electronics*, Vol. 9, Reading, Mass: Addison-Wesley (1982).
47. *Bendro Free Electron Laser Conference, J. Phys. Colloq.* C1, Suppl. 2, p. 44 (Feb. 1983).
48. Brau, C.A., Jacobs, S.F., Scully, M.O., eds. Free electron generators of coherent radiation, *SPIE* (Int. Soc. Opt. Eng.) 453 (1984).

49. Motz, H. Thon, W., Whitehurst, R.N. *J. Appl. Phys.* 24:826 (1953).
50. Phillips, R. M. *IRE Trans. Electron Devices* 17:231 (1960).
51. Schawlow, A.L., Townes, C.H. *Phys. Rev.* 112:1940 (1958); Maiman, T.H. *Phys. Rev. Lett.* 4:564 (1960).
52. Palmer, R.B. *J. Appl. Phys.* 43:3014 (1972); Csonka, P. *Part. Accel.* 8:225 (1978); Robinson, K., unpublished notes.
53. Hopf, F.A., Meystre, P., Scully, M.O., Louisell, W.H. *Phys. Rev. Lett.* 37:1342 (1976).
54. Colson, W.B. *Phys. Lett.* 64A:190 (1977); Colson, W.B., Ride, S.K. *Phys. Lett.* 76A:379 (1980); Tang, C.-M., Sprangle, P. *Appl. Phys.* 53:831 (1982); Shih, C.-C., Yariv, A. *IEEE J. Quantum Electron.* QE-17:1387 (1981); Dattoli, G., et al. *IEEE J. Quantum Electron.* QE-17:1371 (1981); Bonifacio, R., Pellegrini, C., Narducci, L.M. *Opt. Commun.* 50:373 (1984).
55. Madey, J.M.J. *Nuovo Cimento B* 50:64 (1979).
56. Kroll, N.M., Morton, P.L., Rosenbluth, M.N. *IEEE J. Quantum Electron.* QE-27:1436-68 (1981).
57. Vinokurov, N.A., Shrinsky, A.N. *Inst. Nucl. Phys., Novosibirsk, Rep. No. INP 77-59* (unpublished) (1977).
58. Luccio, A., Krinsky, S. See Ref. 45, p. 181 (1982).
59. Dattoli, G., Renieri, A. Experimental and theoretical aspects of the free electron laser. In *Laser Handbook 4*, ed. M.L. Stitch, M.S. Bass. Amsterdam: North Holland (To be published).
60. Scharlemann, E.T. *Lawrence Livermore National Laboratory ELF Note 105P* (published) (1984).
61. Kroll, N., Rosenbluth, M. See Ref. 44, p. 147.
62. Fawley, W.M., Prosnitz, D., Scharlemann, E.T. submitted *Phys. Rev. A* 30:1472 (1984); *Lawrence Livermore Natl. Lab. Rep. UCRL90838* (unpublished) (1984).
63. Scharlemann, E.T., Sessler, A.M., Wurtele, J.S. *Proc. Como Conf., Nucl. Instrum. Methods.* In press; *Lawrence Livermore Natl. Lab. Rep. UCRL-91476* (unpublished) (1984).
64. Scharlemann, E.T., Sessler, A.M., Wurtele, J.S. *Phys. Rev. Lett.* 54:1925 (1985).
65. Moore, G.T. *Opt. Commun.* 52:46 (1984); Moore, G.T. *Proc. Como. Conf., Nucl. Instrum. Methods.* In press; *IMO Rep. 84-14* (unpublished) (1984).
66. Colson, W.B., Elleaume, P. *Appl. Phys. B* 29:1-9 (1982).
67. Colson, W.B., Renieri, A. See Ref. 47, pp. C1-11.
68. Al-Abawi, H., Hopf, F.A., Moore, G.T., Scully, M.O. *Opt. Commun.* 30:235 (1979).
69. Eckstein, J.N., et al. See Ref. 45, p. 49.
70. Benson, S., Deacon, D.A.G. et al. *Phys. Rev. Lett.* 48:235 (1982).
71. Kroll, N.M., Rosenbluth, M.N. See Ref. 44, p. 147.

72. Colson, W.B. *IEEE J. Quantum Electron.* QE-17:1417-27 (1981).
73. Fessenden, T.J., et al. In *Proc. 4th Int. Conf. on High Power Electron and Ion Beam Research and Technology*, ed. H.J. Doucet, J.M. Buzzi, p. 813, Palaiseau, France: Ecole Polytech.
74. Briggs, R.J., et al. *IEEE Trans. Nucl. Sci.* NS-28:3360 (1981).
75. Takeda, S. Workshop on Generation of High Fields, Frascati, Sep. 25- Oct. 1, 1984. *Nucl. Instrum. Methods.* In press (1985).
76. Warren, R.M., et al. *Lasers 84 Tech. Dig.*, p. 20 (1984).
77. Elias, L. *Lasers 84 Tech. Dig.*, p. 25 (1984).
78. Boehmer, H., et al. *Phys. Rev. Lett.* 48:141 (1982).
79. Bix, D.L., et al. A multipurpose 5-MeV linear induction accelerator. In *Proc. IEEE Power Modulator Symp.*, June 1984; Lawrence Livermore Natl. Lab. Rep. UCRL-90554 (unpublished) (1984).
80. Shaw, E.D., Chichester, R.J., Sprenger, W.C. *Lasers 84, Tech. Dig.*, p. 19 (1984).
81. Smith, S.D., et al. See Ref. 45, p. 275.
82. Bizzarri, U., et al. *Lasers 84 Tech. Dig.*, p. 21 (1984).
83. Leiss, J., Norris, N.J., Wilson, M. A. *Part. Accel.* 10:223 (1980).
84. Billardon, M., et al. See Ref. 15, p. 1652.
85. Deacon, D.A.G. *Lasers 84 Tech. Dig.*, p. 27 (1984).
86. Ballili, J.P., et al. *Report of Prospectives for Super ACO, LURE*, Orsay, Internal Report (unpublished) (April 1981).
87. Peterson, J.M., et al. Contributed paper to the Castelgandolfo Conf. *Instrum. Methods in Physics Research.* To be published (1985).
88. Orzechowski, T.J., et al. See Ref. 48, p. 65.
89. Billardon, M., et al. See Ref. 47, pp. C1-29.
90. Elleaume, P. *J. Phys.* 45:997 (1984).
91. Renieri, A. *Nuovo Cimento B* 59:64 (1979).
92. Freund, H.P. See Ref. 48, p. 361; Bernstein, I.B., Friedland, L. *Phys. Rev. A* 23:816 (1981).
93. Lin, A.T. See Ref. 48, p. 336; Friedland, L., Hirschfield, J.L. *Phys. Rev. Lett.* 44:1456 (1980).
94. Tsumoru, S., et al. *Jpn. J. Appl. Phys.* 22:844 (1983).
95. Granatstein, V.L., Carmel, Y., Gover, A. See Ref. 48, p. 344.
96. Elias, L.B. *Phys. Rev. Lett.* 42:977 (1980).
97. Freund, H.P., Ganguly, A.K. See Ref. 48, p. 367.
98. Kimura, W., Wong, D., Piestrup, M., Fauchet, A., Edighoffer, J., Pantell, R. *IEEE J. Quantum Electron.* QE-18:239 (1982); Walsh, J., Johnson, B. See Ref. 48, p. 376.

99. Fauchet, A.M., et al. See Ref. 48, p. 423.
100. Deacon, D.A.G. *Phys. Rev. Lett.* 44:449 (1980).
101. Deacon, D.A.G. *Phys. Rep.* 76:349 (1981).
102. Gaupp, A. See Ref. 47, pp. C1-147.
103. Madey, J.M.J., Pellegrini, C., eds. *AIP Conf. Proc.*, Vol. 118, Brookhaven, Sep. 1983, New York (1984).
104. Proc. Conf. on Coherent and Collective Properties in the Interaction of Relativistic Electrons and Electromagnetic Radiation, Como, Sep. 1984. *Nucl. Instrum. Methods.* In press (1985).

## REPORT DOCUMENTATION PAGE

1a. REPORT SECURITY CLASSIFICATION			1b. RESTRICTIVE MARKINGS		
2a. SECURITY CLASSIFICATION AUTHORITY			3. DISTRIBUTION / AVAILABILITY OF REPORT		
2b. DECLASSIFICATION / DOWNGRADING SCHEDULE					
4. PERFORMING ORGANIZATION REPORT NUMBER(S)			5. MONITORING ORGANIZATION REPORT NUMBER(S)		
6a. NAME OF PERFORMING ORGANIZATION Berkeley Research Associates		6b. OFFICE SYMBOL (if applicable)	7a. NAME OF MONITORING ORGANIZATION Air Force Office of Scientific Research		
6c. ADDRESS (City, State, and ZIP Code) P.O. Box 241 Berkeley, CA 94701			7b. ADDRESS (City, State, and ZIP Code) Bolling Air Force Base Washington, DC 20332		
8a. NAME OF FUNDING / SPONSORING ORGANIZATION		8b. OFFICE SYMBOL (if applicable)	9. PROCUREMENT INSTRUMENT IDENTIFICATION NUMBER F49620-85-C-0087		
8c. ADDRESS (City, State, and ZIP Code)			10. SOURCE OF FUNDING NUMBERS		
			PROGRAM ELEMENT NO.	PROJECT NO.	TASK NO.
11. TITLE (Include Security Classification) The Trapped-Particle Instability in Free Electron Laser Oscillators and Amplifiers					
12. PERSONAL AUTHOR(S) W. B. Colson					
13a. TYPE OF REPORT Final Scientific		13b. TIME COVERED FROM _____ TO _____		14. DATE OF REPORT (Year, Month, Day)	
15. PAGE COUNT					
16. SUPPLEMENTARY NOTATION					
17. COSATI CODES			18. SUBJECT TERMS (Continue on reverse if necessary and identify by block number)		
FIELD	GROUP	SUB-GROUP	free electron lasers                      laser oscillator		
			high-power laser                      laser amplifier		
			trapped-particle instability		
19. ABSTRACT (Continue on reverse if necessary and identify by block number) The electrons in a high-power free-electron laser can become trapped and oscillate in deep potential wells. The oscillating component of the current drives the optical field at frequencies around the fundamental. General features of the trapped-particle instability in free-electron laser oscillators and amplifiers are discussed. Dimensionless parameters clarify the trends for a wide range of FEL designs.					
20. DISTRIBUTION / AVAILABILITY OF ABSTRACT <input type="checkbox"/> UNCLASSIFIED/UNLIMITED <input type="checkbox"/> SAME AS RPT. <input type="checkbox"/> DTIC USERS			21. ABSTRACT SECURITY CLASSIFICATION		
22a. NAME OF RESPONSIBLE INDIVIDUAL			22b. TELEPHONE (Include Area Code)		22c. OFFICE SYMBOL

# **The Trapped-Particle Instability in Free Electron Laser Oscillators and Amplifiers**

*W. B. Colson*

Berkeley Research Associates, P.O. Box 241, Berkeley, California 94701

## **ABSTRACT**

The electrons in a high-power free-electron laser can become trapped and oscillate in deep potential wells. The oscillating component of the current drives the optical field at frequencies around the fundamental. General features of the trapped-particle instability in free-electron laser oscillators and amplifiers are discussed. Dimensionless parameters clarify the trends for a wide range of FEL designs.

## **1. Introduction**

The free-electron laser (FEL) uses a relativistic, high-current electron beam to amplify a copropagating electromagnetic wave [1]. The optical wave and electrons are coupled as they pass through a periodic, transverse magnetic field undulator. A common goal of both the FEL oscillator [2], and the FEL amplifier [3] is large optical power. In strong optical fields, the electrons can be trapped in deep potential wells formed by the combined optical and undulator field forces. Electrons near the bottom of the well oscillate in harmonic orbits at the synchrotron frequency. The synchrotron frequency mixes with the optical carrier wave frequency to form sidebands, and the growth of the sideband power is the trapped-particle instability. In both the amplifier and the overmoded oscillator configurations, the optical amplitude and phase are free to evolve over a wide range so that complicated optical spectra can result from sideband mixing. In this paper, we try to choose examples that clearly show the features of the trapped-particle instability with a minimum of complication from further sideband mixing.

Historically, the instability was first predicted for high-power, low-gain tapered FELs with many synchrotron oscillations in a single pass through the undulator [4]. Later, it was seen in the simulations of pulsed FEL oscillators, and found to have some different properties than originally

predicted [5-7]. The instability has been clearly observed in the high-power FEL oscillator at LANL [2], and possibly in the TRW/Stanford oscillator [8]. It has been termed the sideband, Kroll-Rosenbluth, synchrotron, Raman, and the trapped-particle instability [9-23]. There can be a rich assortment of varied effects ranging from a single sideband to a chaotic frequency spectrum [22]. The shape of ultra-short optical pulse can be controlled to form shorter subpulses in FEL oscillators [5,6,13,21].

Any FEL working at high power is susceptible to the instability. Tapered undulators are used to extend the FEL performance to higher power levels [9], but appear to have less sideband growth. The tapered undulator design is changed along its length to maintain resonance with the electrons as they lose energy to the optical wave. We review simulations of the instability in FEL oscillators, and present new results of the instability in FEL amplifiers. Dimensionless variables are used to determine important regimes of operation.

## 2. Multimode FEL Theory

The wave equation determines the evolution of the radiation field in the presence of the electron current. The carrier wave with frequency  $\omega = kc = 2\pi c/\lambda$  has the single-mode phase  $e^{i(kZ - \omega t)}$  and a complex slowly-varying coefficient. Transverse  $(X, Y)$  dependence is not included, since most FEL designs attempt to minimize the effects of optical diffraction and mode coupling. The intention here is to clarify longitudinal multimode effects without distractions from other FEL topics; many of the effects can be approximately characterized by adjusting the coupling factors in the wave equation. Multimode features are followed with a complex field envelope  $a(z) = |a(z)|e^{i\phi(z)}$  evaluated at many discrete sites  $z$ . With the slowly-varying amplitude and phase approximation and the coordinate change  $Z \rightarrow Z + ct$ , the wave operator reduces to a single derivative in time [24]. The dimensionless optical field envelope is  $a(z) = 4\pi N e K L E(z) / \gamma_0^2 m c^2$  where  $N$  is the number of undulator periods,  $e$  is the electron charge magnitude,  $L = N\lambda_0 = 2\pi N/k_0$  is the undulator length,  $K = e\bar{B}\lambda_0/2\pi m c^2$ ,  $\bar{B}$  is the rms undulator field strength,  $m$  is the electron mass,  $c$  is the speed of light,  $E(z)$  is the complex optical electric field, and  $\gamma_0^2 m c^2$  is the resonant electron energy,  $\gamma_0^2 = k(1 + K^2)/2k_0$  for  $\gamma_0 \gg 1$ . A resonant electron passes through one wavelength of the undulator as one wavelength of light passes over it. The dimensionless coordinate  $z = Z/N\lambda$  is normalized to the "slippage distance"  $N\lambda$ , the characteristic length along the longitudinal axis in FELs. It is defined by the number of optical wavelengths that pass over a resonant electron as that electron traverses the undulator length  $L$ . Simulations of the FEL mode evolution take place within a window of width  $W$  along  $z$  that is an integral number of slippage

distances long.

Electrons in the beam are governed by the Lorentz force. When the relativistic electrons ( $\gamma_0 \gg 1$ ) are properly injected into the undulator, the transverse electron motion is periodic with amplitude  $K\lambda_0/2\pi\gamma_0$  and phase  $\exp(ik_0Z)$ . The electron beam travels along the undulator at an average speed  $\beta_0 c$  where  $\beta_0 \approx 1 - (1+K^2)/2\gamma_0^2$ . At any dimensionless time  $\tau = \beta_0 ct/L$ , electrons at coordinate  $z+\tau$  in the electron beam overlap the light at site  $z$  in the optical wave. The electron phase relative to the optical wave and undulator field is  $\zeta = (k+k_0)Z - \omega t$ , and the phase velocity is  $v = \dot{\zeta} = L[\beta_z k_0 - k(1-\beta_z)]$ ; a resonant electron has  $v = 0$ . The Maxwell-Lorentz equations [24] are

$$\dot{a}(z) = -j(z+\tau) < [1 - v(z+\tau)/2\pi N]^{1/2} e^{-i\zeta(z+\tau)} > \quad (1)$$

$$\ddot{\zeta}(z+\tau) = \dot{v}(z+\tau) = \delta + [1 - v(z+\tau)/2\pi N]^2 |a(z)| \cos(\zeta(z+\tau) + \phi(z)) ,$$

where the dimensionless current density is  $j(z) = 8N(\pi eKL)^2 \rho(z)/\gamma_0^3 mc^2$ ,  $\rho(z)$  is the actual particle density at site  $z$ , time derivatives are with respect to the dimensionless time  $\tau$  (note that  $\tau = 0 \rightarrow 1$  along the undulator length  $L$ ), and  $<...>$  is an average over sample electrons at site  $z+\tau$  in the electron beam. Since we have assumed a slowly-varying amplitude and phase for  $a(z)$ , the sampling sites  $z$  can be taken to be several optical wavelengths apart. The dimensionless current density  $j(z)$  can describe a short, peaked electron pulse or a long, flat beam.

The acceleration term  $\delta$  has been inserted to characterize a possible taper in the undulator design [9]. This can be accomplished by tapering the wavelength  $\lambda_0$ , or the field strength  $\bar{B}$ . As an example, a steady taper in the undulator field strength gives  $\delta = -4\pi NK(1+K^2)^{-1} L dK/dZ$ . No taper in the undulator properties implies  $\delta = 0$ . The accelerating term  $\delta$  in (1) acts continuously to restore the resonance condition as the electrons lose energy to the laser light. The factors  $[1-v/2\pi N]$  in (1) are close to unity unless the electrons lose a significant fraction of their energy. A large change in  $v$ , comparable to  $2\pi N$ , can drastically change the electron-optical coupling strength. We take  $N = 30$  in our examples, since recent oscillator and amplifier experiments have been in that range [2,3].

The dimensionless variables in (1) have been defined to have meaningful physical interpretations for a wide range of FEL designs. Weak optical fields give values of  $|a| < \pi$ , while strong fields give values of  $|a| > \pi$ . The electron-optical coupling is only significant for  $|v|$  not too large, so that the oscillating optical and undulator forces are nearly resonant. The optical power spectrum  $P(k)$  is made more relevant by expressing  $k$ , the optical wavenumber, in terms of the corresponding resonance parameter  $v(k)$ ; similarly, the electron distribution function  $f(\gamma)$  is

expressed in terms of  $v(\gamma)$ . The power spectrum  $P(v(k))$  and the electron distribution function  $f(v(\gamma))$  are more physically meaningful in terms of their effect on the resonance condition. The dimensionless current density  $j$  represents low single-pass gain when  $j \approx 1$ , and high gain when  $j \gg 1$ . Typically, the FEL oscillator configuration uses  $j \approx 1$ , while the FEL amplifier configuration uses  $j \gg 1$ . When Eqs. (1) [24] are cast in dimensional form, they are the same as the Kroll-Morton-Rosenbluth equations [25].

Initial conditions are important to the integration of (1). We represent the beam at each  $z$  with a uniform distribution of initial phases  $\zeta(\tau=0)$  over a  $2\pi$  range; the initial optical phase is therefore arbitrary and we take  $\phi(\tau=0) = 0$  for each  $z$ . In both the amplifier and oscillator cases, we start the optical field at low values  $a(\tau=0) = a_0$ , well below saturation. The initial resonance condition  $v(\tau=0) = v_0$  is taken to be at the maximum of the weak-field gain spectrum. For small current  $j$  and weak fields  $a_0 \ll 1$ , the gain found from (1) is  $G = 0.135j$  at  $v_0 = 2.6$ ; for large current and weak fields, the gain is  $G = \exp((j/2)^{1/3}\sqrt{3})/9$  at  $v_0 = 0$ . The FEL system would normally develop significant coherence and power at  $v_0$  before going on to saturation.

### 3. Trapped-Particle Oscillations

Before starting multimode simulations, it is instructive to present a phase-space picture of the motion of trapped electrons. Fig. 1 shows the  $(\zeta, v)$  phase-space evolution of six sample electrons in a strong optical field  $a_0 = 4\pi^2$ ; this field strength causes one oscillation of the trapped electrons. Many more electrons are used in the simulation, but only six are shown to keep the picture less cluttered. At  $\tau = 0$ , the electron positions are indicated as light grey spots started at  $v_0 = 2.6$  and uniformly spread in phase. They are indicated by darker spots as  $\tau$  increases, and are black at  $\tau = 1$ . A  $2\pi$  span in phase  $\zeta$  corresponds to a span along the electron beam about one optical wavelength in length. Electron motion in  $v$  corresponds to changes in electron energy through  $v \approx 2\pi N(\gamma - \gamma_0)/\gamma_0$ . Most of the electrons shown in Fig. 1 are trapped in closed orbits indicating a strong optical field. The gain,  $\ln(1+G)$  where  $G = (|a|^2 - a_0^2)/a_0^2$ , is plotted to the right as a function of  $\tau$  along the undulator. As bunching develops, the gain and the optical phase  $\phi(\tau)$  grow as shown. The final gain here is small, because the FEL is well into saturation for this current density,  $j = 5$ , and strong field  $|a|$ . Fig. 1 is a single-mode simulation since all sites  $z$  have been given the same values of  $v_0$ , and  $a(z) = a_0$ .

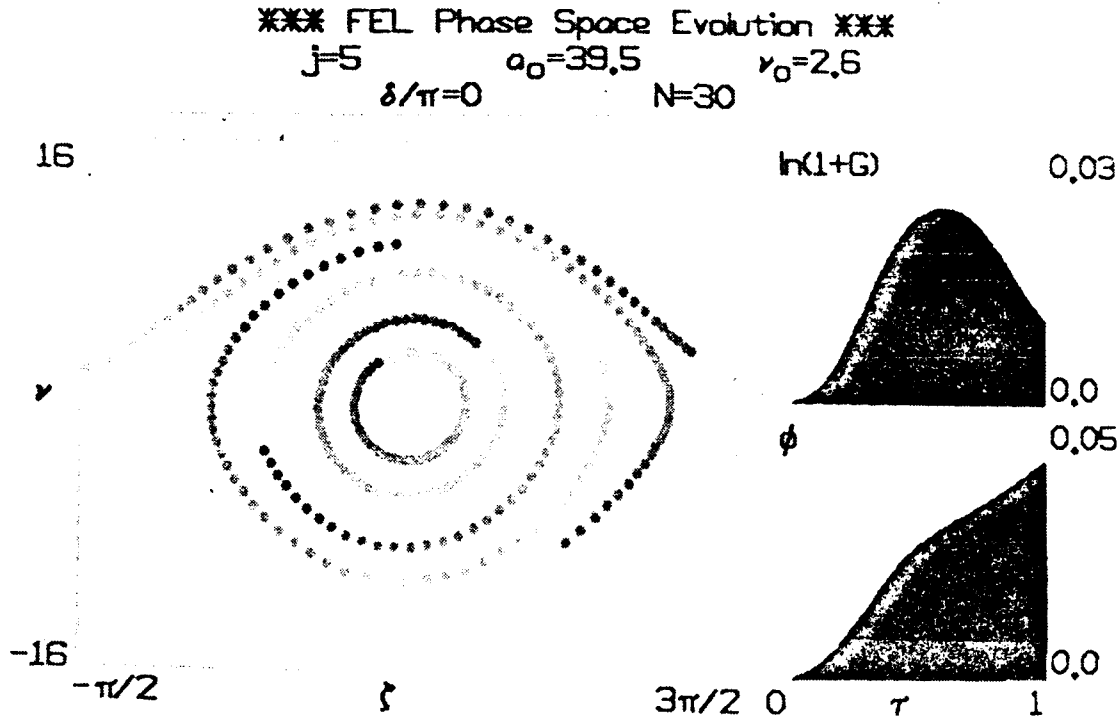


Fig. 1. The phase-space evolution of six sample electrons shows the harmonic oscillations of the trapped particles. At  $\tau=0$ , the electron positions are indicated as light grey spots; as  $\tau \rightarrow 1$  the electron spots gradually become black to show their full phase-space path. The optical field strength  $a_0 = v_s^2 = 4\pi^2$  causes one synchrotron oscillation for those electrons trapped near the stable fixed-point  $\zeta^* = \pi/2$ ; the gain  $G(\tau)$  and optical phase  $\phi(\tau)$  also oscillate at the synchrotron frequency.

The electrons trapped in the center of the phase-space, near phase  $\pi/2$ , execute one synchrotron oscillation at this field strength. The stable fixed-point  $\zeta^*$ , where there is no evolution, is the bottom of the potential well at  $\zeta^* = \cos^{-1}(-\delta/a_0) \approx \pi/2 + \delta/a_0$ . A well-designed tapered undulator reaches a power level sufficient to trap a large fraction of the electrons so that  $\delta/a_0 \ll 1$ . Motion of the trapped electrons near  $\zeta^*$  is described by

$$\zeta = \zeta^* + \frac{v_0}{v_s} \sin(v_s \tau) \quad (2)$$

with the initial position  $(\zeta^*, v_0)$ . The case shown in Fig. 1 has  $\delta = 0$  with small energy extraction, since the changes in resonance are  $< 2\pi N$  and  $N = 30$ . The synchrotron, or trapped-particle, oscillation frequency is  $v_s = (a_0 \sin(\zeta^*))^{1/2} \approx a_0^{1/2}$  when  $\delta/a_0 \ll 1$ . When the trapped electrons oscillate through a synchrotron cycle, the gain in Fig. 1 also oscillates through one cycle. It is the oscillation in the driving phase and the FEL gain that causes the trapped-particle frequency to be imposed on the optical wave as it slips over electrons. The sidebands appear at  $v_0 \pm v_s$ , so that the new FEL power is shifted from the fundamental wavelength by  $\Delta\lambda/\lambda = v_s/2\pi N$ . The shift has a simple interpretation;  $\Delta\lambda/\lambda =$  "the number of synchrotron oscillations"/ "the number of undulator periods".

#### 4. Short Pulse Oscillators

RF accelerators inject a series of short picosecond pulses into the FEL undulator in the oscillator configuration [2]. The optical pulses start from spontaneous emission, and bounce between the mirrors of an optical resonator separated by a distance  $S > L$ . High-power saturation is reached after several hundred passes, and the FEL works in steady-state for an additional  $10^3$  to  $10^4$  passes. The current density of each short pulse  $j(z)$  is taken to be parabolic with the form  $j(z) = j(1 - 2z^2/\sigma_z^2)$  for  $|z| < \sigma_z/\sqrt{2}$  and  $j(z) = 0$  for  $|z| > \sigma_z/\sqrt{2}$ ; the FWHM  $\sigma_z$  is normalized to the slippage distance  $N\lambda$ . Typically, RF accelerators produce current densities that give values of  $j$  in the moderate range  $1 \rightarrow 10$  and  $\sigma_z = 1 \rightarrow 30$ . In addition to gain, there is loss on each pass due to mirror absorption and transmission; in the absence of gain, the optical power decays as  $e^{-n/Q}$  where  $n$  is the pass number. Usually,  $Q$  is from  $10 \rightarrow 200$ .

An important concept in the short pulse FEL configuration is the matching of the electron pulse repetition frequency and the bounce frequency of the light pulse in the resonator  $2Sc$ . These frequencies must be closely synchronized so that each new electron pulse arrives at the beginning of the undulator simultaneous to the rebounding optical pulse. Define  $d$ , the "desynchronism," as the displacement between the pulses on each pass; if the mirrors are too close together by the distance  $\Delta S$ , then  $d = 2\Delta S/N\lambda$ . The desynchronism  $d$  is important to pulse evolution and final saturation. When  $|d|$  is too large, the electron and optical pulses do not overlap over a sufficient number of passes and the FEL is below threshold coupling. Surprisingly, when  $d = 0$ , exact synchronism, the FEL is also below threshold [5-7, 11-13, 21]; this effect has been termed "laser lethargy" [12]. Because of slippage, the gain is preferentially deposited on the trailing edge of the optical pulse; therefore, the optical pulse centroid actually travels slower than  $c$  in vacuum, and the frequency  $2Sc$  is overestimated. To compensate for the "lethargic" light, the

path  $S$  must be reduced by operating at  $d > 0$ . Maximum power is obtained at small  $d > 0$ . The final steady-state power  $P(d)$  is sharply peaked at  $d \approx 0$ , and slopes to zero as  $d$  increases.

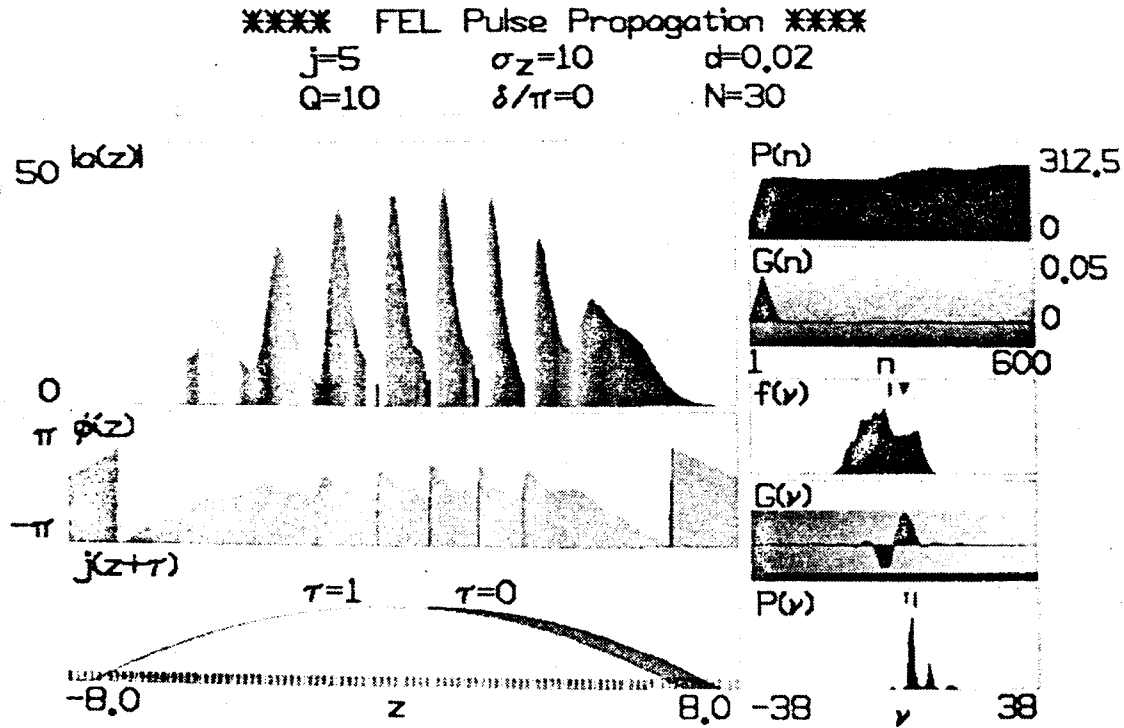


Fig. 2. Several pictures show the results of a short-pulse oscillator simulation affected by the trapped-particle instability. The optical power  $P(n)$  and gain  $G(n)$  evolve through  $n=600$  passes of the oscillator. The final optical field amplitude  $|a(z)|$  and phase  $\phi(z)$  are modulated with the synchrotron period  $\nu_s \approx 2\pi$  while being driven on each pass by the electron pulse  $j(z+\tau)$ .  $G(\nu)$  is the weak-field gain spectrum showing the position of maximum gain for the fundamental; the final optical power spectrum  $P(\nu)$  has additional sidebands  $\nu_0 \pm \nu_s$  due to the instability. The final electron distribution  $f(\nu)$  is broad because of the strong fields.

Figure 2 displays the output of a short pulse simulation for  $n = 600$  passes with  $j = 5$ ,  $\sigma_z = 10$ ,  $N = 30$ ,  $\delta = 0$  (no taper),  $d = 0.02$ , and  $Q = 10$ . The  $Q$  is low in this example so that sidebands will not mix further to produce a chaotic spectrum. After many passes, the initial

conditions are inconsequential, and we look for a final steady-state solution at saturation. The lower left picture shows the electron pulse shape before ( $\tau = 0$ ) and after ( $\tau = 1$ ) slippage of one unit. The evolution of the pulses is followed in a window of width  $W = 16$  so that  $-W/2 < z < W/2$ . The upper left figures show the final optical field amplitude  $|a(z)|$  and the optical phase profile  $\phi(z)$ . The jumps in phase by  $2\pi$  are meaningless, but the slope of the phase profile is a change in the laser light wavenumber and a resonance change  $\Delta v(k) = -\phi'(z)$  away from  $v_0$ . The grey scale on  $\phi(z)$  shows the local frequency component matching the gain spectrum  $G(v)$  on the right. The grey scale superimposed on the field amplitude above shows the gain experienced by each part of  $|a(z)|$  on the last pass in the undulator. This grey scale matches the scale in the gain evolution  $G(n)$  picture on the right. The top right figure follows the power  $P(n)$  averaged over all the sites in the window. Second on the right is  $G(n)$  which is the net gain over the whole pulse. Third is the final electron distribution  $f(v)$ , and fifth is the final optical power spectrum  $P(v)$  found from the Fourier transform of  $a(z)$ . The fourth picture  $G(v)$  is the weak-field, single-mode gain spectrum for the current density  $j$  on a single pass; it is included for reference.

The output of the simulation shows that the FEL oscillator has reached saturation with peak fields near  $|a| \approx 40$ . On each pass, those electrons that are near the center of the pulse, and have initial phases that allow them to become trapped, encounter fields strong enough to cause about one synchrotron oscillation. Normal saturation takes place early and the power is steady for about 350 passes; then the power increases again with the onset of the instability. The extra power is in the sidebands and the fundamental remains saturated [17,23]. Strong optical fields and the resulting trapped-particle oscillations must occur before there is significant gain at the sideband frequency  $v_s$ . A simple calculation shows that the field component at the sideband frequency  $v_s$  grows as

$$a(v_s) = a_s \exp((j_s/4v_s)^{1/2} \tau) \quad (3)$$

where  $v_s = |a|^{1/2}$  at saturation,  $a_s$  is the initial sideband field at  $v_s$ , and  $j_s$  is the trapped fraction of  $j$ ; typically,  $j_s = (0.1 \rightarrow 0.5)j$ . In this simulation,  $(j_s/4v_s)^{1/2} \approx 0.3$  and the loss rate is  $-(2Q)^{-1} \approx -0.05$ , so the sideband gain is above threshold. The sideband structure is clear in  $|a(z)|$ , and the power spectrum  $P(v)$ . The modulation length is close to the slippage distance indicating one synchrotron oscillation of the trapped electrons each pass, and the sideband  $P(v)$  occurs at  $v_s \approx 2\pi$  above the fundamental. At the ends of the pulse where the fields are weaker, the sideband period is slightly longer, in agreement with (2). The full-width of the electron distribution is given by the height of the closed-orbit region in phase-space,  $4|a|^{1/2}$ .

The general features of the trapped-particle instability in short-pulse FELs are briefly outlined below [21]; many features have now been observed in experiments [2,8,11].

1. At small  $d > 0$ , the FEL usually reaches power levels large enough to cause the trapped-particle instability. In this case, the optical pulse will be centered on the electron pulse, and will have sharp spikes due to the instability. This gives a broad, possibly chaotic, optical power spectrum, and a broad electron distribution.
2. At large  $d$ , the steady-state power is smaller due to the reduced coupling, and the trapped-particle instability is less likely to occur. The final optical power spectrum is narrow and in a single-mode; the final electron distribution is narrow due to the weak optical fields. Since the optical pulse is advanced by a large  $d$  on every pass, the center of the optical pulse may actually be ahead of the electron pulse. If the trapped-particle instability is undesirable in an FEL application, it may be easily removed by increasing  $d$ .
3. When  $d$  is in the intermediate range, we have often observed limit-cycle behavior in the simulations [5,6,13,21]. In this case, the pulse continually changes shape while the trapped-particle instability creates new subpulses.
4. Increasing the current density  $j$  or the resonator  $Q$  increases the steady-state power; this increases the synchrotron frequency and the sideband gain. The addition of sideband power is cumulative, since the presence of a strong sideband again increases the steady-state power. Simple modulation as shown in Fig. 2 is not the usual case; most parameter choices lead to a chaotic optical spectrum with many random spikes due to further sideband mixing [22].
5. If taper is introduced into the undulator design, the synchrotron frequency is only slightly modified. But, the depth of the strong-field potential wells is significantly reduced, and a smaller fraction of the electrons are trapped in closed harmonic orbits. Tapered undulators reduce the sideband gain and tend to suppress the trapped-particle instability [2,13,22,23].
6. When the pulse length  $\sigma_z$  is near unity, the short-pulse effects can be dramatic [11]. Adjusting  $d$  affects the total power, the electron distribution, and the optical pulse structure as outlined above. Since the sideband modulation first appears near the slippage distance (normalized to unity), a short pulse may not be long enough to support modulation at the synchrotron frequency. Depending on  $d$  the optical pulse can be made significantly shorter, or longer, than the picosecond electron pulse.

### 5. Long-Pulse Oscillators, "Wrapped-Windows"

In long electron pulses ( $\sigma_z \gg 1$ ) distant slippage sections of length  $\Delta z = 1$  are largely uncoupled and evolve independently in a window  $W > \sigma_z \gg 1$ . Simulations can become time consuming and require large amounts of memory. The straight-forward method used in Fig. 2 becomes wasteful because many of the slippage sections have similar evolutions. A better way to solve the problem [17,22,23] is by sampling a smaller window  $W \ll \sigma_z$  with periodic boundary conditions  $\zeta(z - W/2) = \zeta(z + W/2)$ . This restricts the number of modes that can be examined. Using a number of sites  $N_w$  in the window  $W$  we only represent modes  $v_l = v_0 - (2\pi/W)(l - N_w/2)$  where the integer  $l = 0, 1, 2, \dots, N_w - 1$ ; the mode spacing is  $\Delta v_l = 2\pi/W$ . With the periodic boundary conditions applied to the ends of the windows, we call them "wrapped-window" simulations.

Fig. 3 shows the result of a simulation in a window  $W = 4$ . The FEL is described by  $j = 5$ ,  $Q = 10$ ,  $N = 30$ , and  $\delta = 0$  as in Fig. 2. Without pulses,  $d$  and  $\sigma_z$  don't enter the problem. The individual pictures are the same as in Fig. 2 except for the reference to the pulse shape and slippage. The electron current density  $j(z)$  is constant along the window with a small amount of random noise  $\delta j = 0.01j$  at each site. Without noise, every site  $z$  would evolve identically and no spectral features would develop, but specific sources of noise can vary from one experiment to the next. The dimensionless current density  $j$  depends on several physical quantities which could contribute noise. Fluctuations of the electron particle density  $\rho(z)$ , or undulator errors in  $K^2$ , are both candidates.

After  $n = 600$  passes, the steady-state optical fields peak near  $|a| \approx 40$  just as in Fig. 2, and the final power spectrum  $P(v)$  is nearly identical to Fig. 2. Yet, this wrapped-window simulation takes only 1/4 the computer time of the pulse simulation; a smaller window  $W = 2$  would save more time and give the same result.

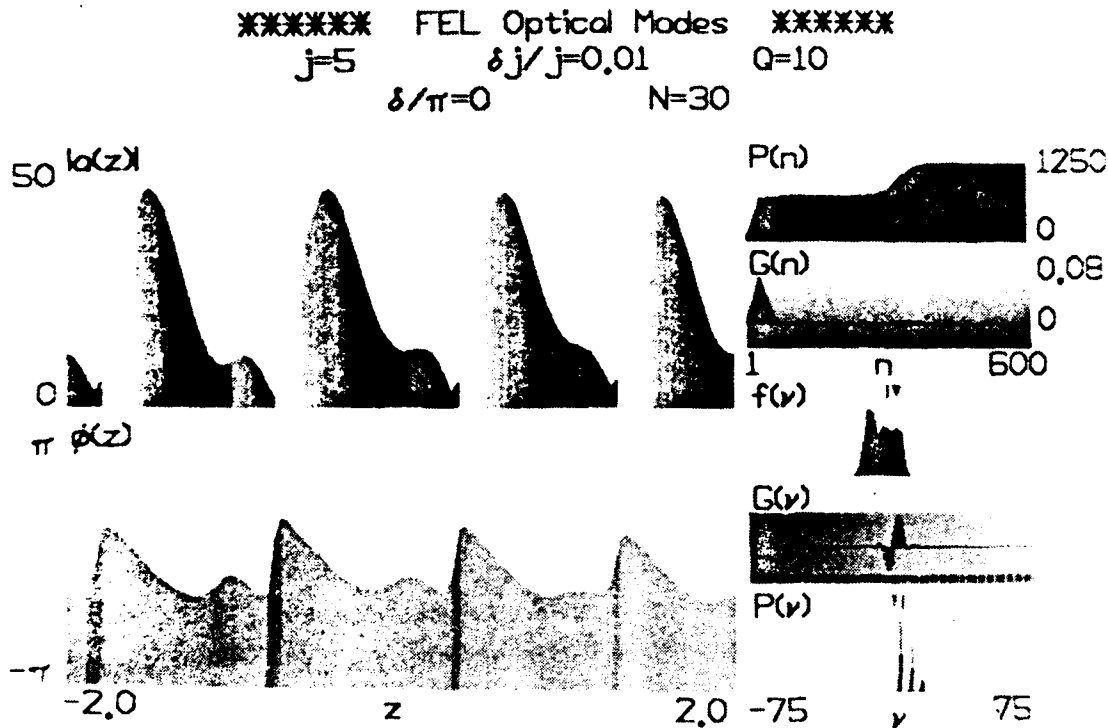


Fig. 3. With periodic boundary conditions in a "wrapped-window" simulation, the modulation and spectral lines resulting from the trapped-particle instability are made more clear. The complicating features of short pulses, seen in Fig. 2, are not present.

The general features of wrapped-window simulations are the same as the short-pulse cases except for desynchronism. An advantage of the wrapped-windows is the reduced number of dimensionless parameters.

1. As with pulse simulations, increases in  $j$  or  $Q$  make the trapped-particle instability more severe. It is unusual to find such even modulation as shown in Fig. 3. The instability increases output power by increasing the laser bandwidth.

2. When there is taper in the undulator design, the instability is less severe for the same reasons stated above.
3. Some source of noise is essential, but details are not important in the oscillator case. For pulse simulations no random noise is introduced, since the spectral features of the electron pulse structure are sufficient. In fact, we typically see the sideband modulations start at the ends of the electron pulse where the Fourier components are larger. In the FEL oscillator case, there are one or more synchrotron oscillations each pass. Over many hundreds of passes, the stored optical wave "sees" many synchrotron oscillations, and even modest sideband gain above threshold gives enormous growth from a small amount of noise. The resulting steady-state features are not affected by the details of the noise source employed.

#### 6. High-Current FEL Amplifiers

The FEL amplifier uses a high current density  $j \gg 1$  to reach high-power in a single pass. It is possible to attain values of  $j = 10^4 \rightarrow 10^5$  with the use of induction linac accelerators and long undulators [3]. The electron pulses are much longer than the slippage distance,  $\sigma_z \rightarrow \infty$ , and the wrapped-window simulation method becomes essential. The FEL growth rates are so large that electrons are trapped early in the undulator and begin executing synchrotron oscillations. There can be from several to many tens of synchrotron oscillations along the undulator, but these are the only synchrotron oscillations experienced by the optical field. Even with far fewer synchrotron cycles than in the oscillator case, the large current density  $j$  can give significant sideband gain once trapping occurs.

Fig. 4 shows the final simulation output for an FEL with high current  $j = 5 \times 10^4$ , no taper  $\delta = 0$ , an initial field  $a_0 = 20$  starting at  $v_0 = 0$ , and  $N = 30$ . A small amount of noise is introduced over a wide range of frequencies using  $\delta j = 0.01j$ ; in addition, there is a specific and comparable contribution from an initial sideband field  $a_s = 0.1$  at  $v_s = 16\pi$ . A high-current beam with some of the electrons trapped by strong fields will provide a source for  $a_s$ ; small fluctuations from shot noise or spontaneous emission in the average  $\langle \dots \rangle$  lead to significant contributions to  $a_s$  because  $j$  is large. The power evolution  $P(\tau)$  shows about eight synchrotron oscillations; these oscillations in  $a(\tau)$  are converted to the  $a(z)$  modulation through the trapped-particle instability. The sideband appears to grow at a rate consistent with (3) as soon as the field  $|a(\tau)|$  becomes sufficiently strong to cause trapped particle oscillations. The final field modulation and sideband in the power spectrum are clear.

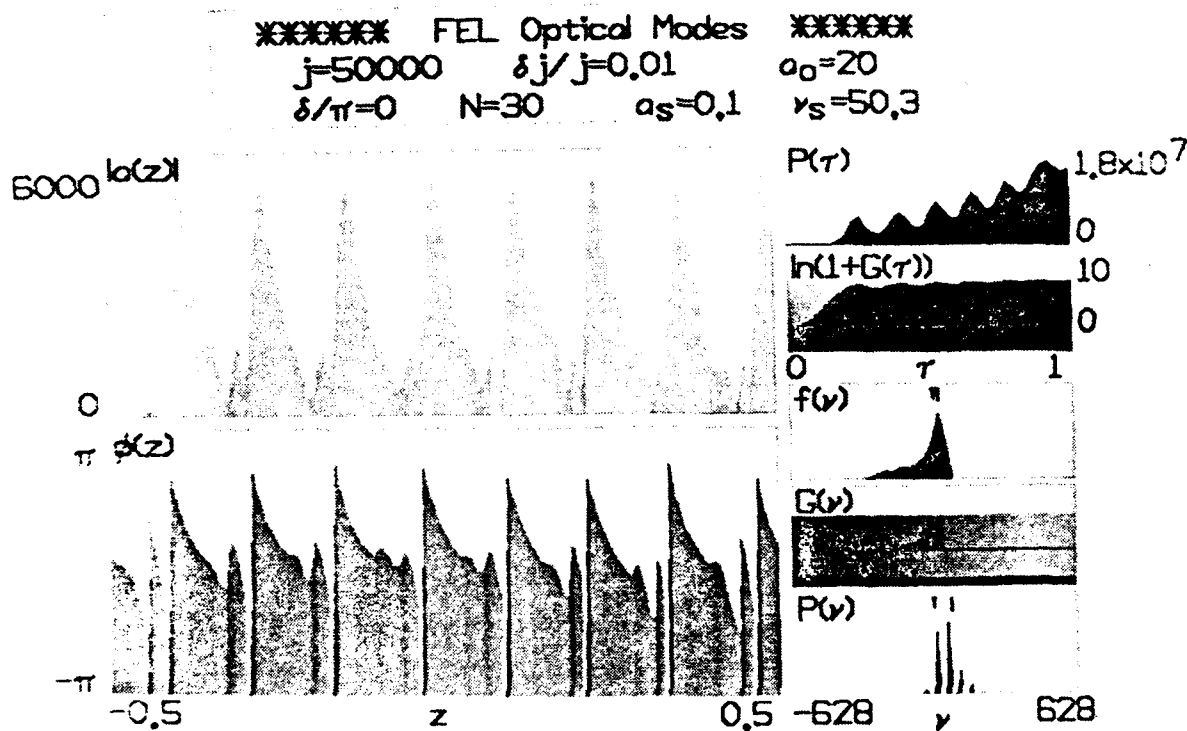


Fig. 4. In the high-current FEL amplifier, the trapped-particle instability must occur in one pass. In much stronger optical fields, the trapped electrons experience eight synchrotron oscillations, and impose a corresponding modulation onto the optical wave envelope. Sidebands are spaced at  $\nu_s \approx 16\pi$ .

The general characteristics of wrapped-window simulations for FEL amplifiers are different in many ways from the oscillator case. There is no resonator  $Q$  to consider, and sources of noise are much more important to FEL amplifiers than to FEL oscillators.

1. As with the oscillator cases, large  $j$  makes the trapped-particle instability more severe. However, it is only the large values of  $j$  that have a possibility of developing a sideband comparable in power to the fundamental. Using (3) we can evaluate the current  $j^*$  needed for the sideband field  $a_s$  to become equal to the fundamental amplitude  $a_0 = \nu_s^2$ . We estimate that most of the current is trapped in harmonic orbits,  $j_s \approx 0.75j^*$ , in the high

current case. With high current, the potential well that traps electrons grows rapidly in height and forces most of the current into harmonic orbits.

$$j^* \approx 20 v_s \ln^2(v_s / \sqrt{a_s}) \quad (4)$$

Assume that at least a few synchrotron oscillations ( say  $v_s \approx 16\pi$  ) are necessary for the optical wave to pick up the synchrotron frequency. The initial sideband field is estimated at  $a_s = 0.1$  for these high current cases;  $j^*$  only has a logarithmic dependence on  $a_s$  so that the estimate is not crucial. Then, we find that a characteristic current density  $j^* \approx 3 \times 10^4$  is needed before sidebands can significantly alter the final FEL amplifier spectrum, and currents below  $j^*$  are not as susceptible to the trapped-particle instability. The example in Fig. 4 uses  $j = 5 \times 10^4 > j^*$  for this reason. We found the trapped-particle instability difficult to excite when  $j \rightarrow j^*$ .

2. When there is taper in the undulator design, the instability is less severe for the same reasons as with the FEL oscillators. Less current is trapped and the synchrotron oscillations have a smaller amplitude.
3. Unlike the FEL oscillators, the spectral features of noise are important to sideband growth in the FEL amplifier. Suppression of input noise at the sideband frequency could be an important method for avoiding the trapped-particle instability in amplifiers. However, shot noise and spontaneous emission cannot be eliminated, and are significant contributions at these current densities.
4. The high current necessary for the trapped-particle instability, also plays a role in suppressing it. For such large  $j > j^*$ , there is no steady-state achieved even in strong fields  $|a|$ ; the power continues to increase and so does the synchrotron frequency. This can be seen in  $P(\tau)$  of Fig. 4. As the synchrotron frequency changes, the sideband power at a particular frequency does not accumulate.

In conclusion, we note that the trapped-particle instability is more likely to be found in the FEL oscillator than in the FEL amplifier, even though it was first predicted for the amplifier case. This is due to the large number of synchrotron oscillations experienced by the light stored in the oscillator resonator for many passes. However, the adjustable desynchronism  $d$  (and even a wavelength selective  $Q(v(\lambda))$ ) can make it relatively easy to reduce the trapped-particle instability in the oscillator case, while the FEL amplifier allows no such control in just one pass. To suppress sidebands in the amplifier, it may prove most fruitful to explore particular taper designs  $\delta(Z)$ , the

input wavelength  $\nu_0(\lambda)$  and field strength  $a_0$ , and controllable sources of noise like undulator errors and current fluctuations. It should also be remembered that while the trapped-particle instability has already been observed in the FEL oscillator, it has not yet been found in the FEL amplifier.

#### Acknowledgments

The author is grateful for support from Los Alamos National Laboratory Contract No. 9-X35-U8327, the U.S. Office of Naval Research Contract No. N00014-85-C-0493, and the U.S. Air Force Office of Scientific Research Contract No. F49620-85-C-0087.

#### References

- [1] W. B. Colson and A. M. Sessler, "Free Electron Lasers," Annual Rev. Nucl. Nucl. and Part. Science, **35**, 25 (1985).
- [2] B. E. Newman, R. W. Warren, R. L. Sheffield, W. E. Stein, M. T. Lynch, J. S. Fraser, J. C. Goldstein, J. E. Sollid, T. A. Swann, J. M. Watson, and C. A. Brau, Journal of Quantum Electronics, **QE-21**, 867 (1985).
- [3] T. J. Orzechowski, E. T. Scharlemann, B. Anderson, V. K. Neil, W. M. Fawley, D. Prosnitz, S. M. Yarema, D. B. Hopkins, A. C. Paul, A. M. Sessler and J. S. Wurtele, Journal of Quantum Electronics, **QE-21**, 831 (1985).
- [4] N. M. Kroll and M. N. Rosenbluth, *Physics of Quantum Electronics*, **7**, 147 (1980).
- [5] W. B. Colson and S. K. Ride, *Physics of Quantum Electronics*, **7**, 377 (1980).
- [6] W. B. Colson, International Summer School of Quantum Electronics, Erice (Sicily), eds. S. Martellucci and A. N. Chester, Plenum Press (1980), p. 189.
- [7] G. Dattoli, A. Marino, A. Renieri and F. Romanelli, Journal of Quantum Electronics, **QE-17**, 1371 (1981).
- [8] J. A. Edighoffer, G. R. Nell, C. E. Hess, T. I. Smith, S. W. Fornaca, H. A. Schwettman, Physical Rev. Lett. **B. 52**, 344 (1984).
- [9] N. M. Kroll, P. L. Morton and M. N. Rosenbluth, Journal of Quantum Electronics, **QE-17**, 1436 (1981).

- [10] J. C. Goldstein and W. B. Colson, Proc. of the Int. Conf. on Lasers '81, ed. C.B. Collins (STS Press, McLean, VA, 1981), p. 93.
- [11] J. N. Eckstein, J. M. J. Madey, K. Robinson, T. I. Smith, S. Benson, D. Deacon, R. Taber, and A. Gaupp, *Physics of Quantum Electronics*, 8 , 49 (1982).
- [12] H. Al-Abawi, J. K. McIver, G. T. Moore, and M. O. Scully, *Physics of Quantum Electronics*, 8 , 415 (1982).
- [13] W. B. Colson, *Physics of Quantum Electronics*, 8 , 457 (1982).
- [14] G. Dattoli, A. Marino, and A. Renieri, *Physics of Quantum Electronics*, 8 515 (1982).
- [15] A. T. Lin, *Physics of Quantum Electronics*, 9 , 867 (1982).
- [16] J. C. Goldstein and W. B. Colson, Proc. Int. Conf. LASERS '82, New Orleans, LA, Dec. 13-17, p. 218 (1982), ed. R.C. Powell.
- [17] W. B. Colson and R. A. Freedman, *Opt. Commun.*, 40 , 37 (1983).
- [18] J. C. Goldstein, *Free Electron Generators of Coherent Radiation*, eds. S. F. Jacobs and M. O. Scully, SPIE 453 , 2 (1983).
- [19] C.-M. Tang, P. Sprangle, *Free Electron Generators of Coherent Radiation*, eds. S. F. Jacobs and M. O. Scully, SPIE 453 , 11 (1983).
- [20] M. N. Rosenbluth, H. V. Wong, B. N. Moore, *Free Electron Generators of Coherent Radiation*, eds. S. F. Jacobs and M. O. Scully, SPIE 453 , 25 (1983).
- [21] W. B. Colson and A. Renieri, *J. de Physique* 44 , C1-11 (1983).
- [22] W. B. Colson, *Free Electron Generators of Coherent Radiation*, eds. S. F. Jacobs and M. O. Scully, SPIE 453 , 289 (1983).
- [23] R. A. Freedman and W. B. Colson, *Opt. Commun.*, 52 , 409 (1985).
- [24] W. B. Colson and S. K. Ride, *Phys. Lett. A* 76 , 379 (1980).
- [25] N. M. Kroll, P. L. Morton, and M. N. Rosenbluth, *Physics of Quantum Electronics*, 7 , 89 (1980).

## REPORT DOCUMENTATION PAGE

1a. REPORT SECURITY CLASSIFICATION			1b. RESTRICTIVE MARKINGS		
2a. SECURITY CLASSIFICATION AUTHORITY			3. DISTRIBUTION / AVAILABILITY OF REPORT		
2b. DECLASSIFICATION / DOWNGRADING SCHEDULE					
4. PERFORMING ORGANIZATION REPORT NUMBER(S)			5. MONITORING ORGANIZATION REPORT NUMBER(S)		
6a. NAME OF PERFORMING ORGANIZATION Berkeley Research Associates		6b. OFFICE SYMBOL (If applicable)	7a. NAME OF MONITORING ORGANIZATION Air Force Office of Scientific Research		
6c. ADDRESS (City, State, and ZIP Code) P.O. Box 241 Berkeley, CA 94701			7b. ADDRESS (City, State, and ZIP Code) Bolling Air Force Base Washington, DC 20332		
8a. NAME OF FUNDING / SPONSORING ORGANIZATION		8b. OFFICE SYMBOL (If applicable)	9. PROCUREMENT INSTRUMENT IDENTIFICATION NUMBER F49620-85-C-0087		
8c. ADDRESS (City, State, and ZIP Code)			10. SOURCE OF FUNDING NUMBERS		
			PROGRAM ELEMENT NO.	PROJECT NO.	TASK NO.
			WORK UNIT ACCESSION NO.		
11. TITLE (Include Security Classification) The Effect of Electron Trapping in Free-Electron Laser Oscillators and Amplifiers					
12. PERSONAL AUTHOR(S) W. B. Colson					
13a. TYPE OF REPORT Final Scientific		13b. TIME COVERED FROM _____ TO _____		14. DATE OF REPORT (Year, Month, Day)	
15. PAGE COUNT					
16. SUPPLEMENTARY NOTATION					
17. COSATI CODES			18. SUBJECT TERMS (Continue on reverse if necessary and identify by block number)		
FIELD	GROUP	SUB-GROUP	high-power laser		
			free electron laser		
			trapped-particle instability		
			laser oscillator		
			laser amplifier		
19. ABSTRACT (Continue on reverse if necessary and identify by block number) In high-power free-electron lasers, the electrons can become trapped in deep potential wells formed by the combined optical and undulator field forces. The trapped current oscillates at the synchrotron frequency, and can drive the optical wave at sideband frequencies around the fundamental. This "trapped-particle instability" can occur in both the oscillator and amplifier configurations.					
20. DISTRIBUTION / AVAILABILITY OF ABSTRACT <input type="checkbox"/> UNCLASSIFIED/UNLIMITED <input type="checkbox"/> SAME AS RPT. <input type="checkbox"/> DTIC USERS			21. ABSTRACT SECURITY CLASSIFICATION		
22a. NAME OF RESPONSIBLE INDIVIDUAL			22b. TELEPHONE (Include Area Code)		22c. OFFICE SYMBOL

# **The Effect of Electron Trapping in Free-Electron Laser Oscillators and Amplifiers**

*W. B. Colson*

Berkeley Research Associates, P.O. Box 241, Berkeley, California 94701

## **ABSTRACT**

In high-power free-electron lasers, the electrons can become trapped in deep potential wells formed by the combined optical and undulator field forces. The trapped current oscillates at the synchrotron frequency, and can drive the optical wave at sideband frequencies around the fundamental. This "trapped-particle instability" can occur in both the oscillator and amplifier configurations.

## **1. Introduction**

Many free-electron laser (FEL) oscillators [1], and FEL amplifiers [2] are designed to produce large optical power. In both configurations, a relativistic, high-current electron beam amplifies a copropagating electromagnetic wave as they pass through a periodic, transverse magnetic field undulator. The trapped-particle instability starts when electrons become trapped in deep potential wells formed by the combined optical and undulator fields. Electrons near the bottom of the well oscillate in harmonic orbits at the synchrotron frequency causing the carrier wave to develop sidebands. The "trapped-particle instability" was first predicted using a single-mode theory describing high-power, low-gain FEL oscillators with a tapered undulator [3]; the tapered undulator design reaches high power by trapping electrons in potential wells that remain resonant as the electrons lose energy [4]. At the same time, multimode simulations of short-pulse FEL oscillators observed the effects of the instability as pulse modulation [5-7]. Recently, the instability has been observed in the high-power FEL oscillator at LANL [1], and possibly in the TRW/Stanford oscillator [8]. It has been termed the sideband, Kroll-Rosenbluth, synchrotron, Raman, and the trapped-particle instability [9-23]. Here, the multimode sideband theory is reviewed with examples from short-pulse FELs, oscillators, and amplifiers. Common features and differences are discussed.

## 2. Multimode Simulation Theory

The electrons injected into the FEL undulator evolve due to the combined optical and undulator electromagnetic fields. When the relativistic electrons of energy  $\gamma_0 mc^2$  ( $\gamma_0 \gg 1$ ) are properly injected into the undulator, the transverse electron motion is periodic with amplitude  $K\lambda_0/2\pi\gamma_0$  and phase  $\exp(ik_0 Z)$  where  $K = e\bar{B}\lambda_0/2\pi mc^2$ ,  $e$  is the electron charge magnitude,  $\bar{B}$  is the rms undulator field strength,  $\lambda_0 = 2\pi/k_0$  is the undulator wavelength,  $m$  is the electron mass, and  $c$  is the speed of light in vacuum. The average speed of the beam along the  $Z$ -axis is  $\beta_0 c$  where  $\beta_0 = 1 - (1+K^2)/2\gamma_0^2$ . We follow the beam evolution with the dimensionless time  $\tau = \beta_0 ct/L = 0 \rightarrow 1$  along the undulator length  $L = N\lambda_0$  with  $N$  periods.

The light wave evolves in the presence of the electron beam according to the transverse wave equation. The optical carrier wave with frequency  $\omega = kc = 2\pi c/\lambda$  has the single-mode phase  $\exp[i(kZ - \omega t)]$  and a complex slowly-varying coefficient  $a(z) = a_R(z) + ia_I(z) = |a(z)|e^{i\phi(z)}$  evaluated at many discrete sites  $z$ . The dimensionless coordinate  $z$  is the ratio  $Z/N\lambda$  where the "slippage distance"  $N\lambda$  is defined by the number of optical wavelengths that pass over a resonant electron as that electron traverses the undulator length  $L$ . With the slowly-varying amplitude and phase approximation, and the coordinate change  $Z \rightarrow Z + ct$ , the wave operator reduces to a single derivative in time. The dimensionless optical field envelope is  $a(z) = 4\pi NeKLE(z)/\gamma_0^2 mc^2$  where  $E(z)$  is the complex optical electric field, and  $\gamma_0 mc^2$  is the resonant electron energy,  $\gamma_0^2 = k(1+K^2)/2k_0$ . Simulations take place within a window of width  $W$  along  $z$  that is an integral number of slippage distances long. At any  $\tau$ , electrons at coordinate  $z + \tau$  in the electron beam overlap the light at coordinate  $z$  in the optical wave. The electron phase relative to the optical wave and undulator fields is  $\zeta = (k+k_0)Z - \omega t$ , and the phase velocity is  $v = \dot{\zeta} = L[(k+k_0)\beta_z - k]$ . The self-consistent electron and optical equations [24] are

$$\dot{v}(z+\tau) = [1 - v(z+\tau)/2\pi N]^2 (a_R(z)\cos(\zeta(z+\tau)) - a_I(z)\sin(\zeta(z+\tau))) \quad (1)$$

$$\dot{\zeta}(z+\tau) = v(z+\tau) \quad (2)$$

$$\dot{a}_R(z) = -j(z+\tau) < [1 - v(z+\tau)/2\pi N]^{1/2} \cos(\zeta(z+\tau)) > \quad (3)$$

$$\dot{a}_I(z) = j(z+\tau) < [1 - v(z+\tau)/2\pi N]^{1/2} \sin(\zeta(z+\tau)) > \quad (4)$$

where the dimensionless current density is  $j(z) = 8N(e\pi KL)^2 \rho(z)/\gamma_0^3 mc^2$ ,  $\rho(z)$  is the actual particle density at site  $z$ , time derivatives are with respect to the dimensionless time  $\tau$ , and  $<...>$  is an average over sample electrons at site  $z + \tau$  in the electron beam.

In order to maintain strong coupling between the electrons and light, the phase velocity  $v$  cannot be too far from resonance,  $v = 0$ . The initial resonance condition  $v(\tau=0) = v_0$  is taken to be at the maximum of the weak-field gain spectrum. In both the amplifier and oscillator cases, we start the optical field at low values  $a(\tau=0) = a_0$ , well below saturation. The dimensionless current density  $j$  represents low single-pass gain when  $j \approx 1$ , and high gain when  $j \gg 1$ . Typically, the FEL oscillator configuration uses  $j \approx 1$ , while the FEL amplifier configuration uses  $j \gg 1$ . Weak optical fields give values of  $|a| < \pi$ , while strong fields give values of  $|a| > \pi$ . For small current and weak fields, maximum gain is at  $v_0 = 2.6$ ; for large current and weak fields, maximum gain is at  $v_0 = 0$ . The electron beam at each  $z$  has a uniform distribution of initial phases  $\zeta(\tau=0)$  over a  $2\pi$  range so that the initial optical phase is arbitrary; we take  $\phi(\tau=0) = 0$  at each  $z$ . The factors  $[1 - v/2\pi N]$  in (1)-(4) are close to unity unless the electrons lose a significant fraction of their energy and become less relativistic. Electron motion in terms of  $v$  corresponds to changes in the electron energy through the relation  $v \approx 4\pi N(\gamma - \gamma_0) / \gamma_0$ . We take  $N = 50$  in our examples as a common value typical of both amplifiers and oscillators. The final optical power spectrum  $P(k)$  is made more relevant by expressing  $k$ , the optical wavenumber, in terms of the corresponding resonance parameter  $v(k)$ ; similarly, the electron distribution function  $f(\gamma)$  is expressed in terms of  $v(\gamma)$ . The power spectrum  $P(v(k))$  and the electron distribution function  $f(v(\gamma))$  are more physically meaningful in terms of their affect on the resonance condition.

The single-mode version of (1)-(4) is obtained by removing all  $z$  dependence; all sites are given the same initial values of  $\zeta_0$ ,  $v_0$ , and  $a(z) = a_0$ . An estimate of the trapped-particle motion is obtained by considering the electrons in harmonic orbits near the stable fixed-point  $\zeta^* = \pi/2$ . With  $j$  not too large, and small energy extraction ( $N \gg 1$ ),  $|a|$  remains approximately constant during the synchrotron oscillations at saturation. Then, the motion of a trapped electron is  $\zeta(\tau) = \zeta^* + (v_0 / v_s) \sin(v_s \tau)$  with the initial position  $(\zeta^*, v_0)$ . The synchrotron or trapped-particle oscillation frequency is  $v_s = a_0^{1/2}$ . When the trapped electrons oscillate through a synchrotron cycle, part of the current driving the optical field in (3) and (4) also oscillates through one cycle. It is the oscillation of the driving phase in the average  $\langle \dots \rangle$  that causes the trapped-particle frequency to be imposed on the optical wave as it slips over electrons. The sidebands appear at  $v_0 \pm v_s$ , so that the new FEL power is shifted from the fundamental wavelength by  $\Delta\lambda/\lambda = v_s/2\pi N$ . The shift has a simple interpretation;  $\Delta\lambda/\lambda = \text{"the number of synchrotron oscillations"} / \text{"the number of undulator periods"}$ .

### 3. The Trapped-Particle Instability in Short-Pulse Oscillators

An FEL oscillator that is powered by an RF accelerator injects a series of short picosecond electron pulses into the undulator while the optical pulse bounces between mirrors separated by a distance  $S > L$ . High-power saturation is reached after many passes, and the FEL continues to work for an additional  $10^3$  to  $10^4$  passes. The current density of each short pulse  $j(z)$  is taken to be parabolic with the form  $j(z) = j (1 - 2z^2/\sigma_z^2)$  for  $|z| < \sigma_z/\sqrt{2}$  and  $j(z)=0$  for  $|z| > \sigma_z/\sqrt{2}$ ; the length  $\sigma_z$  is normalized by the slippage distance  $N\lambda$ . Typically, RF accelerators produce current densities which give values of  $j$  in the moderate range  $1 \rightarrow 100$  and  $\sigma_z = 1 \rightarrow 30$ . The loss on each pass (due to mirror absorption and transmission) is described by  $e^{-n/Q}$  where  $n$  is the pass number. Usually,  $Q$  is from  $2 \rightarrow 200$ .

The repetition frequency of successive electron pulses must be matched to the bounce frequency of the light pulse,  $2Sc$ . When synchronized, each new electron pulse arrives at the beginning of the undulator simultaneous to the rebounding optical pulse. The "desynchronism,"  $d = 2\Delta S/N\lambda$ , is the displacement between the pulses after each pass when the mirrors are separated by  $S - \Delta S$ . If  $|d|$  is too large, the electron and optical pulses do not overlap for a sufficient number of passes and the FEL operates below threshold coupling. If  $d = 0$ , exact synchronism, the FEL is also below threshold [5-7,11-14,21] due to an effect termed "laser lethargy" [12]. Because of slippage, gain is preferentially deposited on the trailing edge of the optical pulse causing the optical pulse centroid to travel slower than  $c$  in vacuum; therefore, the optical bounce frequency  $2Sc$  is overestimated. To compensate for the "lethargic" light, the path  $S$  must be reduced by operating at  $d > 0$ .

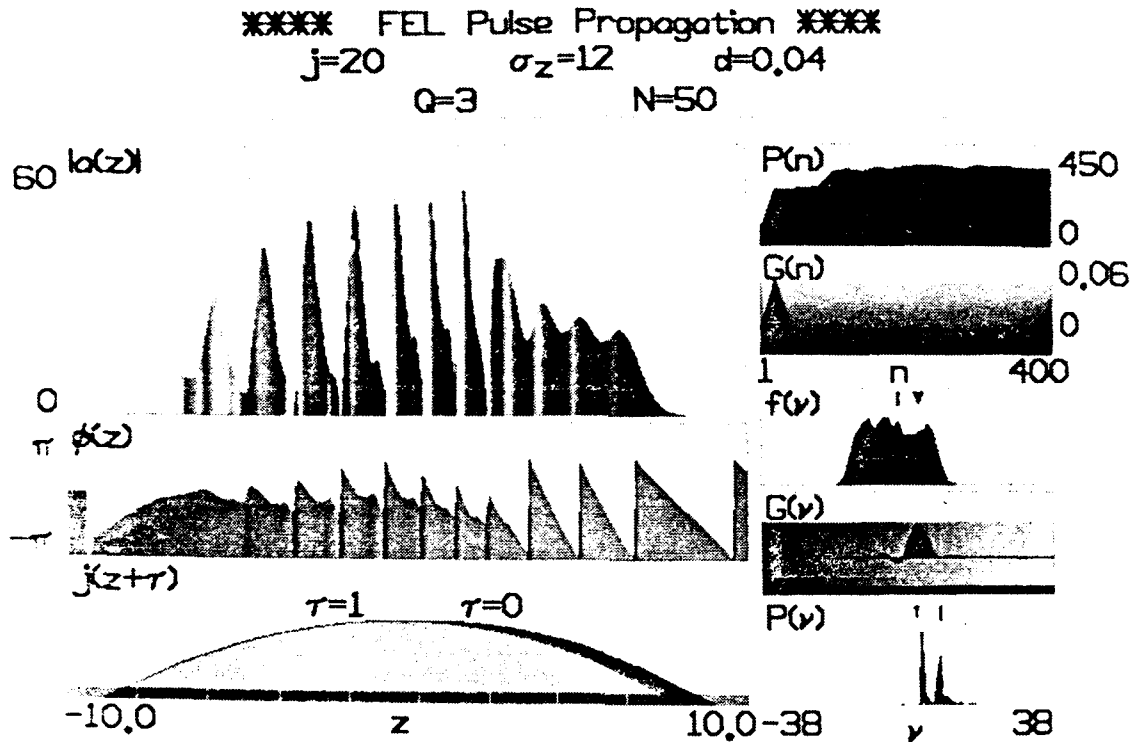


Fig. 1. Driven by the short electron pulse  $j(z+\tau)$ , the trapped-particle instability has modulated the optical pulse envelope  $a(z)$  at the synchrotron period  $\nu_s \approx 2\pi$ . The total optical power  $P(n)$  and gain  $G(n)$  reach steady-state after  $n=400$  passes through the oscillator.  $G(v)$  is the weak-field gain spectrum, included for reference. The final optical power spectrum  $P(v)$  has an additional sideband at  $\nu_0 + \nu_s$  due to the instability. The final electron distribution  $f(v)$  is broad because of the strong fields.

A short-pulse simulation is shown in Fig. 1. Steady-state is reached after  $n = 400$  passes with moderately high current  $j = 20$ , an intermediate pulse length  $\sigma_z = 12$ ,  $N = 50$ , desynchronism  $d = 0.04$ , and  $Q = 3$ . Large output coupling is used ( low  $Q$  ) because the gain is far above threshold. The top right figure follows the power  $P(n)$  averaged over the whole window. Second on the right is the net gain  $G(n)$  experienced by the pulse each pass. The lower left picture shows the electron pulse shape before ( $\tau = 0$ ) and after ( $\tau = 1$ ) the slippage of one unit per pass in a window of width  $W = 20$ . The upper left figures show the final optical field amplitude  $|a(z)|$  and the optical phase profile  $\phi(z)$  plotted along  $z$  where  $-W/2 < z < W/2$ . The jumps in phase of  $2\pi$  are meaningless, but the slope of the phase profile indicates a local change in the laser light

wavenumber and a resonance change  $\Delta v(k) = -\phi'(z)$  away from  $v_0$ . The grey scale on  $\phi(z)$  shows the local frequency component matching the gain spectrum  $G(v)$  on the right. The grey scale superimposed on the field amplitude shows the local gain experienced by each part of  $a(z)$  on the last pass in the undulator. This grey scale matches the scale in  $G(v)$  pictured on the right. Third on the right is the final electron distribution  $f(v)$ , and fifth is the final optical power spectrum  $P(v)$  found from the Fourier transform of  $a(z)$ . The fourth picture  $G(v)$  is the weak-field gain spectrum for the current density  $j = 20$ .

The simulation has reached saturation with peak fields near  $|a| \approx 60$ . Each pass, those electrons near the center of the pulse, that become trapped, encounter fields strong enough to cause about one synchrotron oscillation since  $\sqrt{a} \approx 2\pi$ . Normal saturation takes place early and the power is steady for about 50 passes; then the power increases again as the sideband grows. Strong optical fields and the resulting trapped-particle oscillations must occur before there is significant gain at the sideband frequency  $v_s$ . The extra power is in the sidebands and the fundamental remains saturated [17,23]. A simple calculation shows that the field component at the sideband frequency grows as  $a(\tau) = a_s \exp((j/4v_s)^{1/2} \tau)$  where  $v_s = |a|^{1/2}$  at saturation, and  $a_s$  is the initial sideband field at  $v_s$ . In this simulation,  $(j/4v_s)^{1/2} \approx 0.8$  and the loss rate is  $-(2Q)^{-1} \approx -0.2$ , so the sideband gain is above threshold. The sideband structure is clear in  $|a(z)|$ , and the power spectrum  $P(v)$ . The modulation length is close to the slippage distance indicating  $v_s \approx 2\pi$ , and the sideband in  $P(v)$  occurs at  $\Delta v \approx 2\pi$  above the fundamental. The full-width of the electron distribution is given by the height of the closed-orbit region in phase-space,  $4|a|^{1/2}$ .

The characteristics of the trapped-particle instability in short-pulse FELs are briefly outlined below [21]. Most characteristics have now been confirmed by experiments [1,8,11].

1. At small  $d > 0$ , the FEL usually reaches power levels large enough to cause the trapped-particle instability. This gives a broad, possibly chaotic, optical power spectrum, and a broad electron distribution.
2. At large  $d$ , the steady-state power is small due to the reduced coupling, and the trapped-particle instability is less likely to occur. The final optical power spectrum is narrow and in a single-mode; the final electron distribution is narrow due to the weak optical fields.

3. When  $d$  is in the intermediate range, we have often observed limit-cycle behavior in the simulations [5,6,13,21]. In this case, the pulse continually changes shape while the trapped-particle instability creates new subpulses.
4. Increasing the current density  $j$  or the resonator  $Q$  increases the steady-state power, the synchrotron frequency, and the sideband gain. The addition of sideband power is cumulative, since the presence of a strong sideband again increases the steady-state power.
5. If taper is introduced into the undulator design, the synchrotron frequency is only slightly modified, and the sideband gain is reduced [13,22,23].
6. When the pulse length  $\sigma_z$  is near unity, the short-pulse effects can be dramatic [11]. Since the sideband modulation first appears near the slippage distance, a short pulse may not be long enough to support modulation at the synchrotron frequency. The optical pulse can be made significantly shorter or longer than the picosecond electron pulse by adjusting  $d$ .

#### 4. Simulations in a "Wrapped-Window"

If the electron pulse is not short ( $\sigma_z \gg 1$ ) it is prudent to simulate the FEL by sampling a smaller window  $W \ll \sigma_z$  with periodic boundary conditions such that  $\zeta(z - W/2) = \zeta(z + W/2)$ ; these can be called "wrapped-window" simulations [17,22,23]. Using a number of sites  $N_W$  in a window of width  $W$  we follow a restricted number of modes  $\nu_l = \nu_0 - (2\pi/W)(l - N_W/2)$  where  $l = 0, 1, 2, \dots, N_W - 1$ ; the mode spacing is  $\Delta\nu = 2\pi/W$ . The desynchronization  $d$  and the pulse length  $\sigma_z$  don't enter the problem, and the current density  $j(z) = j$  is constant along the window.

The FEL simulation in Fig. 2 uses  $j = 20$ ,  $Q = 3$ , and  $N = 50$  (as in Fig. 1), but for a long pulse  $\sigma_z \gg W = 4$ . The individual pictures are the same as in Fig. 1 except for the reference to pulse shape. Without some noise source, no power would develop at frequencies other than the fundamental and every site  $z$  would evolve identically. Specific sources of noise can vary from one experiment to the next. In Fig. 2, the initial electron phases are uniformly spread over a  $2\pi$  range, but with an additional random phase of zero mean and standard deviation  $\delta\zeta \approx 1.0 \times 10^{-6}$ . Electron shot noise is a typical source of this kind of noise. In the pulse simulations no random noise is introduced, since the spectral features of  $j(z)$  are sufficient. After  $n = 400$  passes, the steady-state optical fields peak at  $|\alpha| \approx 60$  just as in Fig. 1, and the final power spectrum  $P(\nu)$  is similar to Fig. 1, but without the short pulse features.

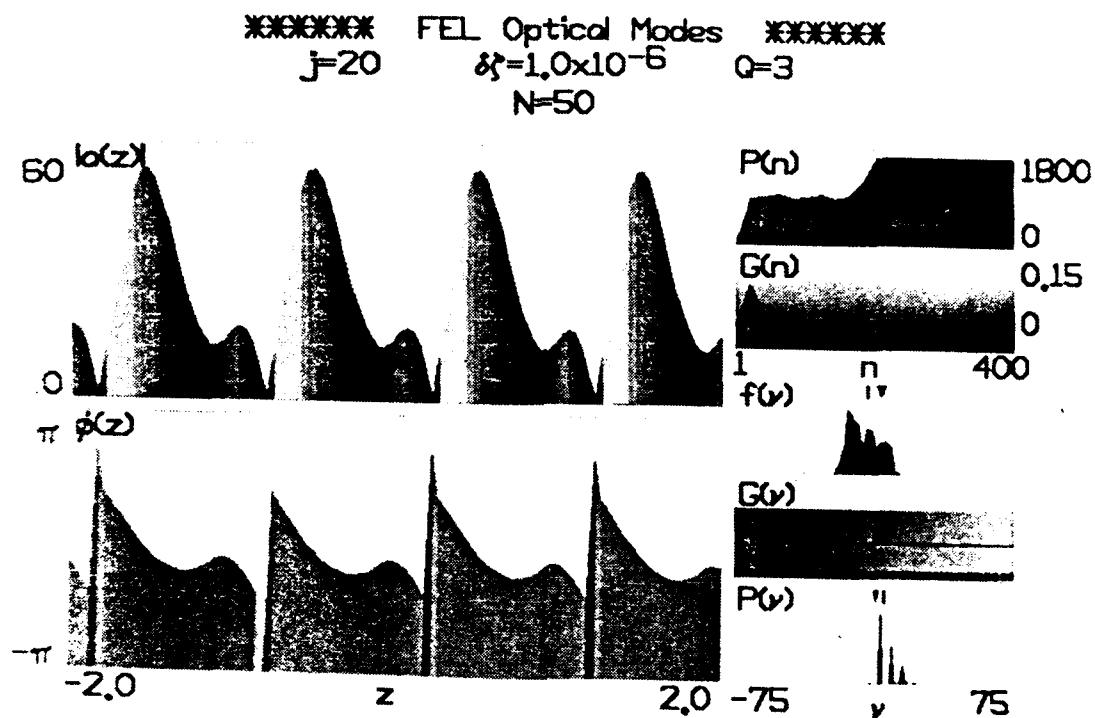


Fig. 2. The "wrapped-window" simulation gives a clear example of the trapped-particle instability in the FEL oscillator without the complicating features of short pulses.

Wrapped-window simulations have many of the same characteristics as for pulses, but without the effects of desynchronization. As  $\sigma_z \rightarrow \infty$  the wrapped-window approach is the only viable solution to the FEL multimode simulation.

1. Increases in  $j$  or  $Q$  make the trapped-particle instability more severe. It is unusual to find the periodic, even modulation shown in Fig. 2.
2. When there is taper in the undulator design, the instability is less prominent for the same reasons as stated in the pulse case.

3. Over many hundreds of passes, the stored optical wave "sees" many synchrotron oscillations, so that any sideband gain above threshold gives large growth from a small amount of noise. The resulting steady-state features are therefore not affected by the details of the noise source employed.

### 5. The Trapped-Particle Instability in High-Current FEL Amplifiers

In the high-current FEL amplifier,  $j \gg 1$ , large optical power can be produced in a single pass through the undulator. An induction linac accelerator and a long undulator can result in values  $j = 10^4 \rightarrow 10^5$  [2]. The electron pulses are long,  $\sigma_z \rightarrow \infty$ , so that the wrapped-window simulation method is essential. The FEL growth rates are so large that electrons become trapped early in the undulator and begin executing synchrotron oscillations. There can be from several to many tens of synchrotron oscillations along the undulator so that the optical field experiences far fewer synchrotron cycles than in the oscillator case. However, even the limited number of synchrotron cycles can result in significant sideband gain owing to the large current density  $j$ .

The wrapped-window simulation in Fig. 3 follows the power and gain from  $\tau = 0 \rightarrow 1$  for an FEL with high current  $j = 8 \times 10^4$ , an initial field  $a_0 = 20$  starting at  $v_0 = 0$ , and  $N = 50$ . No electron phase noise is present, but a small initial sideband field  $a_s = 0.01$  is introduced at  $v_s = 20\pi$ . Spontaneous emission or electron shot noise from the trapped electrons can lead to a contribution of this size because  $j$  is large. The power  $P(\tau)$  and gain  $G(\tau)$  are seen to oscillate with the synchrotron frequency  $v_s \approx 20\pi$  and impose a strong modulation on the light wave envelope  $a(z)$ . The final power spectrum  $P(v)$  shows that the sideband has grown to almost equal the fundamental power.

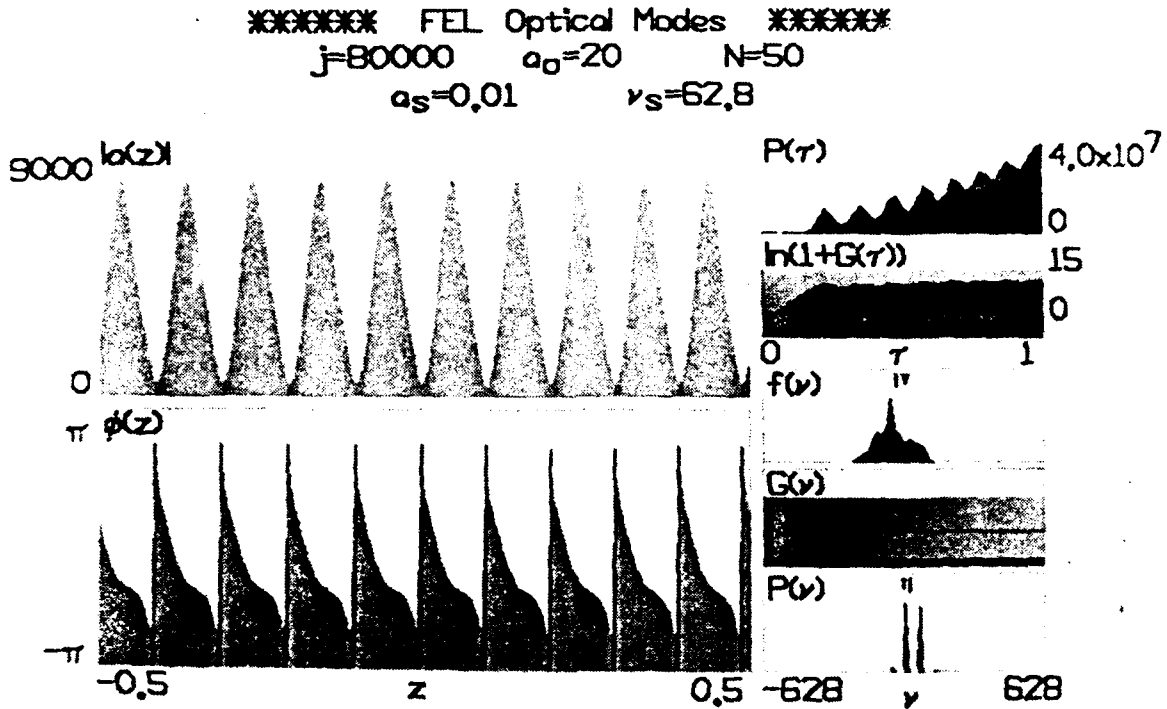


Fig. 3. The trapped-particle instability can create significant sideband power during one pass in the FEL amplifier. The high-currents used in amplifiers give much stronger optical fields at early stages of the undulator that can cause several synchrotron oscillations, and impose a corresponding modulation onto the optical wave envelope. In this example, the sideband is spaced at  $\nu_s \approx 20\pi$ .

The trapped-particle instability in FEL amplifiers differs in many ways from the oscillator case. Sources of noise are much more important, and there is no resonator  $Q$  to consider.

1. Large current  $j$  makes the trapped-particle instability more likely. Using the sideband growth rate, we can evaluate the current  $j^*$  needed to make the sideband field  $a_s$  equal to the fundamental,  $a_0 = \nu_s^2$ . This gives

$$j^* \approx 16\nu_s \ln^2(\nu_s/\sqrt{a_s})$$

The current  $j^*$  has a slow logarithmic dependence on the initial sideband field  $a_s$  so that an accurate estimate is not too crucial; we take  $a_s = 0.01$ . We also estimate that there must be at least a few synchrotron oscillations, say  $\nu_s \approx 16\pi$ , before the optical wave could accurately determine the synchrotron frequency. This gives a characteristic current density  $j^* \approx 3 \times 10^4$  where sidebands could be expected to significantly alter the final FEL amplifier spectrum.

2. In the tapered undulator case, less current is trapped, and the synchrotron oscillations have a smaller amplitude so that the trapped-particle instability is observed to be less severe, as in FEL oscillators.
3. Input noise at the sideband frequency is important to the development of significant sideband power in FEL amplifiers. Shot noise and spontaneous emission cannot be eliminated, and may be a significant contribution at large current densities.
4. For the large currents  $j > j^*$ , the FEL does not reach steady-state operation even in strong optical fields  $|a|$ . The power continues to increase and so does the synchrotron frequency. This continual change in the synchrotron frequency may play a useful role in suppressing the growth at any particular sideband frequency.

In conclusion, we find that the trapped-particle instability is more difficult to suppress in the FEL oscillator than in the FEL amplifier. The large number of synchrotron oscillations experienced by the light stored in the oscillator make the effective gain over for many passes large. But, while the trapped-particle instability has already been observed in the FEL oscillator, it has not yet been found in the FEL amplifier. The many differences between FEL oscillator and amplifier simulations implies that we should not use the oscillator case as a direct proof that there will be an equally prominent instability in real FEL amplifiers.

#### Acknowledgments

The author is grateful for support from Naval Research Lab Contract No. N00014-86-C-2006, the U.S. Office of Naval Research Contract No. N00014-85-C-0493, and the U.S. Air Force Office of Scientific Research Contract No. F49620-85-C-0087.

### References

- [1] B. E. Newman, R. W. Warren, R. L. Sheffield, W. E. Stein, M. T. Lynch, J. S. Fraser, J. C. Goldstein, J. E. Sollid, T. A. Swann, J. M. Watson, and C. A. Brau, *IEEE Journal of Quantum Electronics*, QE-21, 867 (1985).
- [2] T. J. Orzechowski, E. T. Scharlemann, B. Anderson, V. K. Neil, W. M. Fawley, D. Prosnitz, S. M. Yarema, D. B. Hopkins, A. C. Paul, A. M. Sessler and J. S. Wurtele, *IEEE Journal of Quantum Electronics*, QE-21, 831 (1985).
- [3] N. M. Kroll and M. N. Rosenbluth, "*Physics of Quantum Electronics*," 7, 147 (1980).
- [4] N. M. Kroll, P. L. Morton, and M. N. Rosenbluth, "*Physics of Quantum Electronics*," 7, 89 (1980).
- [5] W. B. Colson and S. K. Ride, "*Physics of Quantum Electronics*," 7, 377 (1980).
- [6] W. B. Colson, International Summer School of Quantum Electronics, Erice (Sicily), eds. S. Martellucci and A. N. Chester, Plenum Press (1980), p. 189.
- [7] G. Dattoli, A. Marino, A. Renieri and F. Romanelli, *IEEE Journal of Quantum Electronics*, QE-17, 1371 (1981).
- [8] J. A. Edighoffer, G. R. Neil, C. E. Hess, T. I. Smith, S. W. Fornaca, H. A. Schwettman, *Phys. Rev. Lett.* 52, 344 (1984).
- [9] N. M. Kroll, P. L. Morton and M. N. Rosenbluth, *IEEE Journal of Quantum Electronics*, QE-17, 1436 (1981).
- [10] J. C. Goldstein and W. B. Colson, *Proc. of the Int. Conf. on Lasers '81*, ed. C.B. Collins (STS Press, McLean, VA, 1981), p. 93.
- [11] J. N. Eckstein, J. M. J. Madey, K. Robinson, T. I. Smith, S. Benson, D. Deacon, R. Taber, and A. Gaupp, "*Physics of Quantum Electronics*," 8, 49 (1982).
- [12] H. Al-Abawi, J. K. Mclver, G. T. Moore, and M. O. Scully, "*Physics of Quantum Electronics*," 8, 415 (1982).
- [13] W. B. Colson, "*Physics of Quantum Electronics*", 8, 457 (1982).
- [14] G. Dattoli, A. Marino, and A. Renieri, "*Physics of Quantum Electronics*," 8, 515 (1982).

- [15] A. T. Lin, "*Physics of Quantum Electronics*," 9, 867 (1982).
- [16] J. C. Goldstein and W. B. Colson, Proc. Int. Conf. LASERS '82, New Orleans, LA, Dec. 13-17, p. 218 (1982), ed. R. C. Powell.
- [17] W. B. Colson and R. A. Freedman, Opt. Commun., 40, 37 (1983).
- [18] J. C. Goldstein, "*Free Electron Generators of Coherent Radiation*," eds. C. A. Brau, S. F. Jacobs and M. O. Scully, SPIE 453, 2 (1983).
- [19] H. Freund, P. Sprangle, and C.-M. Tang, Phys. Rev. A25, 3121 (1982).
- [20] M. N. Rosenbluth, H. V. Wong, and B. N. Moore, "*Free Electron Generators of Coherent Radiation*," eds. C. A. Brau, S. F. Jacobs and M. O. Scully, SPIE 453, 25 (1983);  
N. M. Kroll, M. N. Rosenbluth, H. V. Wong, B. N. Moore, and S. Tsunoda, Conf. on Lasers and Electro-Optics, CLEO/IQEC '84, Anaheim CA (May 1984);
- [21] W. B. Colson and A. Renieri, J. de Physique 44, C1-11 (1983).
- [22] W. B. Colson, "*Free Electron Generators of Coherent Radiation*," eds. C. A. Brau, S. F. Jacobs and M. O. Scully, SPIE 453, 289 (1983).
- [23] R. A. Freedman and W. B. Colson, Opt. Commun., 52, 409 (1985).
- [24] W. B. Colson and S. K. Ride, Phys. Lett. A76, 379 (1980).

## REPORT DOCUMENTATION PAGE

1a. REPORT SECURITY CLASSIFICATION			1b. RESTRICTIVE MARKINGS		
2a. SECURITY CLASSIFICATION AUTHORITY			3. DISTRIBUTION/AVAILABILITY OF REPORT		
2b. DECLASSIFICATION/DOWNGRADING SCHEDULE					
4. PERFORMING ORGANIZATION REPORT NUMBER(S)			5. MONITORING ORGANIZATION REPORT NUMBER(S)		
6a. NAME OF PERFORMING ORGANIZATION Berkeley Research Associates		6b. OFFICE SYMBOL (if applicable)	7a. NAME OF MONITORING ORGANIZATION Air Force Office of Scientific Research		
6c. ADDRESS (City, State, and ZIP Code) P.O. Box 241 Berkeley, CA 94701			7b. ADDRESS (City, State, and ZIP Code) Bolling Air Force Base Washington, DC 20332		
8a. NAME OF FUNDING/SPONSORING ORGANIZATION		8b. OFFICE SYMBOL (if applicable)	9. PROCUREMENT INSTRUMENT IDENTIFICATION NUMBER F49620-85-C-0087		
8c. ADDRESS (City, State, and ZIP Code)			10. SOURCE OF FUNDING NUMBERS		
			PROGRAM ELEMENT NO.	PROJECT NO.	TASK NO.
11. TITLE (Include Security Classification) Free-Electron Laser Gain Degradation and Electron Beam Quality					
12. PERSONAL AUTHOR(S) W. B. Colson, J. C. Gallardo, P. M. Bosco					
13a. TYPE OF REPORT Final Scientific		13b. TIME COVERED FROM _____ TO _____		14. DATE OF REPORT (Year, Month, Day)	
15. PAGE COUNT					
16. SUPPLEMENTARY NOTATION					
17. COSATI CODES			18. SUBJECT TERMS (Continue on reverse if necessary and identify by block number)		
FIELD	GROUP	SUB-GROUP	free electron laser energy spread angular spread		
			high-gain laser emittance		
			weak-field laser electron beam quality		
19. ABSTRACT (Continue on reverse if necessary and identify by block number)					
<p>The free electron laser can be described by an integral equation that allows the inclusion of an arbitrary electron distribution function in a simple way. Contour maps show the gain degradation due to an energy spread and an angular spread. For low gain, the gain spectrum is related to the spontaneous emission line-shape through successively higher derivatives. For high gain, the growth rate becomes less susceptible to degradation from the electron beam quality.</p>					
20. DISTRIBUTION/AVAILABILITY OF ABSTRACT <input type="checkbox"/> UNCLASSIFIED/UNLIMITED <input type="checkbox"/> SAME AS RPT. <input type="checkbox"/> DTIC USERS			21. ABSTRACT SECURITY CLASSIFICATION		
22a. NAME OF RESPONSIBLE INDIVIDUAL			22b. TELEPHONE (Include Area Code)		22c. OFFICE SYMBOL

# Free-Electron Laser Gain Degradation and Electron Beam Quality

*W. B. Colson*

Berkeley Research Associates, P.O. Box 241, Berkeley, CA 94701

*J. C. Gallardo and P. M. Bosco*

Quantum Institute, University of California, Santa Barbara, CA 93106

## ABSTRACT

The free electron laser can be described by solving the Lorentz-Maxwell equations self-consistently in weak optical fields. The field evolution is determined by an integral equation that allows the inclusion of an arbitrary electron distribution function in a simple way. Contour maps are used to show the gain degradation due to an electron beam energy spread and an electron beam angular spread. In the limit of low gain, the gain spectrum is related to the spontaneous emission line-shape through successively higher derivatives. In the limit of high gain, it is shown that the growth rate becomes less susceptible to degradation from the electron beam quality.

## I. Introduction

In a free-electron laser (FEL), a relativistic electron beam amplifies a co-propagating, coherent optical wave traveling through a periodic undulator magnetic field [1]. In the oscillator configuration, coherent electron bunching develops on each pass while resonator mirrors allow the stored optical power to grow over many passes. In the amplifier configuration, coherent electron bunches develop rapidly in the first part of the undulator followed by rapid growth of the optical field. Maintaining the coherence of the electron bunches over a significant interaction length imposes important restrictions on the electron beam quality. An energy or angular spread (due to emittance) contributes a random component to the electron motion that decreases the coherent bunching in time.

Some of the earliest FEL experiments used electron beams that were essentially monoenergetic [2-5], but practically all subsequent experiments have made use of higher current sources with significant energy spread or emittance. Many accelerators present a design trade-off between high current and high beam quality. This makes it essential to accurately evaluate the effects of beam quality in present and future experiments. It is particularly important for FELs designed to operate at XUV or X-ray wavelengths [6]. Several theoretical models involving simulations and plasma dispersion relations have discussed the detrimental effects of electron beam quality in the FEL interaction [7-24]. The theory presented here uses a convenient, yet powerful, method of including an arbitrary electron distribution function in a self-consistent integral equation for the complex optical field. FEL gain and the effects of beam quality can then be calculated analytically or integrated on a small computer.

Since the basic equations solved here are the same as in computer simulations or the plasma dispersion methods, specific physical results have been shown to agree with those methods when a direct comparison is possible. The computer simulations have proved to be a useful method of understanding many aspects of the FEL interaction, but one of the most difficult effects to accurately characterize is that of electron beam quality. Even a prohibitively large number of sample particles is far short of the number in a real experiment, and yet introduces a large amount of numerical noise when distributed over a large volume of phase-space. To reproduce some of the results shown later in this paper, we found the simulation method to be several hundred to a thousand times less efficient. While many other FEL topics are most efficiently studied through simulations, the detrimental effects of beam quality are probably better handled through a combination of analytic and numerical techniques. The stability analysis used to obtain plasma dispersion relations usually calculates the reduced FEL growth rates due to poor beam quality. This method can lead to analytical expressions, but depends upon specific models for the electron beam distribution, and does not easily describe more complicated transient behavior where the FEL growth rate is not constant; the FEL is often designed to operate in this regime. In addition, the exact formulation presented here works smoothly between different regimes of operation like high and low gain. The only requirement is weak optical fields.

## II. Basic Theory

We solve the electron Lorentz and optical wave equations self-consistently with the assumption of weak optical fields. The effects of beam quality are typically less important when the optical field strength is large near saturation, and the issue of beam quality is most important in weak fields where the accurate evaluation of gain can determine whether the FEL is above or below threshold.

The electrons travel through a periodic undulator with the field on the  $z$ -axis described by  $\vec{B} = B [\cos(k_0 z), \sin(k_0 z), 0]$  where  $B$  is the peak magnetic field amplitude. The undulator field extends over a length  $L = N\lambda_0$  with a number of periods  $N$ , and wavelength  $\lambda_0 = 2\pi/k_0$ . The electron velocity in a perfect helical orbit is  $c\vec{\beta} = c [-(K/\gamma) \cos(k_0 z), -(K/\gamma) \sin(k_0 z), \beta_0]$  where  $K = eB\lambda_0/2\pi mc^2$ ,  $e$  is the electron's charge magnitude,  $m$  is the electron's mass,  $c$  is the speed of light,  $\beta_0 = (1 - (K/\gamma)^2)^{1/2}$ , and  $\gamma mc^2$  is the electron's energy. Imperfect injection due to poor beam quality is more meaningfully introduced after some further theoretical development. A typical undulator uses  $B \approx 2\text{kG}$  and  $\lambda_0 \approx 5\text{cm}$ , so that  $K \approx 1$ . Since the electrons are relativistic ( $\gamma \gg 1$ ), the transverse excursions are small compared to  $\lambda_0$ .

The optical vector potential with the polarization that best couples to the above trajectory is  $\vec{A} = k^{-1}|E|[\sin\psi, \cos\psi, 0]$  where  $\psi = kz - \omega t + \phi$ , and  $\lambda = 2\pi/k = 2\pi c/\omega$  is the optical carrier wavelength. The complex electric field envelope,  $E(z, t) = |E(z, t)|e^{i\phi(z, t)}$ , is taken to vary slowly in  $z$  and  $t$ , so that terms containing two derivatives in the wave equation are small compared to terms with single derivative [25]. No transverse  $(x, y)$ -dependence is included so that diffraction is taken to be a small over the interaction length  $L$ , and the electron beam remains aligned near the center of the optical mode. The transverse motion above, proportional to  $(K/\gamma)$ , defines the transverse current for each electron in the beam. If the current density is uniform over a sufficient length, each point  $z + ct$  in the optical field envelope evolves according to the slowly-varying wave equation [25]

$$\frac{da}{d\tau} = -j \langle e^{-i\zeta} \rangle, \quad (1)$$

where  $a = 4N\pi e K L E / \gamma^2 mc^2$  is the dimensionless optical field strength,  $\tau = ct/L$  is the dimensionless time ( $0 \leq \tau \leq 1$ ),  $j = 8N(\pi e K L)^2 \rho / \gamma^3 mc^2$  is the dimensionless current density,  $\rho$  is the actual electron particle density,  $\zeta = (k + k_0)z - \omega t$  is the electron phase in the combined optical and undulator fields, and  $\langle \dots \rangle$  represents a normalized average over all electrons in the beam

driving  $a(\tau)$ . The electrons are labeled by their initial phase-space coordinates; the initial phase is  $\zeta_i = \zeta(0)$ , and the initial phase velocity is  $v_i = d\zeta(0)/d\tau = L[(k + k_0)\beta_0 - k]$ . There are a large number of electrons spread randomly over each optical wavelength ( $\sim 10^7$ ), so that the  $\zeta_i$  can be accurately taken to be uniformly spread along each section of the electron beam one wavelength of light long. It can be easily seen in (1) that bunching the electrons near the relative phase  $\zeta + \phi \approx \pi$  drives the optical wave amplitude producing gain, while bunching near  $\zeta + \phi \approx \pi/2$  drives the optical phase  $\phi$  without gain. Bunching electrons near  $\zeta + \phi \approx 0$  results in negative gain, or absorption. The dimensionless electron phase velocity  $v_i$  has an initial spread associated with the beam quality.

The electron motion in the presence of the optical wave is described by the Lorentz force equation;  $d\gamma/dt = -(e/mc)\beta \cdot \vec{E}$ . In the FEL, it is important to distinguish between collective Coulomb forces and collective high-gain effects [26]. Most FELs do not use current densities large enough for Coulomb forces to be a significant effect for the relativistic electrons; yet, high gain is possible and will be included. Using the definitions and assumptions above, the Lorentz force takes on the form of the pendulum equation [27],

$$\frac{d^2\zeta}{d\tau^2} = \frac{dv}{d\tau} = |a| \cos(\zeta + \phi) \quad (2)$$

The combined equations (1) and (2) are valid in weak or strong optical fields, for large or small gain, and for an arbitrary electron distribution. Strong fields near saturation mean that  $|a| \gg \pi$ , and weak fields occur when  $|a| \ll \pi$ . High gain is achieved when  $j \gg 1$  and low gain occurs when  $j \leq 1$  [28]. Useful FEL configurations display a wide range of current densities. The electron beam area is typically between 1mm and 5mm, but the current ranges from 1A up to 10kA. Undulator lengths  $L$  now range from 1m to 5m, but will soon be made to  $L = 20$ m and beyond. With electron energies in the range 10MeV to 1GeV, the corresponding values of  $j$  are from unity to more than  $5 \times 10^4$  [1]. Both the high-gain, single-pass and the low-gain, oscillator configurations have important applications.

Equations (1) and (2) were originally derived [25] for the more general case where the electron energy can change significantly during a single pass; in this case, an additional factor  $\eta = (1 - v/2\pi N)$  alters the wave and electron equations so that  $\dot{a} = -j < \sqrt{\eta} e^{-i\zeta} >$  and,  $\ddot{\zeta} = \dot{v} = |a| \eta^2 \cos(\zeta + \phi)$  with  $(\dot{\phantom{x}}) = d(\phantom{x})/d\tau$ . The following work, however, will be confined to weak optical fields where  $\eta \approx 1$ . An extension to higher harmonics and linearly polarized undulators is

also possible without any change in form of (1) and (2), so that the general conclusions and methods of this paper are immediately applicable to a wide range of FEL designs.

We now proceed to solve (1) and (2) in weak fields,  $|a| \ll \pi$ , to obtain an integral equation for  $a(\tau)$  incorporating an arbitrary electron distribution function. The electron phase can be expressed as  $\zeta = \zeta_i + v_i \tau + \zeta^{(1)}$  where  $\zeta^{(1)}$  is the first-order perturbation in  $a$ . Expanding (1) and (2) we have

$$a(\tau) = a_0 + ij \int_0^\tau ds \langle \exp[-i(\zeta_i + v_i s)] \zeta^{(1)}(s) \rangle, \quad (3)$$

$$\zeta^{(1)}(s) = \frac{1}{2} \int_0^s dq \int_0^q du [a(u) \exp(i(\zeta_i + v_i u)) + a^*(u) \exp(-i(\zeta_i + v_i u))] ,$$

where the initial optical field is  $a(0) = |a(0)| = a_0$  and  $\phi(0) = 0$ . We have made use of  $\langle \exp(-i\zeta_i) \rangle = \int_0^{2\pi} d\zeta_i \exp(-i\zeta_i) / 2\pi = 0$ , since the initial electrons are spread uniformly in phase. The reference to the individual electron phases  $\zeta^{(1)}$  can be explicitly removed by combining the equations in (3). Then, we have an integral equation governing the evolution of the optical field  $a(\tau)$ :

$$a(\tau) = a_0 + \frac{ij}{2} \int_0^\tau ds \int_0^s dq \int_0^q du \langle \exp(-iv_i(s-u)) \rangle a(u), \quad (4)$$

where  $\langle \dots \rangle$  is now an average over the initial electron velocity distribution, and all reference to the electron phases has been removed. Since (4) is an iterated triple integral, it may be rewritten [29] as a double integral,

$$a(\tau) = a_0 + \frac{ij}{2} \int_0^\tau ds \int_0^s dq \langle \exp(-iv_i(s-q)) \rangle (s-q) a(q). \quad (5)$$

A normalized electron distribution function  $f(v_i)$  can be used to evaluate the remaining average:

$$\langle \dots \rangle \equiv \int_{-\infty}^{\infty} dv_i f(v_i) (\dots) \text{ with } \int_{-\infty}^{\infty} dv_i f(v_i) = 1.$$

### III. Simple Electron Distributions

We begin by considering two simple examples with perfect beam quality. In the first, we start the FEL on resonance where the electron-optical wave coupling is largest,  $f(v_i) = \delta(v_i)$ . The optical wave is most simply determined from (4).

$$a(\tau) = a_0 + \frac{ij}{2} \int_0^\tau ds \int_0^s dq \int_0^q du a(u) \quad (6)$$

The integral equation (6) can also be written in a differential form by taking successive derivatives,  $\ddot{a}(\tau) = ija(\tau)/2$ . The complete solution uses the form  $a(\tau) = \sum_{n=1}^3 a_n \exp(\alpha_n \tau)$  where the  $\alpha_n$  are the three complex roots of the cubic equation  $\alpha^3 - ij/2 = 0$ , and the coefficients  $a_n$  are determined by the initial conditions  $a(0) = a_0$ , and  $\dot{a}(0) = \ddot{a}(0) = 0$  [1]. The solution for  $a(\tau)$  is

$$a(\tau) = \frac{a_0}{3} \left[ \exp((j/2)^{1/3} (i+\sqrt{3}) \tau/2) + \exp((j/2)^{1/3} (i-\sqrt{3}) \tau/2) + \exp(-i(j/2)^{1/3} \tau) \right] \quad (7)$$

If the current density is small  $j \rightarrow 0$ , or  $\tau \ll 1$ , we have the trivial result  $a(\tau) = a_0 (1 + ij\tau^3/12 + \dots)$  for an FEL starting on resonance. There is no change in the optical amplitude  $|a| = a_0 + \dots$  to lowest order, and therefore no gain. The optical phase  $\phi(\tau)$  increases slowly in proportion to  $\tau^3$ . The FEL gain is defined as  $G(\tau) = (|a(\tau)|^2 - a_0^2)/a_0^2$ , and

$$G(\tau) = \frac{1}{9} \left[ 2 \cosh((j/2)^{1/3} \sqrt{3} \tau) + 4 \cos((j/2)^{1/3} 3 \tau/2) \cosh((j/2)^{1/3} \sqrt{3} \tau/2) - 6 \right] \quad (8)$$

In the high current limit,  $j \gg 1$  on resonance, the expressions simplify because one fastest-growing root dominates and describes exponential growth in  $\tau$ . As seen from (7) there is little change in the field during the bunching time,  $\tau < \tau_B \approx (2/j)^{1/3}$ , that precedes exponential growth. During this time, the electrons move from their initially uniform phase distribution to bunch near the phase  $\zeta + \phi = \pi/2$ . As soon as bunching forms, the high current immediately causes exponential field growth and high gain. Then,

$$a(\tau) \approx \frac{a_0}{3} \exp[(j/2)^{1/3} \sqrt{3} \tau/2], \quad \text{and} \quad G(\tau) \approx \frac{1}{9} \exp[(j/2)^{1/3} \sqrt{3} \tau] \quad (9)$$

A second simple example is a high quality electron beam starting off resonance at  $\nu_0$ . This is characterized by  $f(\nu_i) = \delta(\nu_i - \nu_0)$ . The optical field is then determined by

$$a(\tau) = a_0 + \frac{ij}{2} \int_0^\tau ds \int_0^s dq \int_0^q du e^{-i\nu_0(s-u)} a(u) \quad (10)$$

For low current,  $j \leq 1$ , the optical field evolution away from  $a_0$  is small so that  $a(u) \approx a_0$  can be extracted from the integrand in (10). The resulting integrals are easily solved to obtain the

usual low current gain and phase shift formulas [27].

$$G(\tau) = j \frac{2 - 2\cos(v_0\tau) - v_0\tau \sin(v_0\tau)}{v_0^3}, \quad \text{and} \quad \phi(\tau) = j \frac{2 \sin(v_0\tau) - v_0\tau (1 + \cos(v_0\tau))}{2v_0^3} \quad (11)$$

The maximum final gain is  $G = 0.135j$  at  $v_0 = 2.6$  and  $\tau = 1$ , while the range of modes with significant gain is  $\delta v_0 \approx 1$  about the peak.

In order to obtain the general solution, use the substitution  $b = a e^{iv_0\tau}$  in (10). Successive derivatives then lead to the differential form of (10),  $\ddot{b} - iv_0\ddot{b} - j\dot{b}/2 = 0$ . Solutions of the form  $b = \sum_{n=1}^3 b_n \exp(\alpha_n \tau)$  have roots  $\alpha_n$  that satisfy the cubic equation  $\alpha_n^3 - iv_0\alpha_n^2 - j/2 = 0$ . In the limit of high current  $j \gg 1$ , the exponential gain coefficient is reduced by the factor  $-v_0^2 / 3\sqrt{3} (j/2)^{1/3}$  so that the gain spectrum is centered about  $v_0 = 0$  with a characteristic range  $\delta v_0 \approx 4.22j^{1/6}$ . In the high current case, the range of modes with significant gain increases slowly as  $j$  increases. We go on now to look at more interesting FEL distributions describing less than perfect electron beams.

#### IV. More General Electron Distributions

New cases of interest involve more complicated distributions  $f(v_i)$  describing the initial electron beam in the integral equation (5). Two electrons starting at the same phase  $\zeta_i$  at the beginning of the undulator ( $\tau = 0$ ), but with different z-velocities,  $c\beta_0$  and  $c(\beta_0 + \Delta\beta_0)$ , will drift apart as they travel through the undulator. The amount of drift is not easily predicted without solving the full problem, because electrons can influence each other through the self-consistently evolving optical wave. In this sense, the effect of FEL beam quality is collective. However, the times for the two electrons to traverse the undulator are nearly identical since they are relativistic,  $L/\beta_0 c \approx L/(\beta_0 + \Delta\beta_0)c \approx L/c$ . An estimate of their separation at the end of the undulator ( $\tau = 1$ ) is  $\Delta z \approx \Delta\beta_0 L$ , and their approximate phase difference is  $\Delta\zeta = (k + k_0)\Delta z \approx k\Delta z \approx kL\Delta\beta_0$ . If the velocity difference  $\Delta\beta_0$  is due to an initial energy difference  $\Delta\gamma mc^2$ , we have  $\Delta\beta_0 \approx (1 + K^2)\Delta\gamma/\gamma^3$ , and an approximate final phase separation  $\Delta\zeta \approx 4\pi N \Delta\gamma/\gamma$ .

Any random phase difference  $\Delta\zeta \sim \pi$ , or larger, between electrons in the beam is important to the FEL operation, because bunching on the optical wavelength scale is diminished significantly. At the end of the undulator, the final phase difference is roughly estimated by  $\Delta\zeta \approx \Delta v_i$  for each electron. From the definition of the electron phase velocity  $v_i$ , we see that a

small change in the initial electron energy  $\Delta\gamma mc^2$  corresponds to a change in the initial phase velocity,  $\Delta v_i \approx 4\pi N \Delta\gamma / \gamma$  ,  $\gamma \gg 1$ . A distribution of initial electron energies from an accelerator or storage ring is often accurately represented by the normal distribution function so that we can take

$$f(v_i) = \frac{\exp(-(v_i - v_0)^2 / 2\sigma^2)}{\sqrt{2\pi}\sigma} \quad (12)$$

where  $\sigma$  is the standard deviation of  $v_i$  away from the peak phase velocity  $v_0$ . If  $\Delta\gamma mc^2$  is taken to be the standard deviation of the electron energy away from  $\gamma mc^2$ , then  $\sigma \approx 4\pi N \Delta\gamma / \gamma$ . Two electrons starting at the same phase  $\zeta_i$ , but with an energy difference  $\Delta\gamma = \gamma / 4N$  will drift apart by roughly half of one optical wavelength at the end of the undulator. A random spread of width  $\sigma = \pi$  causes a random phase spread of approximately  $\Delta\zeta \approx \pi$  at the end of the undulator and impairs bunching. Inserting (12) into (5) gives

$$a(\tau) = a_0 + \frac{ij}{2} \int_0^\tau ds \int_0^s dq e^{-\sigma^2(s-q)^2/2} e^{-iv_0(s-q)} (s-q) a(q) \quad (13)$$

The gaussian factor in the integrand decreases the coupling current  $j$  as  $\tau$  increases, and describes the degradation of bunching due to the spread in electron phase velocities. The complicated self-consistent evolution of the electron beam distribution and the optical field are described exactly in (13), but before evaluation, we can generalize its form further.

An angular spread is also possible due to the finite emittance of an electron beam. An electron of energy  $\gamma mc^2$  entering the undulator with a small injection angle  $\theta_i$  has a reduced  $z$ -velocity,  $\beta_0 \rightarrow \beta_0 \cos \theta_i \approx \beta_0 (1 - \theta_i^2 / 2)$ . The resulting  $z$ -velocity change is  $\Delta\beta_0 \approx -\theta_i^2 / 2$ , reducing the initial phase velocity by  $\Delta v_i = -2\pi N \gamma^2 \theta_i^2 / (1 + K^2)$ . A gaussian distribution of angles about the  $z$ -axis with standard deviation  $\Delta\theta_i$  gives the exponential distribution function

$$f(v_i) = \frac{\exp(-(v_0 - v_i) / \sigma_\theta)}{\sigma_\theta} \quad \text{for } v_i < v_0, \text{ and } f(v_i) = 0 \quad \text{for } v_i > v_0 \quad (14)$$

where  $\sigma_\theta = 4\pi N \gamma^2 \Delta\theta_i^2 / (1 + K^2)$ , and  $v_0$  is the phase velocity for electrons entering on-axis. The distribution function (14) is sharply peaked at  $v_i = v_0$  where electrons enter on-axis, and decays exponentially for  $v_i < v_0$  because the injection at any angle  $\theta_i$  can only decrease the electron's longitudinal velocity and its phase velocity  $v_i$ . If each element of the energy distribution (12) is given an angular spread according to (14), then the resulting integral equation for the optical field becomes

$$a(\tau) = a_0 + \frac{ij}{2} \int_0^\tau ds \int_0^s dq \frac{e^{-\sigma^2(s-q)^2/2}}{1 - i\sigma_0(s-q)} e^{-iv_0(s-q)} (s-q) a(q) . \quad (15)$$

The transverse motion of electrons injected at an angle is sometimes confined by either the natural off-axis undulator fields or external focusing elements. The focusing forces result in transverse betatron oscillations about the undulator axis. When the electron beam is injected to match the natural focusing properties of an undulator, the number of betatron oscillations along the undulator is  $N_\beta \approx NK\sqrt{2}\gamma$ . In the limit of large  $\gamma$  and/or small  $K$ , the angular spread of electrons can be important,  $\sigma_0 > 1$ , while the transverse focusing can be made negligible,  $N_\beta < 1$ . In this limit, the integral equation (15) applies.

The complex optical field  $a(\tau)$  now depends on an input energy spread characterized by  $\sigma$ , and an input angular spread characterized by  $\sigma_0$ . Other types of distribution functions can be added in a similar way. If (5) is solved numerically, even experimental distribution functions peculiar to a given accelerator or transport system can be added. The general result (5) and the specific example (15) are important results of this paper. They provide analytic expressions describing FEL performance with an arbitrary electron distribution function.

## V. Low-Current FELs

One of the cases of general interest is the low current FEL oscillator. Radiation energy is stored in an optical resonator, and repeatedly driven by successive electron pulses from an accelerator like a linac or storage ring. An important issue for the oscillator is the detrimental effect of the electron energy and angular distributions when the oscillator is starting from weak optical fields. In the low-current case, we can simplify (15) by taking  $a(q) \approx a_0$  in the integrand of the integral equation, and neglecting higher-order terms in  $j$ . Without  $a(q)$  in the integrand, the integral can be further simplified by noticing that  $iqe^{-iv_0q} = -\partial_{v_0} e^{-iv_0q}$ . Then,

$$\frac{a(\tau) - a_0}{a_0} = -\frac{j}{2} \frac{\partial}{\partial v_0} \int_0^\tau ds \int_0^s dq \frac{e^{-\sigma^2 q^2/2}}{1 - i\sigma_0 q} e^{-iv_0 q} . \quad (16)$$

Direct integration of (16) is possible, but the result is a complicated expression containing many error-functions [30].

We can alter the form of (16), however, to obtain some important physical interpretations. The factors  $e^{-\sigma^2 q^2/2}$  and  $(1 - i\sigma_0 q)^{-1}$  can be interpreted as power series expansions in  $q$

multiplying the factor  $e^{-iv_0 q}$ ; then  $(-iq)^n e^{-iv_0 q} \rightarrow \partial_{v_0}^n e^{-iv_0 q}$ . Now, write

$$\frac{a(\tau) - a_0}{a_0} = -\frac{j}{2} \frac{\exp(\sigma^2 \partial_{v_0}^2 / 2)}{1 + \sigma_0 \partial_{v_0}} \partial_{v_0} \int_0^\tau ds \int_0^s dq e^{-iv_0 q} . \quad (17)$$

The double integral is simply  $v_0^{-2} (1 - iv_0 \tau - e^{-iv_0 \tau})$ , so that the complex integrations in (16) have been replaced with a power series expansion to all orders in  $\sigma$  and  $\sigma_0$ . To first order in  $\sigma$  and  $\sigma_0$ , an explicit expression for  $a(\tau)$  is easily obtained from (17). This is a useful limiting case since a low-current FEL system would not typically use a low quality electron beam (large  $\sigma$  or  $\sigma_0$ ) and remain above threshold. From (17), the low-current FEL gain at the end of the undulator is

$$G = -\frac{j}{2} \frac{\exp(\sigma^2 \partial_{v_0}^2 / 2)}{1 + \sigma_0 \partial_{v_0}} \partial_{v_0} \left[ \frac{\sin^2(v_0/2)}{(v_0/2)^2} \right] . \quad (18)$$

We recognize the factor in brackets [...] as the FEL spontaneous emission line-shape for an electron in a perfect trajectory through the undulator. It has been known for some time that the gain is fundamentally related to the derivative of the spontaneous emission line-shape [31]. The new feature presented in (18) is to express how the electron beam energy and angular spreads affect that relationship through successively higher derivatives.

With the physical interpretation of the line-shape factor [...], we can substitute alternate forms. One convenient choice is  $[...] \rightarrow \exp(-v_0^2/4\pi)$  which approximately reproduces the correct features of the simple FEL gain spectrum,  $G \approx (jv_0/4\pi) \exp(-v_0^2/4\pi)$ . The successive derivatives evaluating the effects of beam quality lead to more compact expressions, and illustrate how (18) can be used in practical situations. Even an experimental line-shape could be used in (18).

While the analytic results presented have their merit, the complete integral (15) is easy to integrate on a small computer. The values needed for the contour plots of this paper were evaluated in this way. Figure 1 shows a combined intensity and contour plot of  $\ln(1+G(\sigma, v_0))$  where the final gain at the end of the FEL undulator is  $G = (a^*(1) a(1) - a_0^2) / a_0^2$ . In Fig. 1  $\sigma_0 = 0$ , so that gain degradation is only due to an energy spread with no angular spread. The current density is  $j = 1$ , and gives low gain so that  $\ln(1+G) \approx G$ . The brightest points (white) on the  $(\sigma, v_0)$ -surface indicate peak gain  $G \approx 0.13j$ , while the darkest points (black) indicate maximum absorption  $G \approx -0.13j$ . Zero gain is indicated by the intermediate grey shown in the scale at the

top. Specific contours of constant gain,  $\ln(1+G) = \pm 0.06, \pm 0.08, \pm 0.1$ , and  $\pm 0.12$ , are superimposed on the intensity plot. The gain surface is approximately antisymmetric about  $v_0 = 0$ , and in the limit  $j \rightarrow 0$ , the gain  $G(\sigma, v_0)$  becomes exactly antisymmetric. The characteristic amount of spread required to decrease the gain is seen from Fig. 1 and (18) to be  $\sigma^* \approx 1$ . Note also that as the spread  $\sigma$  increases, the phase velocity for peak gain  $v_0^* \approx 2.6$  increases slightly. Peak absorption occurs at  $-v_0^*$  and slightly decreases with increasing  $\sigma$ .

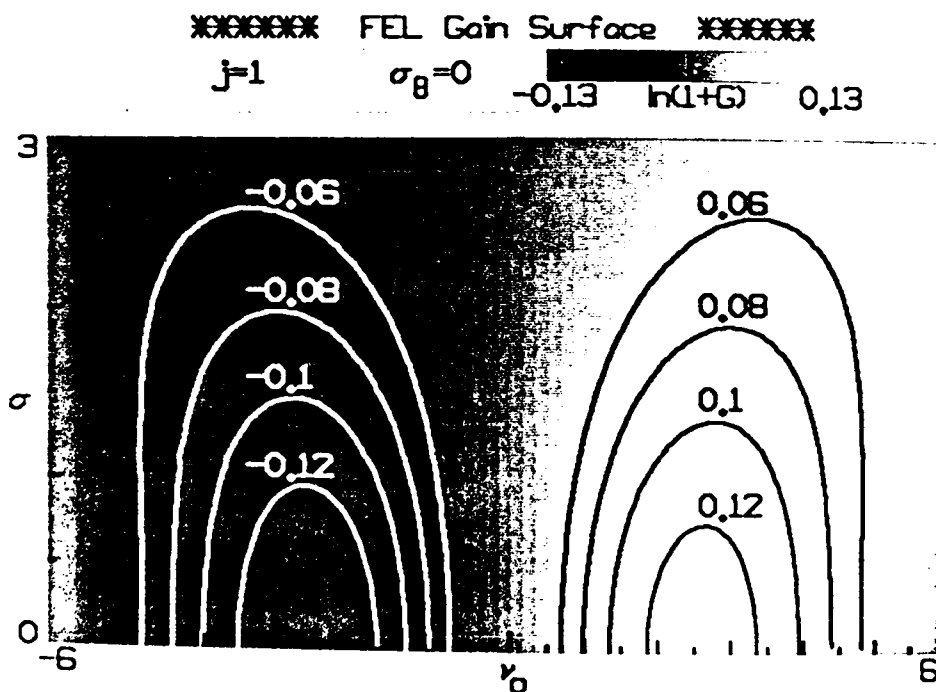


Fig. 1. Intensity and contour plot of  $\ln(1+G(\sigma, v_0))$  with  $j = 1$  and  $\sigma_0 = 0$ . The weak-field gain degradation in this low-current FEL is due to an electron beam energy spread with a normal distribution function.

Figure 2 shows a combined intensity and contour plot of  $\ln(1+G(\sigma_0, v_0))$  evaluated by (15) with  $j = 1$  and  $\sigma = 0$ . The gain degradation here is due to a monoenergetic electron beam entering the undulator with an angular spread described by  $\sigma_0$ . The grey scale and contours of gain are the same as in Fig. 1. Unlike Fig. 1, the absorption contours (white) have a much different shape than the gain contours (black). Since the distribution function  $f(v_i)$  due to an angular spread is skewed, there is no reason to expect the antisymmetric properties of  $G(\sigma_0 = 0, v_0)$  to be

maintained at  $\sigma_0 > 0$ . As seen in Fig. 1 and (18), the characteristic value for the degradation of gain is  $\sigma_0^* \approx 1$ . The phase velocity for peak gain, and peak absorption, both increase with increasing  $\sigma_0$  roughly as  $v_0^* \approx \sigma_0$ . Note that the general features of Figs. 1 and 2 are quite different owing to the different forms of the electron distributions. This emphasizes the importance of the shape of the electron distribution in evaluating gain degradation in FELs, and the need for an accurate, flexible theory as presented here.

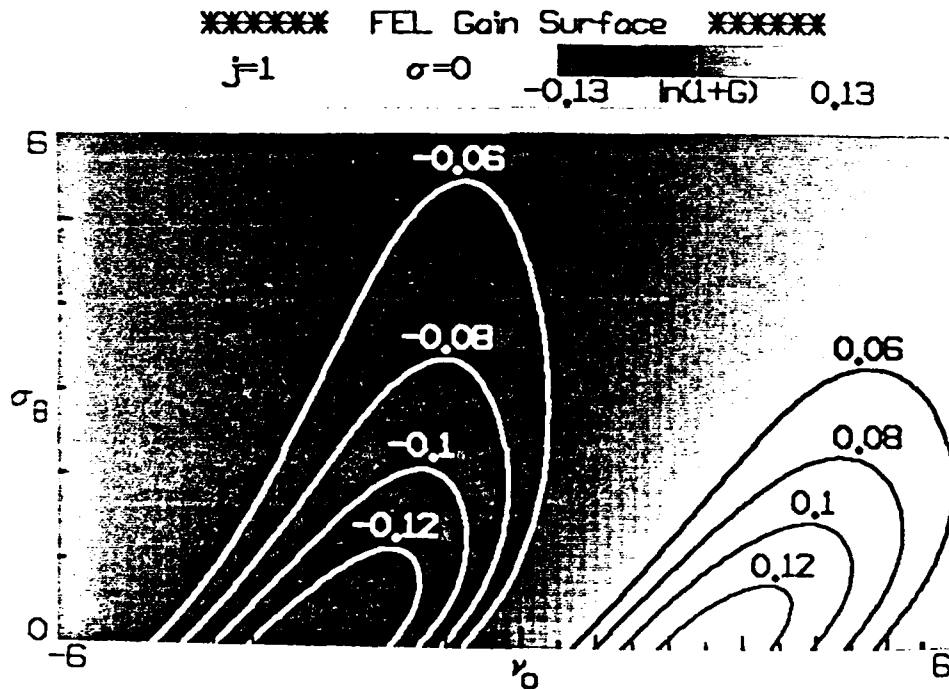


Fig. 2. Intensity and contour plot of  $\ln(1+G(\sigma_0, v_0))$  with  $j = 1$  and  $\sigma = 0$ . The weak-field gain degradation in this low-current FEL is due to an electron beam angular spread with a normal distribution; the resultant phase-velocity distribution is the exponential distribution function.

## VI. High-Current FELs

The integral representation of the optical field in (15) is also valid for high-current FELs where  $j \gg 1$ . In this case,  $a(\tau)$  acquires a non-linear dependence on  $j$  ( recall expression (7) ) and cannot be removed from the integrand of (15). To proceed analytically, it is convenient to remove one integral from (15) by taking the  $\tau$ -derivative of both sides, and use the form  $a = a_0 e^{a\tau}$

for the optical field. Since  $j \gg 1$ , assume that  $\alpha$  has some large real part, even though the exponential growth may be somewhat diminished by the presence of  $\sigma$  and  $\sigma_0$ . The magnitude  $a_0$  cancels on both sides, and a change of variables gives the form

$$\alpha^3 \approx \frac{ij}{2} \int_0^\infty ds s e^{-s} \frac{e^{-\sigma^2 s^2 / 2\alpha^2}}{1 - i\sigma_0 s / \alpha} e^{-i v_0 s / \alpha} . \quad (19)$$

The upper integration limit in (19) has been extended to infinity because the integrand containing the factor  $e^{-s}$  becomes negligible for large  $s$ .

Eqn. (19) describes several properties of high-gain FELs without integration. If  $\sigma$ ,  $v_0$ , and  $\sigma_0$  all  $\rightarrow 0$ , then  $\alpha$  has the same roots found in (7). If the current density  $j \rightarrow \infty$  so that a real part of  $\alpha \rightarrow \infty$ , then we obtain the same limit, since  $\sigma$ ,  $v_0$ , and  $\sigma_0$  all appear divided by  $\alpha$  in (19). Unlike the low-current FEL, the importance of beam quality in a high-current FEL depends on the current density  $j$ . This feature has been seen in FEL experiments and simulations, but is now expressed analytically. The importance of beam quality can be made more quantitative by iterating (19). Estimating the real part of the fast-growing root as  $\alpha^* = (j/2)^{1/3} \sqrt{3}/2$ , the integrand of (19) is only significantly modified when  $\sigma^* = (j/2)^{1/3} \sqrt{3}/2$  or when  $\sigma_0^* = (j/2)^{1/3} \sqrt{3}/2$ . In the high-current FEL, the characteristic values of beam quality,  $\sigma^*$  and  $\sigma_0^*$ , are not equal, and increase with the current density  $j$ . These expressions should be helpful in designing high-gain experiments where there is a trade-off between beam quality and beam current.

Figure 3 shows a combined intensity and contour plot of  $\ln(1+G(\sigma, v_0))$  for moderately high current  $j = 100$  and  $\sigma_0 = 0$ . The points at the peak gain  $\ln(1+G) = 4.3$  are indicated by white on the  $(\sigma, v_0)$ -surface; black indicates zero gain. Contours of constant gain,  $\ln(1+G) = 2.0, 2.5, 3.0, 3.5$ , and 4.0 are superimposed on the intensity plot. For the high quality electron beam, small  $\sigma$ , gain is confined to a region near resonance, but extends to a broader range in  $v_0$  than in the low-current cases of Figs. 1 or 2. This agrees with the discussion below (11), and gives the range of optical wavelengths over which there is significant gain  $\delta v_0 \approx 4j^{1/6} \approx 7$ . To find the range of wavelengths, use  $\Delta\lambda/\lambda \approx \Delta v_0 / 2\pi N$  about the resonant wavelength  $\lambda = \lambda_0(1+K^2)/2\gamma^2$ . The maximum available gain decreases significantly as  $\sigma \rightarrow \sigma^* \approx 4.5$  as predicted in the previous paragraph, and the phase velocity for peak gain roughly follows  $v_0^* \approx \sigma$ .

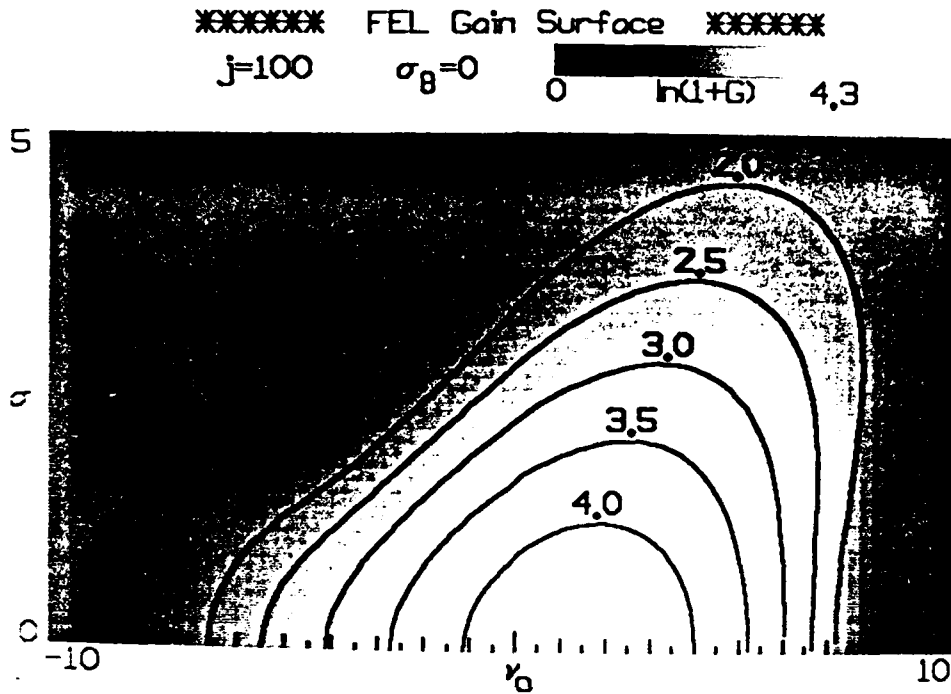


Fig. 3. Intensity and contour plot of  $\ln(1+G(\sigma, v_0))$  with  $j = 100$  and  $\sigma_8 = 0$ . The weak-field gain degradation in this FEL is due to an electron beam with a normal distribution in energy.

Figure 4 shows the plot of  $\ln(1+G(\sigma_8, v_0))$  with  $\sigma = 0$  so that the gain degradation is caused by an angular spread in the electron beam. The contours of constant gain differ from Fig. 3 because of the new shape of the electron distribution function. As  $\sigma_8$  increases, there is a slower decrease in gain because  $\sigma_8^* > \sigma^*$  as found above. When expressed in dimensionless form, an angular spread is better tolerated in an FEL than is an energy spread. The points of peak gain increase with increasing  $\sigma_8$  similar to Fig. 3.

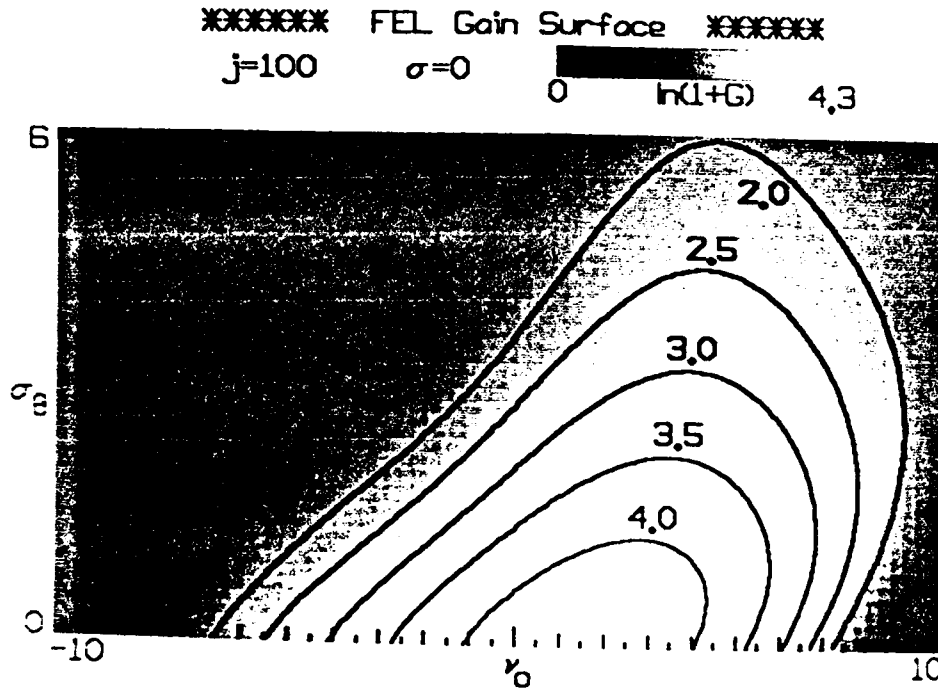


Fig. 4. Intensity and contour plot of  $\ln(1+G(\sigma_0, v_0))$  with  $j = 100$  and  $\sigma = 0$ . The weak-field gain degradation in this FEL is due to an electron beam with an angular spread producing an exponential distribution in phase velocities.

Figure 5 shows the combined intensity and contour plot of  $\ln(1+G(\sigma, v_0))$  for high current  $j = 10^4$  with  $\sigma_0 = 0$ . There are no negative gain regions, and the available peak gain is much larger than for the lower current. For  $\sigma \approx 0$ , the position of peak gain is essentially at resonance  $v_0 = 0$ , but again increases roughly as  $v_0^* \approx \sigma$  while beam quality diminishes. The width of the gain spectrum at  $\sigma = 0$  is wider than the lower current case, and agrees well with  $\delta v_0 \approx 4j^{1/6} \approx 12$ . The contours of constant gain,  $\ln(1+G) = 14, \dots, 24$ , show that the range of wavelengths for gain becomes narrower as  $\sigma$  increases, and the maximum available gain decreases significantly as  $\sigma \rightarrow \sigma^* \approx 20$ .

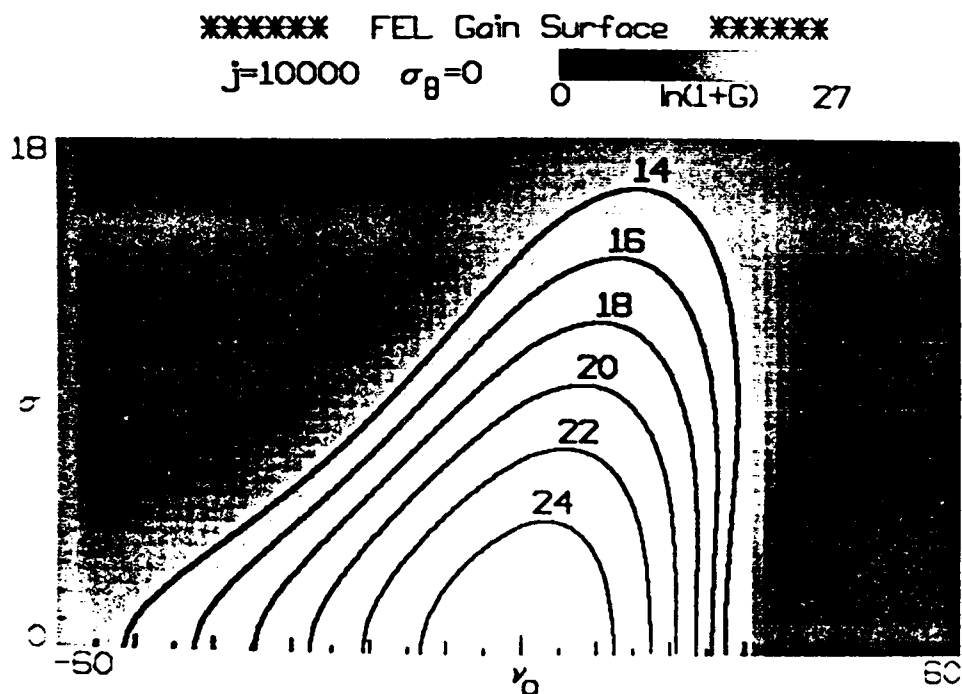


Fig. 5. Intensity and contour plot of  $\ln(1+G(\sigma, \nu_0))$  with  $j = 10^4$  and  $\sigma_0 = 0$ . The weak-field gain degradation in this high-gain FEL is due to an electron beam with a normal distribution in energy.

Figure 6 shows the plot of  $\ln(1+G(\sigma_0, \nu_0))$  for high current  $j = 10^4$  with  $\sigma = 0$ . Again, the contours of constant gain,  $\ln(1+G) = 14, \dots, 24$ , are distinct from Fig. 5 showing the importance of the electron beam distribution function even at high gain. As  $\sigma_0 \rightarrow \sigma_0^*$ , the gain decreases significantly, but again the angular spread is seen to be less harmful than an energy spread. Unlike Fig. 5, the position of peak gain stays closer to resonance as  $\sigma_0$  increases.

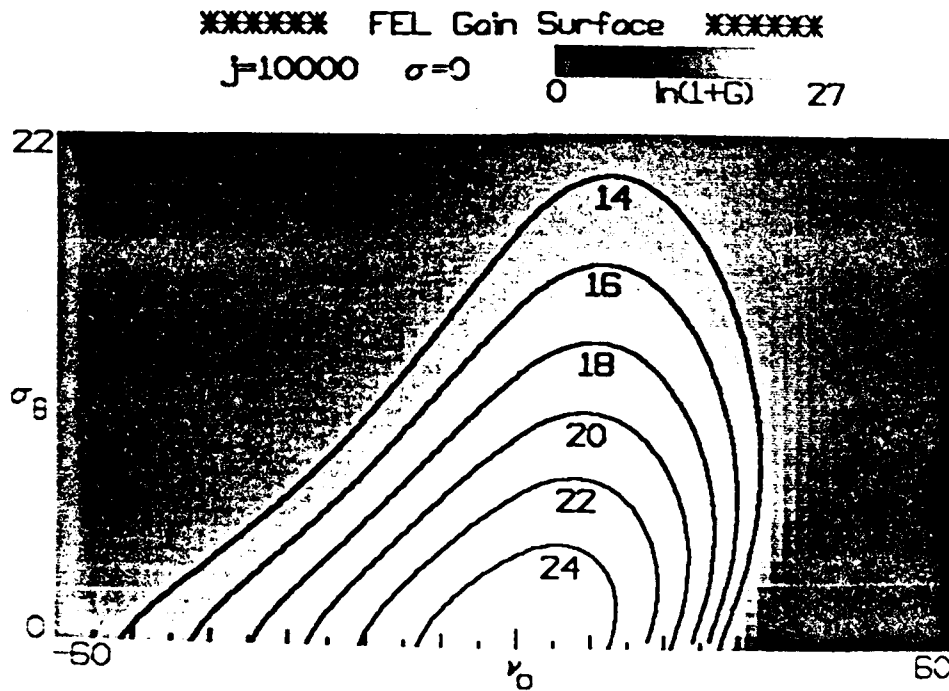


Fig. 6. Intensity and contour plot of  $\ln(1+G(\sigma_0, v_0))$  with  $j = 10^4$  and  $\sigma = 0$ . The weak-field gain degradation in this high-gain FEL is due to an electron beam with an angular spread producing an exponential distribution in phase velocities.

#### References

1. W. B. Colson and A. M. Sessler, *Annuals Reviews of Nuclear and Particle Science* 35, 25 (1985).
2. S. Benson, D. A. G. Deacon, J. N. Eckstein, J. M. J. Madey, K. Robinson, T. I. Smith and R. Taber, *J. de Physique* 44, Colloque C1, 353 (1983).
3. J. A. Edighoffer, G. R. Neil, C. E. Hess, T. I. Smith, S. W. Fornaca and H. A. Schwettman, *Phys. Rev. Lett.* 52, 344 (1984).
4. Billardon, M. et. al., *Phys. Rev. Lett.* 51, 1652 (1983).
5. L. R. Elias, J. Hu, and G. Ramian, *Nucl. Instr. and Math. in Phys. Res.* A237, 203 (1985).

6. *Free-Electron Generators of Extreme Ultraviolet Coherent Radiation*, AIP Conf. Proc. No. 118, eds. Madey and Pellegrini, Brookhaven National Lab, Upton NY (1984).
7. V. K. Neil, JASON Technical Report JSR-79-10 (1979).
8. Ira B. Bernstein and J. L. Hirshfield, Phys. Rev. Lett. **40**, 761 (1978).
9. Ira B. Bernstein and J. L. Hirshfield, Phys. Rev. **20A**, 1661 (1979).
10. N. M. Kroll and W. A. McMullin, Phys. Rev. **A17**, 300 (1978).
11. P. Sprangle, Cha-Mei Tang, and W. M. Manheimer, Phys. Rev. **A21**, 302 (1980).
12. P. Sprangle and Robert A. Smith, Phys. Rev. **A21**, 293 (1980).
13. W. B. Colson and S. K. Ride, *Physics of Quantum Electronics*, **7**, 377, eds. Jacobs, Pilloff, Sargent, Scully, and Spitzer (Addison-Wesley 1980).
14. F. Ciocci, G. Dattoli and A. Renieri, Lettere Al Nuovo Cimento **34**, 342 (1982).
15. I. Boscolo, M. Leo, R. A. Leo and G. Soliani, Il Nuovo Cimento **2D**, 64 (1983).
16. J. C. Goldstein, W. B. Colson, and R. W. Warren, Bendor Free Electron Laser Conference, J. de Physique **44**, C1-371 (1983).
17. L. F. Ibanez and S. Johnston, IEEE Journal of Quantum Electron. **QE-19**, 339 (1983).
18. J. Gea-Banacloche, G. T. Moore, and M. O. Scully, *Free Electron Generators of Coherent Radiation*, SPIE **453**, 393 (Society of Photo-Optical Inst. Eng. 1983).
19. J. Gea-Banacloche, G. T. Moore, and M. O. Scully, *Free Electron Generation of Extreme Ultraviolet Coherent Radiation*, AIP Conf. Proceedings No. 118, eds. J. M. J. Madey and C. Pellegrini, p. 161 (American Inst. of Physics 1984).
20. G. T. Moore, Opt. Commun. **54**, 121 (1985).
21. L. K. Grover, J. Feinstein, R. H. Pantell, IEEE J. Quant. Electron. **QE-21**, 470 (1985).
22. K.-J. Kim, Seventh Annual Free Electron Laser Conference, Lake Tahoe CA (1985).
23. G. Dattoli and A. Renieri, *Experimental and Theoretical Aspects of the Free Electron Laser*, Laser Handbook, **4**, eds. M. L. Stich and M. S. Bass (North-Holland, Amsterdam, 1985).
24. E. Jerby and A. Gover, IEEE J. Quantum Electron. **QE-21**, 1041 (1985).
25. W. B. Colson and S. K. Ride, Phys. Lett. **76A**, 379 (1980).
26. W. B. Colson, IEEE J. Quantum Electron. **QE-17**, 1417 (1981).
27. W. B. Colson, Phys. Lett. **A64**, 190 (1977).
28. W. B. Colson and R. A. Freedman, Phys. Rev. **A27**, 1399 (1983).
29. M. Abramowitz and I. A. Stegun, Handbook of Mathematical Functions, p. 891, National Bureau of Standards, 1972.

AD-A172 996

FREE ELECTRON LASER THEORY(U) BERKELEY RESEARCH  
ASSOCIATES INC CA W B COLSON 10 JUL 86 BRA-86-313R  
AFOSR-TR-86-0912 F49620-85-C-0007

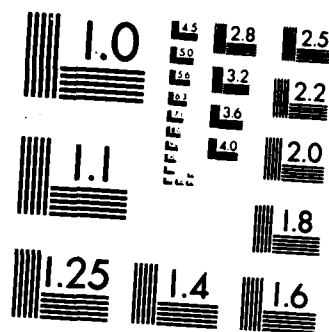
2/2

UNCLASSIFIED

F/G 20/5

NL





MICROCOPY RESOLUTION TEST CHART  
NATIONAL BUREAU OF STANDARDS-1963-A

30. P. M. Bosco, Ph.D. Thesis, University of California at Santa Barbara, 1985.
31. J. M. J. Madey, J. Appl. Phys. 42, 1906 (1971).

# REPORT OF INVENTIONS AND SUBCONTRACTS

(Pursuant to "Patent Rights" Contract Clause) (See Instructions on Reverse Side.)

FORM APPROVED  
OMB NO. 0704-0016

1. NAME OF CONTRACTOR/ SUBCONTRACTOR Berkeley Research Associates	2a. NAME OF GOVERNMENT PRIME CONTRACTOR Same	3. TYPE OF REPORT (check one) <input type="checkbox"/> INTERIM <input checked="" type="checkbox"/> FINAL
2. CONTRACT NUMBER F49620-85-C-0087	4. AWARD DATE (YYMMDD)	4. REPORTING PERIOD (YYMMDD) FROM: TO:
3. ADDRESS (include Zip Code) P.O. Box 241 Berkeley, CA 94701	4. AWARD DATE (YYMMDD)	

## SECTION I - SUBJECT INVENTIONS

a. NAME OF INVENTOR(S) (Last, First, M.I.)	b. TITLE OF INVENTION(S)	c. DISCLOSURE NO. PATENT APPLICATION SERIAL NO. OR PATENT NO.	d. ELECTION TO FILE PATENT APPLICATIONS				e. CONFIRMATORY INSTRUMENT OR ASSIGNMENT FORWARDED TO CONTRACTING OFFICER
			UNITED STATES	FOREIGN	YES	NO	
NONE	NONE	NONE	YES	NO	YES	NO	

i. EMPLOYER OF INVENTOR(S) NOT EMPLOYED BY CONTRACTOR/SUBCONTRACTOR.	g. ELECTED FOREIGN COUNTRIES IN WHICH A PATENT APPLICATION WILL BE FILED.	
	ii. NAME OF INVENTOR (Last, First, M.I.)	ii. FOREIGN COUNTRIES OF PATENT APPLICATION
ii. NAME OF EMPLOYER NONE	NONE	NONE
iii. ADDRESS OF EMPLOYER (include Zip Code)		

## SECTION II - SUBCONTRACTS (Containing a "Patent Rights" clause)

a. NAME OF SUBCONTRACTOR(S)	b. ADDRESS (include Zip Code)	c. SUBCONTRACT NO. (\$)	d. "PATENT RIGHTS"		e. DESCRIPTION OF WORK TO BE PERFORMED UNDER SUBCONTRACT(S)	f. SUBCONTRACT DATES (YYMMDD)	
			CLAUSE NO.	DATE (YYMM)		AWARD	ESTIMATED COMPLETION
NONE	NONE	NONE			NONE		

## SECTION III - CERTIFICATION

7. CERTIFICATION OF REPORT BY CONTRACTOR/SUBCONTRACTOR. (Not required if <input checked="" type="checkbox"/> Small Business or <input type="checkbox"/> Non-Profit organization.) (Check appropriate box)	
a. NAME OF AUTHORIZED CONTRACTOR/SUBCONTRACTOR OFFICIAL (Last, First, M.I.) MAGANN, KATHERINE B.	c. I certify that the reporting party has procedures for prompt identification and timely disclosure of "Subject Inventions," that such procedures have been followed and that all "Subject Inventions" have been reported.
b. TITLE CORPORATION SECRETARY	SIGNATURE OF AUTHORIZED CONTRACTOR/SUBCONTRACTOR OFFICIAL <i>Katherine B. Magann</i> 860722 DATE (YYMMDD)

END

12-86

DTIC